



NATIONAL AERONAUTICS AND SPACE ADMINISTRATION

APOLLO 9 MISSION REPORT  
SUPPLEMENT 2

GUIDANCE, NAVIGATION, AND CONTROL  
SYSTEM PERFORMANCE ANALYSIS

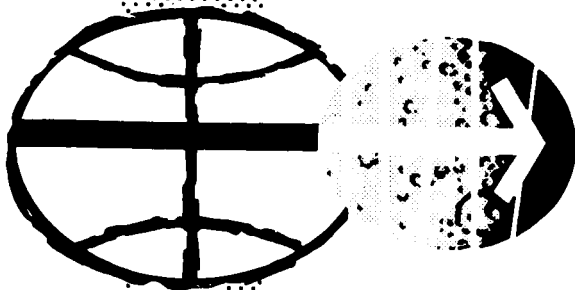
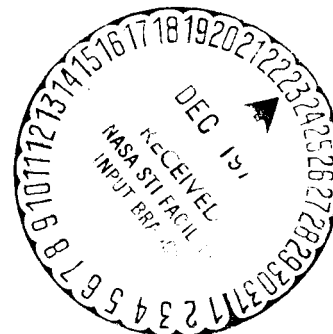
(NASA-TM-X-72261) APOLLO 9 MISSION  
REPORT. SUPPLEMENT 2: GUIDANCE,  
NAVIGATION, AND CONTROL SYSTEM PERFORMANCE  
ANALYSIS (NASA) 162 p

N75-70467

Unclas

00/98

17335



MANNED SPACECRAFT CENTER  
HOUSTON, TEXAS  
NOVEMBER 1969

APOLLO 9 MISSION REPORT

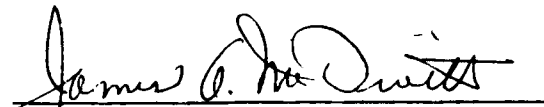
SUPPLEMENT 2

GUIDANCE, NAVIGATION, AND CONTROL  
SYSTEM PERFORMANCE ANALYSIS

PREPARED BY

TRW Systems Group

APPROVED BY



---

James A. McDivitt  
Manager, Apollo Spacecraft Program

NATIONAL AERONAUTICS AND SPACE ADMINISTRATION  
MANNED SPACECRAFT CENTER  
HOUSTON, TEXAS  
November 1969

---

PROJECT TECHNICAL REPORT  
TASK E-38B

---

APOLLO IX GUIDANCE, NAVIGATION AND  
CONTROL SYSTEM PERFORMANCE ANALYSIS  
REPORT

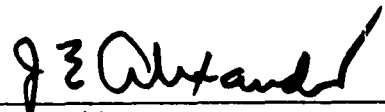
---

NAS 9-8166

15 MAY 1969

Prepared for  
NATIONAL AERONAUTICS AND SPACE ADMINISTRATION  
MANNED SPACECRAFT CENTER  
HOUSTON, TEXAS

Approved by



J. E. Alexander, Manager  
Guidance and Control  
Systems Department

## TABLE OF CONTENTS

	Page
1.0 INTRODUCTION	1-1
1.1 General	1-1
1.2 Background	1-1
2.0 SUMMARY	2-1
3.0 CSM IMU PERFORMANCE	3-1
3.1 Ascent Velocity Comparison	3-1
4.0 CSM DIGITAL AUTOPILOT	4-1
4.1 TVC DAP Performance	4-1
4.1.1 Attitude Errors	4-2
4.1.2 Ignition Transients	4-3
4.1.3 Manual Takeover	4-4
4.1.4 Roll TVC DAP	4-5
4.1.5 Stroking Tests	4-5
4.2 RCS DAP Performance	4-6
4.2.1 RCS DAP Automatic Maneuvers	4-6
4.2.2 RCS DAP Attitude Hold	4-7
4.3 Entry DAP Performance	4-7
4.3.1 Roll DAP Performance	4-7
4.3.2 Pitch and Yaw Rate Damping	4-8
5.0 LM IMU PERFORMANCE	5-1
5.1 DPS 1 Velocity Comparison	5-1

TABLE OF CONTENTS  
(Continued)

	Page
6.0 LM DIGITAL AUTOPILOT	6-1
6.1 LM/CSM Docked Configuration	6-1
6.1.1 Docked DPS Burn	6-1
6.1.2 Slosh	6-3
6.1.3 Compliance	6-5
6.2 Descent Configuration	6-5
6.2.1 DPS Insertion Burn	6-6
6.2.2 Attitude Hold	6-7
6.3 Ascent Configuration	6-7
6.3.1 Automatic Maneuver	6-7
6.3.2 Attitude Hold	6-8
6.3.3 Manual Control	6-8
6.3.4 CSI Burn	6-9
6.3.5 APS Burn to Depletion	6-9
7.0 LM/AGS/CES CONTROLLABILITY	7-1
7.1 DPS Phasing Burn (AGS)	7-1
7.1.1 Telemetry Quantization Versus the Rate - Attitude Phase Plane	7-1
7.1.2 GTS Performance	7-4

TABLE OF CONTENTS  
(Continued)

	Page
7.1.3 CG Offsets	7-4
7.2 Descent Stage Attitude Hold (AGS)	7-5
7.2.1 Propellant Consumption	7-5
8.0 RENDEZVOUS	8-1
8.1 Onboard Navigation	8-1
8.2 Rendezvous Targeting	8-1
8.2.1 CSI Maneuver Evaluation	8-2
8.2.2 TPI Maneuver Evaluation	8-2
REFERENCES	R-1

## LIST OF ILLUSTRATIONS

Figure	Page
3-1 DELVX G&N Minus Final S-IVB OMPT, W/O Compensation - Ascent	3-3
3-2 DELVY G&N Minus Final S-IVB OMPT, W/O Compensation - Ascent	3-5
3-3 DELVZ G&N Minus Final S-IVB OMPT, W/O Compensation - Ascent	3-7
3-4 DELVX G&N Minus S-IVB IU/TM, W/O Compensation - Ascent	3-9
3-5 DELVY G&N Minus S-IVB IU/TM, W/O Compensation - Ascent	3-11
3-6 DELVZ G&N Minus S-IVB IU/TM W/O Compensation - Ascent	3-13
3-7 DELVX G&N Minus S-IVB IU/TM, With Compensation - Ascent	3-15
3-8 DELVY G&N Minus S-IVB IU/TM, With Compensation - Ascent	3-17
3-9 DELVZ G&N Minus S-IVB IU/TM, With Compensation - Ascent	3-19
4-1 SPS 2 - Attitude Errors	4-15
4-2 SPS 2 - Gimbal Commands and Gimbal Positions	4-16
4-2a SPS 2 - Gimbal Position During Ignition Transient and 40% Stroking Tests	4-17
4-3 SPS 2 - Trim Angles	4-18
4-4 SPS 3 - Attitude Errors	4-19
4-5 SPS 3 - Pitch Rates and Attitude Errors During Rate MTVC	4-20
4-6 SPS 3 - Yaw Rates and Attitude Errors During Rate MTVC	4-21
4-7 SPS 3 - Gimbal Commands and Gimbal Positions	4-22

## LIST OF ILLUSTRATIONS (Continued)

Figure	Page
4-8 SPS 3 - Trim Angles	4-24
4-9 SPS 4 - Attitude Errors	4-25
4-10 SPS 4 - Gimbal Commands and Gimbal Positions	4-26
4-11 SPS 4 - Trim Angles	4-27
4-12 SPS 5 - Attitude Errors	4-28
4-13 SPS 5 - Gimbal Commands and Gimbal Positions	4-29
4-14 SPS 5 - Trim Angles	4-30
4-15 SPS 5 - Comparison of Measured Filter Output and Computed Filter Output	4-31
4-16 SPS 5 - Measured Gimbal Positions	4-32
4-17 Automatic Maneuver to SPS 2 Attitude - Body Rates	4-33
4-18 Automatic Maneuver to SPS 2 Attitude - CDU Angles	4-34
4-19 Automatic Maneuver to Docked DPS Burn Attitude - Body Rates	4-35
4-20 Automatic Maneuver to Docked DPS Burn Attitude - CDU Angles	4-36
4-21 Orbit Rate Automatic Maneuver - Body Rates	4-37
4-22 Orbit Rate Automatic Maneuver - CDU Angles	4-38
4-23 Attitude Hold Prior to SPS 3 - Roll Phase Plan	4-39
4-24 Attitude Hold Prior to SPS 3 - Pitch Phase Plan	4-40
4-25 Attitude Hold Prior to SPS 3 - Yaw Phase Plan	4-41
4-26 Attitude Hold Prior to SPS 4 - Roll Phase Plan	4-42
4-27 Attitude Hold Prior to SPS 4 - Pitch Phase Plan	4-43
4-28 Attitude Hold Prior to SPS 4 - Yaw Phase Plan	4-44

## LIST OF ILLUSTRATIONS (Continued)

Figure	Page
4-29 Commanded and Actual Roll Angles During Entry	4-45
4-30 Yaw Thruster Activity During Bank Angle Reversal	4-46
4-31 Yaw Thruster Activity During Bank Angle Reversal	4-47
5-1 DELVX LM Minus CSM W/O Compensation - DPS 1	5-5
5-2 DELVY LM Minus CSM W/O Compensation - DPS 1	5-7
5-3 DELVZ LM Minus CSM W/O Compensation - DPS 1	5-9
5-4 DELVX LM Minus CSM With Compensation - DPS 1	5-11
5-5 DELVY LM Minus CSM With Compensation - DPS 1	5-13
5-6 DELVZ LM Minus CSM With Compensation - DPS 1	5-15
6-1 Docked DPS Burn P Axis Phase Plane	6-12
6-2 LGC Angular Rates Versus Time During Manual Throttle Profile	6-13
6-3 Docked DPS Burn - CSM BMAG Rates	6-14
6-4 Docked DPS Burn - Velocity-to-be-gained	6-15
6-5 Docked DPS Burn - Time History of GDA's and Throttle Setting	6-16
6-6 DPS Insertion Burn - U Axis Attitude Errors and Jet Firings	6-17
6-7 DPS Insertion Burn - P Axis Phase Plane	6-18
6-8 DPS Insertion Burn - V Axis Phase Plane	6-19
6-9 DPS Insertion Burn - Velocity-to-be-gained	6-20
6-10 DPS Insertion Burn - GDA Time History	6-21

LIST OF ILLUSTRATIONS (Continued)

Figure		Page
6-11	Descent Configuration - Attitude Hold - P Axis Phase Plane	6-22
6-12	Descent Configuration - Attitude Hold - U Axis Phase Plane	6-23
6-13	Descent Configuration - Attitude Hold - V Axis Phase Plane	6-24
6-14	Ascent Configuration Automatic Maneuver - Rates	6-25
6-15	Ascent Configuration Automatic Maneuver - Gimbal Angles	6-26
6-16	Ascent Configuration - Attitude Hold - P Axis Phase Plane	6-27
6-17	Ascent Configuration - Attitude Hold - U Axis Phase Plane	6-28
6-18	Ascent Configuration - Attitude Hold - V Axis Phase Plane	6-29
6-19	Ascent Configuration - P Axis Phase Plane	6-30
6-20	Ascent Configuration - U Axis Phase Plane	6-31
6-21	Ascent Configuration - V Axis Phase Plane	6-32
6-22	CSI Burn - P Axis Phase Plane	6-33
6-23	CSI Burn - U Axis Phase Plane	6-34
6-24	CSI Burn - V Axis Phase Plane	6-35
6-25	CSI Burn - Velocity-to-be-gained	6-36
6-26	APS Burn to Depletion - U Axis Phase Plane	6-37
6-27	APS Burn to Depletion - U Axis Attitude Errors and Jet Firings	6-38

## LIST OF ILLUSTRATIONS (Continued)

Figure	Page
6-28 APS Burn to Depletion - V Axis Attitude Errors and Jet Firings	6-39
7-1 Phase Plane of Attitude & Rate Versus Logic Volt. Polarity	7-8
7-2 Logic Input Volts as Generated by Attitude Errors & Body Rates	7-9
7-3 LM 3/Apollo 9 Time History Plot of Logic Input Volts During DPS 2 Burn	7-10
7-4 LM 3/Apollo 9 Time History Plot of Calculated Rates During DPS 2 Burn	7-11
7-5 LM 3/Apollo 9 Time History Plot of Pitch Rate as Telemetered	7-12
7-6 LM 3/Apollo 9 Time History Plot of Attitude Errors During DPS 2 Burn	7-13
7-7 LM 3/Apollo 9 Time History Plot of Roll Rate Recorded Inflight	7-14
7-8 LM 3/Apollo 9 Time History Plot of DPS Engine Position During DPS 2 Burn	7-15
8-1 State Vector Comparison Versus Rendezvous Radar Marks - $P_x$	8-4
8-2 State Vector Comparison Versus Rendezvous Radar Marks - $P_y$	8-5
8-3 State Vector Comparison Versus Rendezvous Radar Marks - $P_z$	8-6
8-4 State Vector Comparison Versus Rendezvous Radar Marks - $V_x$	8-7
8-5 State Vector Comparison Versus Rendezvous Radar Marks - $V_y$	8-8
8-6 State Vector Comparison Versus Rendezvous Radar Marks - $V_z$	8-9

LIST OF ILLUSTRATIONS (Continued)

Figure		Page
8-7	Comparison of CMC and BET Relative Position Vector - X Component (NBY Coordinates)	8-10
8-8	Comparison of CMC and BET Relative Position Vector - Y Component (NBY Coordinates)	8-11
8-9	Comparison of CMC and BET Relative Position Vector - Z Component (NBY Coordinates)	8-12

## LIST OF TABLES

	Page
3.1 IMU Error Sources, CSM Ascent	3-21
4.1 SPS Burn Data	4-10
4.2 Pre-Ignition Data	4-11
4.3 Rates and Attitude Errors During SPS Burns	4-12
4.4 Engine Gimbal Trim	4-13
4.5 Velocity-to-be-gained and Velocity Residuals for SPS Burns	4-14
5.1	
8.1 Rendezvous Targeting Summary	8-13
8.2 Rendezvous Targeting Solutions	8-14
8.3 CDH Maneuver Evaluation	8-15
8.4 Comparison of TPI Solutions	8-15
8.5 PGNC S TPI Maneuver Evaluation	8-16

## 1.0 INTRODUCTION

### 1.1 GENERAL

This report presents the conclusions of the analyses of the in-flight performance of the Apollo 9 mission (AS-504/CSM-104/LM-3) onboard guidance and navigation equipment and is intended as a supplement to the MSC Mission Report for Apollo 9. The report was prepared and submitted under MSC/TRW Task E-38B (G&C Test Analysis). The work reported reflects a working interface between Task E-38B, MSC/TRW Task A-50 (Trajectory Reconstruction) and MSC/TRW Task E-72A (Guidance and Control System Analysis). The results of these tasks are highly interdependent and the cooperation and support of the A-50 and E-72A task personnel are gratefully acknowledged.

### 1.2 BACKGROUND

The Apollo 9 mission was the first manned Lunar Module (LM) flight test. The primary purpose of the mission was to evaluate the LM systems performance and perform selected Command and Service Module and Lunar Module (CSM/LM) Operations. This was the first flight for the operation and checkout of the Abort Guidance System (AGS). The most significant GN&C activity occurred during the fifth day of the mission when the LM undocked from the CSM, performed burns simulating the lunar mission and concluded with a rendezvous and docking with the CSM. Overall, spacecraft performance data and mission event times are presented in the MSC Mission Report for Apollo 9.

## 2.0 SUMMARY

The inertial subsystem performance was excellent during the mission. The capability of a docked LM/CSM IMU alignment was successfully demonstrated.

Performance of the LM and CSM DAP was very good and completely nominal. No external torques were apparent during the periods of CSM attitude hold investigated, except the torque due to the cg offsets during the ullages. During the period of CSM-LM docked attitude hold preceding the docked DPS burn, the crew reported the presence of apparent aerodynamic torquing. Inadequate data were available during that period to either substantiate or refute the cause of the experienced torquing. Prior to the LM DPS Insertion burn, an external disturbing torque about the V-axis was evident.

CES operation during the AGS DPS Phasing burn was nominal.

Performance of the spacecraft navigation systems during the rendezvous period was excellent. All updates supplied to the LM guidance computer during the rendezvous were from the rendezvous radar. All Concentric Flight Plan burn solutions used were generated by the LGC.

### 3.0 CSM IMU PERFORMANCE

#### 3.1 ASCENT VELOCITY COMPARISON

Analysis of the CM and LM IMU's were based on separate studies. The analysis of the CM system was based on the S-IVB as a standard. Analysis of the LM IMU is presented in Section 5.0 and is based on the DPS docked burn.

Two final trajectories were generated by MSFC as a basis for comparison for the ascent phase, these being the "Edited S-IVB IU TM" trajectory and the "Final S-IVB Observed Point Mass Trajectory," (OPMT). Reasons for rejection of the latter are shown in comparisons of Figures 3-1 through 3-3 with Figures 3-4 through 3-6 which present the uncompensated velocity residuals for the ascent phase. As in the past, the OPMT was rejected because of more erratic trends, and reasonable error sets which effected a good boost comparison were unachievable.

In the analysis of Apollo 9, flight load values were used in place of the data means as a basis of comparison with the derived errors because the number of preflight data points were small and because some of the instruments were showing strong trends immediately prior to flight. The inflight (free fall) measured values were used as comparisons to the derived data values for PIPA and IRIG biases. The CM error sources are presented in Table 3.1. None of the error sources exceeded the one-sigma bounds from the expected errors. Comparison with the preflight data trends lends confidence to the derived error set. The compensated residuals for the ascent phase are presented in Figures 3-7 through 3-9.

Due to the exceptionally good fit to the derived data with respect to the expected errors, no discussion of the individual error sources is necessary. One problem unrelated to Apollo is evident from

Figures 3-2 and 3-9. The first few seconds of velocity error could not be corrected by using the standard technique of applying an offset velocity to the Apollo data equivalent to the time zero velocity difference between Apollo and Saturn data. The problem is more apparent in the acceleration domain where it was observed that the Saturn S-IVB Y accelerometer sensed output was approximately  $1 \text{ ft/sec}^2$  higher for the first four seconds of flight than the Apollo sensed acceleration. It has subsequently been established that Saturn accelerometers are susceptible to the lift-off vibration environment and the first few seconds of Saturn data are suspect.

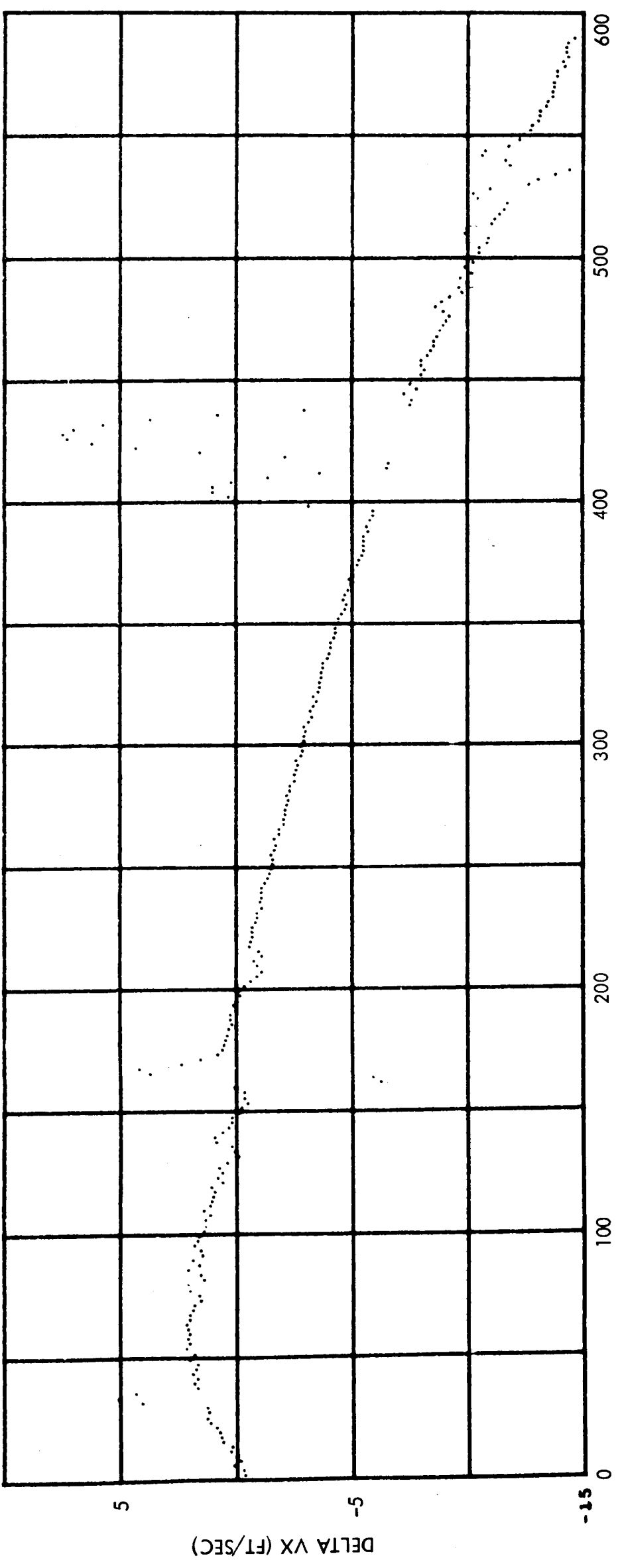


Figure 3-1 G&N MINUS FINAL S-IVB OMPT,  
WITHOUT COMPENSATION - ASCENT

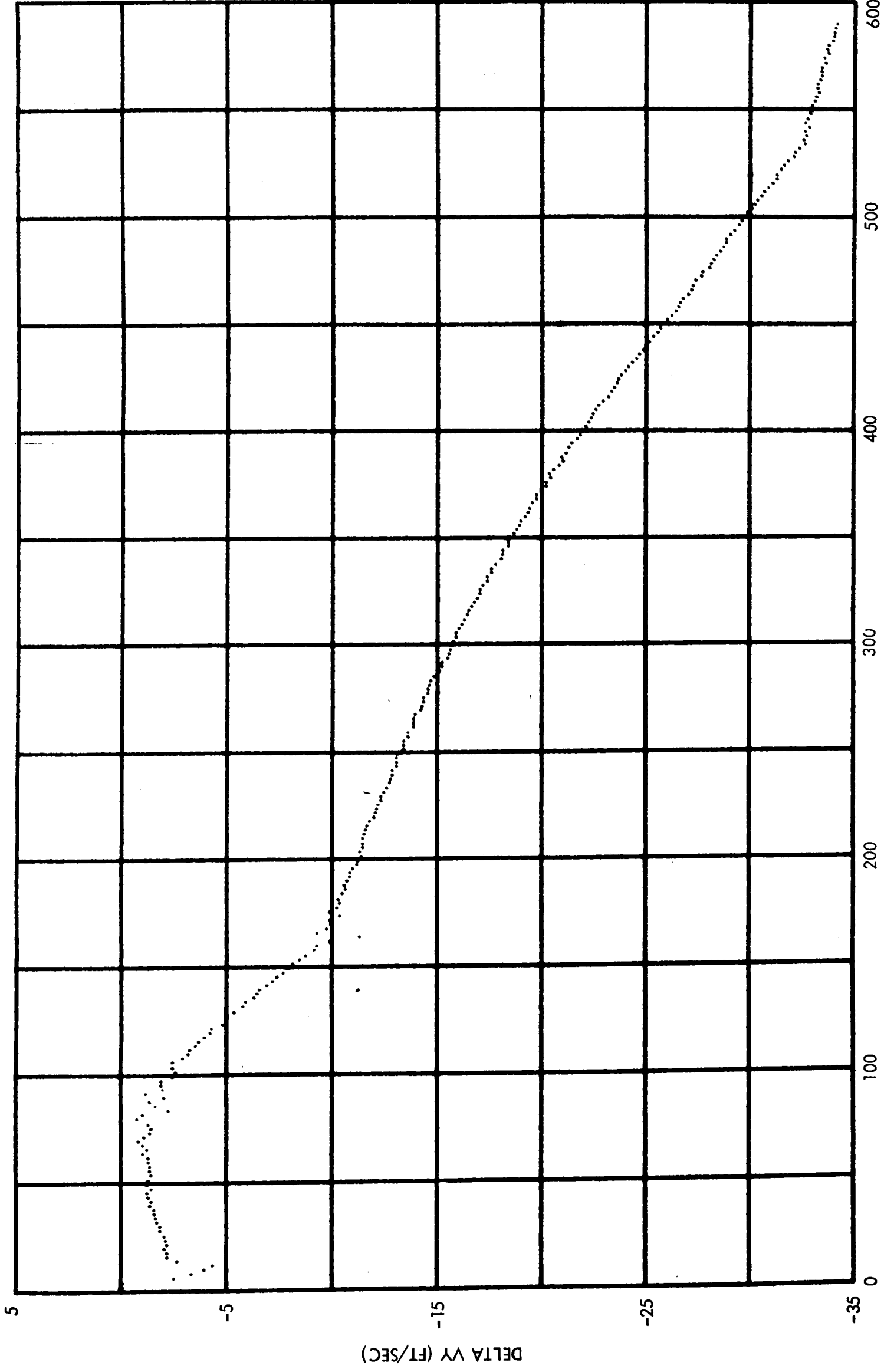


Figure 3-2 G&N MINUS FINAL S-IVB OMPT,  
WITHOUT COMPENSATION - ASCENT

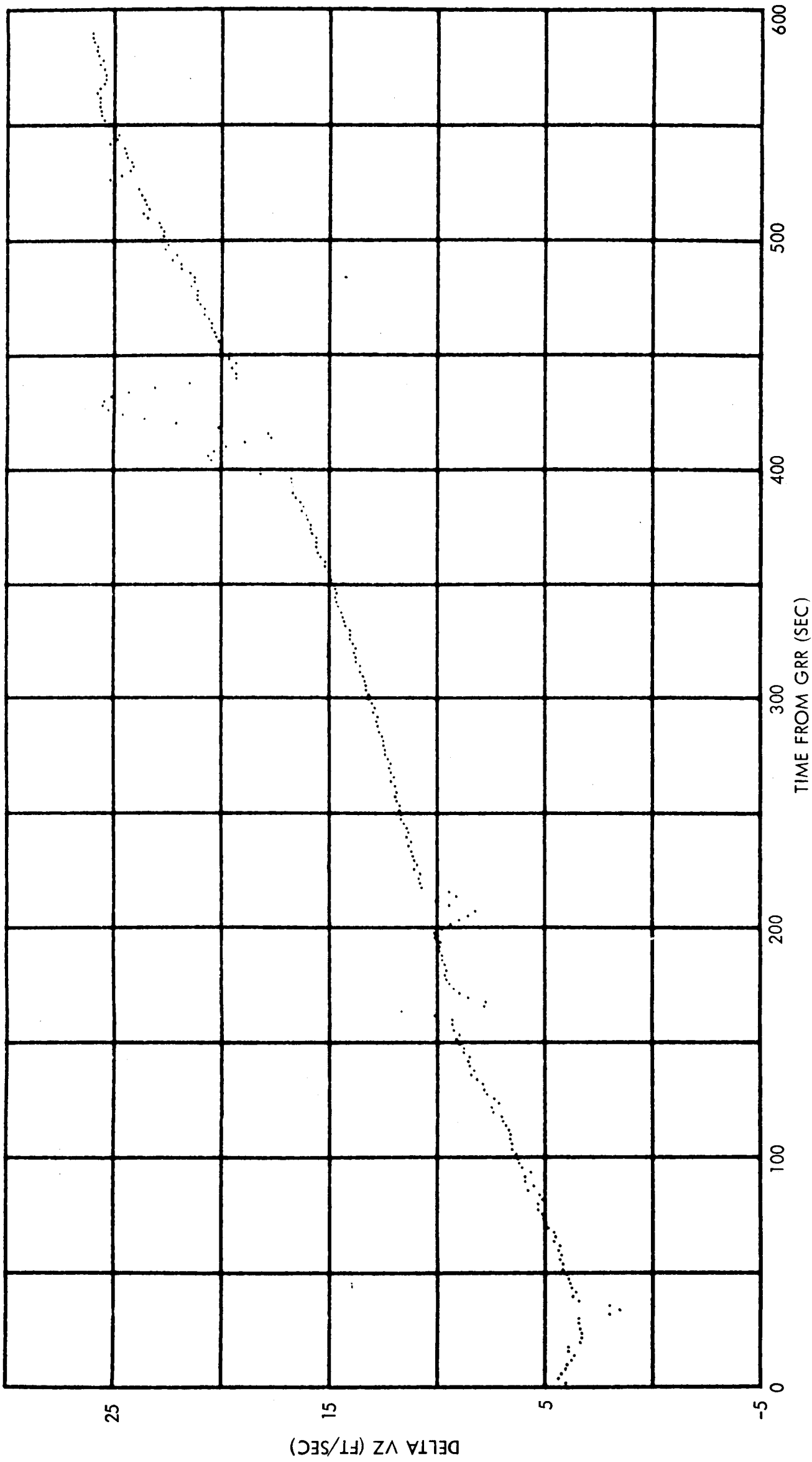


Figure 3-3 G&N MINUS FINAL S-IVB OMPT,  
WITHOUT COMPENSATION - ASCENT

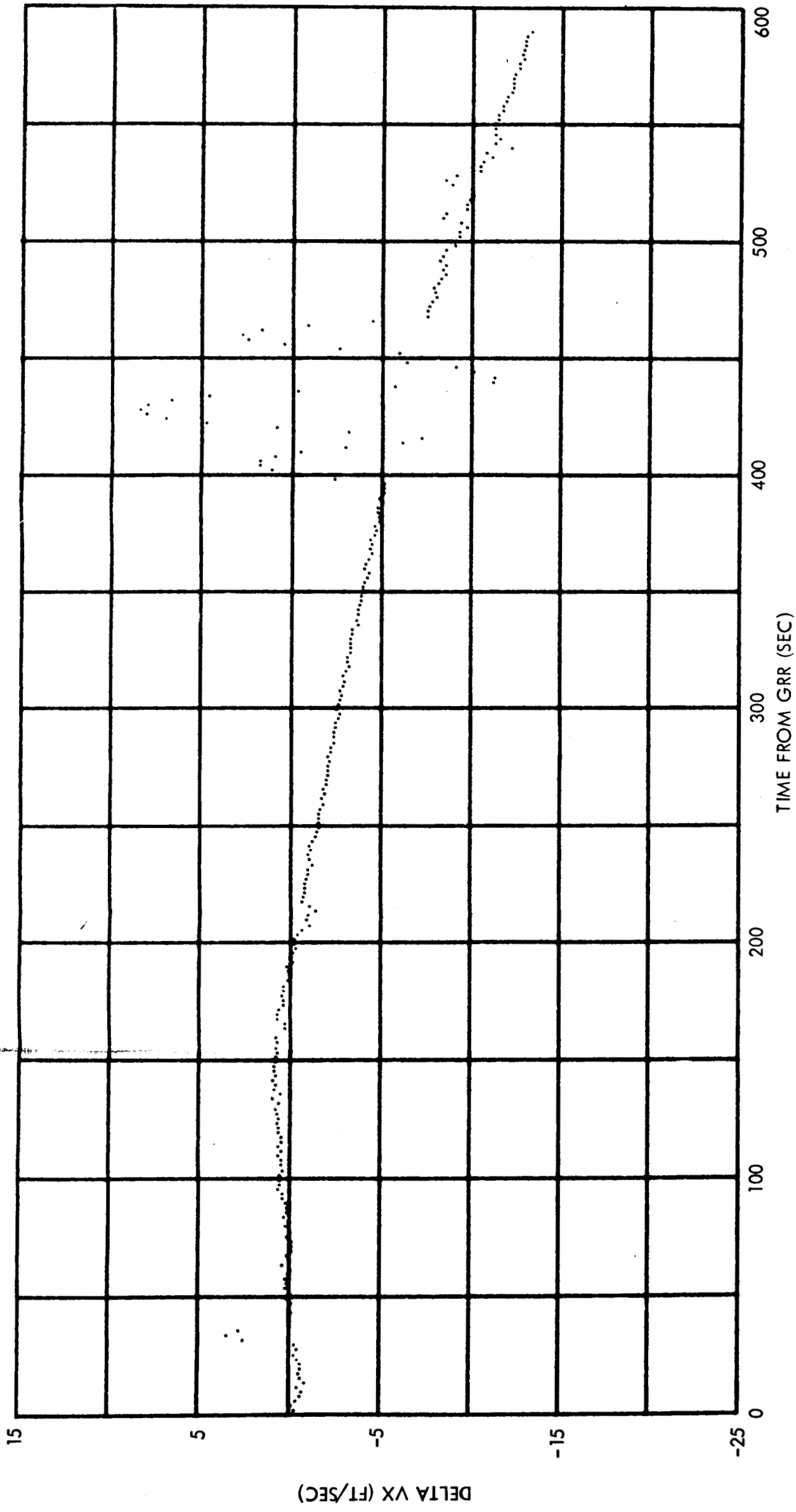


Figure 3-4 G&N MINUS S-IVB IU/TM, WITHOUT COMPENSATION - ASCENT

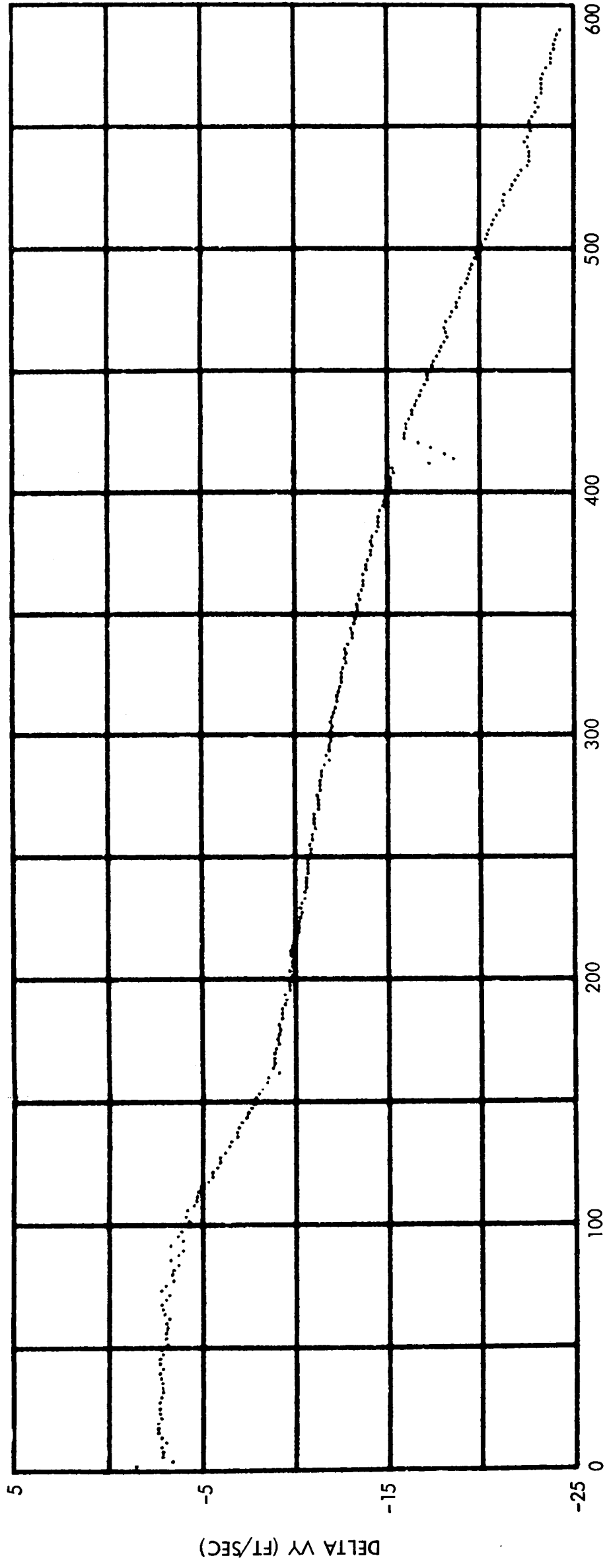


Figure 3-5 G&N MINUS S-IVB IU/TM, WITHOUT COMPENSATION - ASCENT

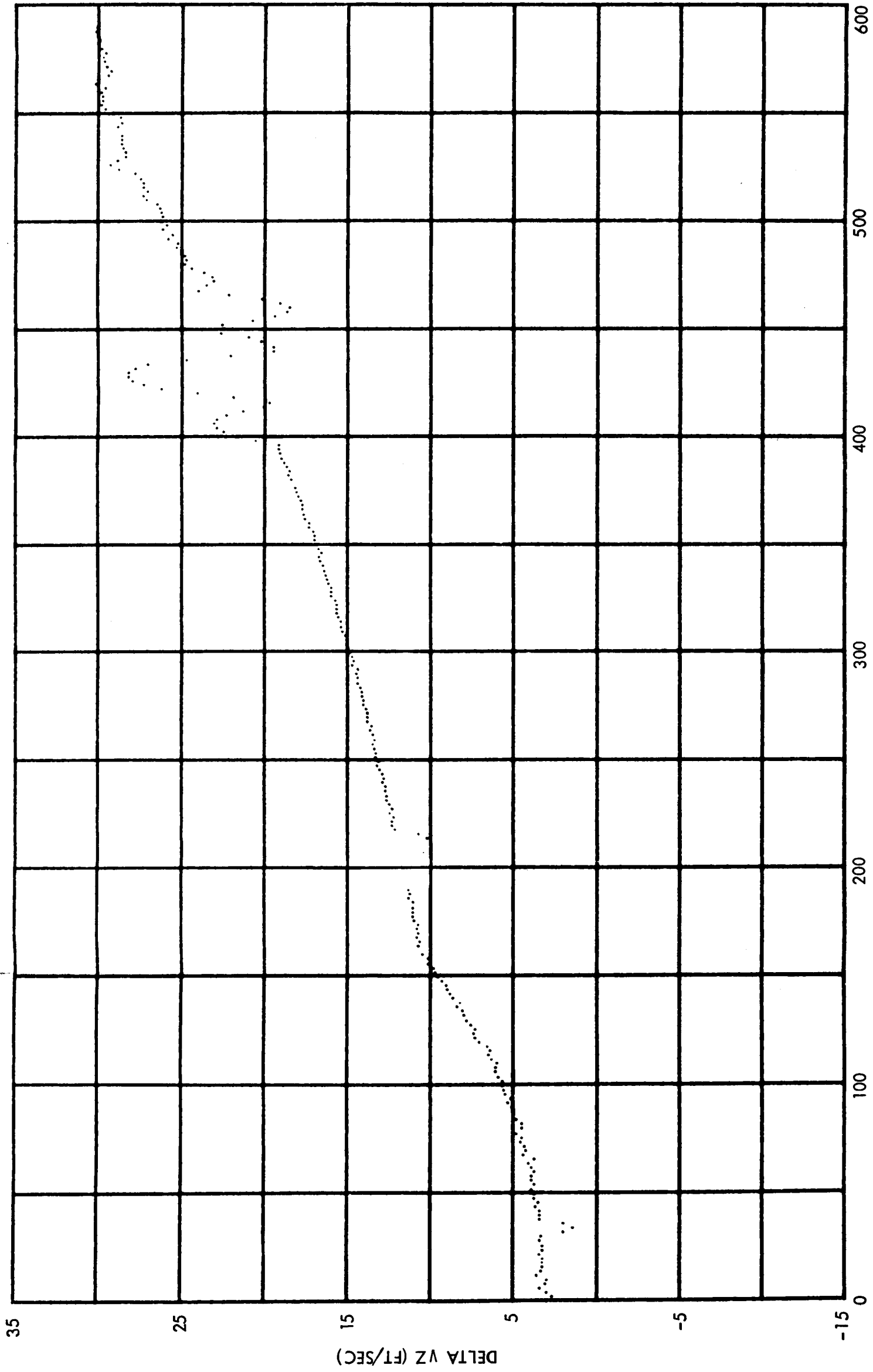


Figure 3-6 G&N MINUS S-IVB IU/TM, WITHOUT COMPENSATION - ASCENT

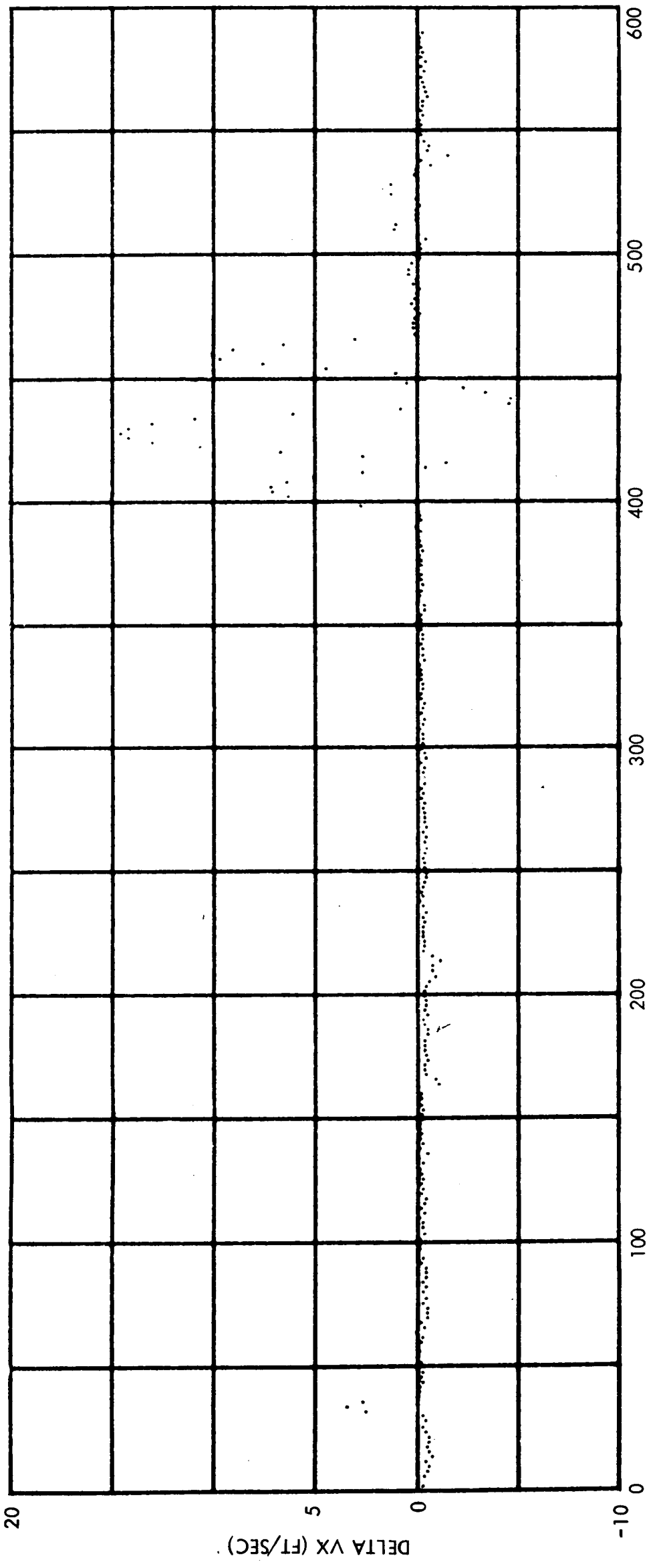


Figure 3-7

G&N MINUS S-IVB IU/TM, WITH  
COMPENSATION - ASCENT

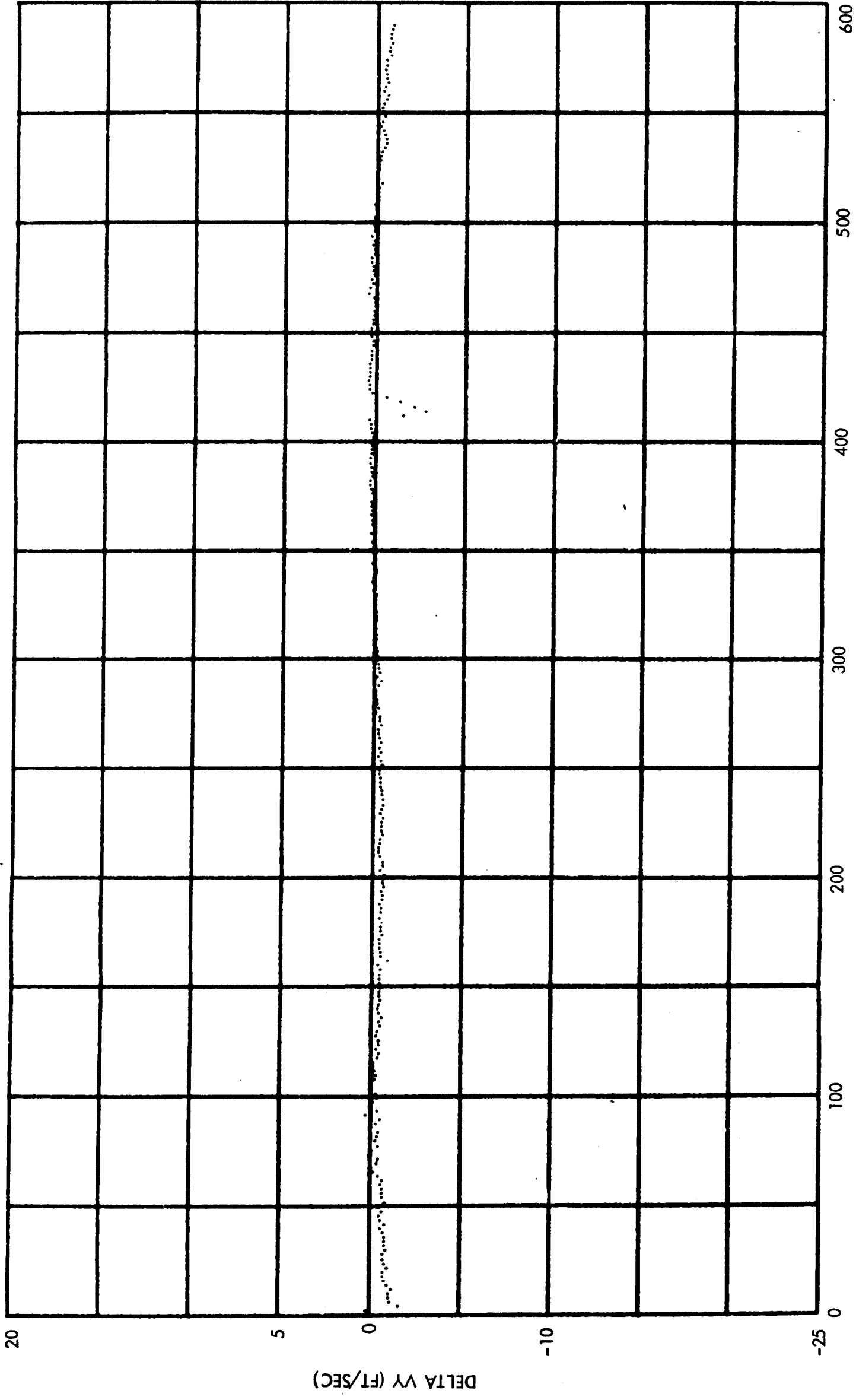


Figure 3-8

G&N MINUS S-IVB IU/TM, WITH  
COMPENSATION - ASCENT

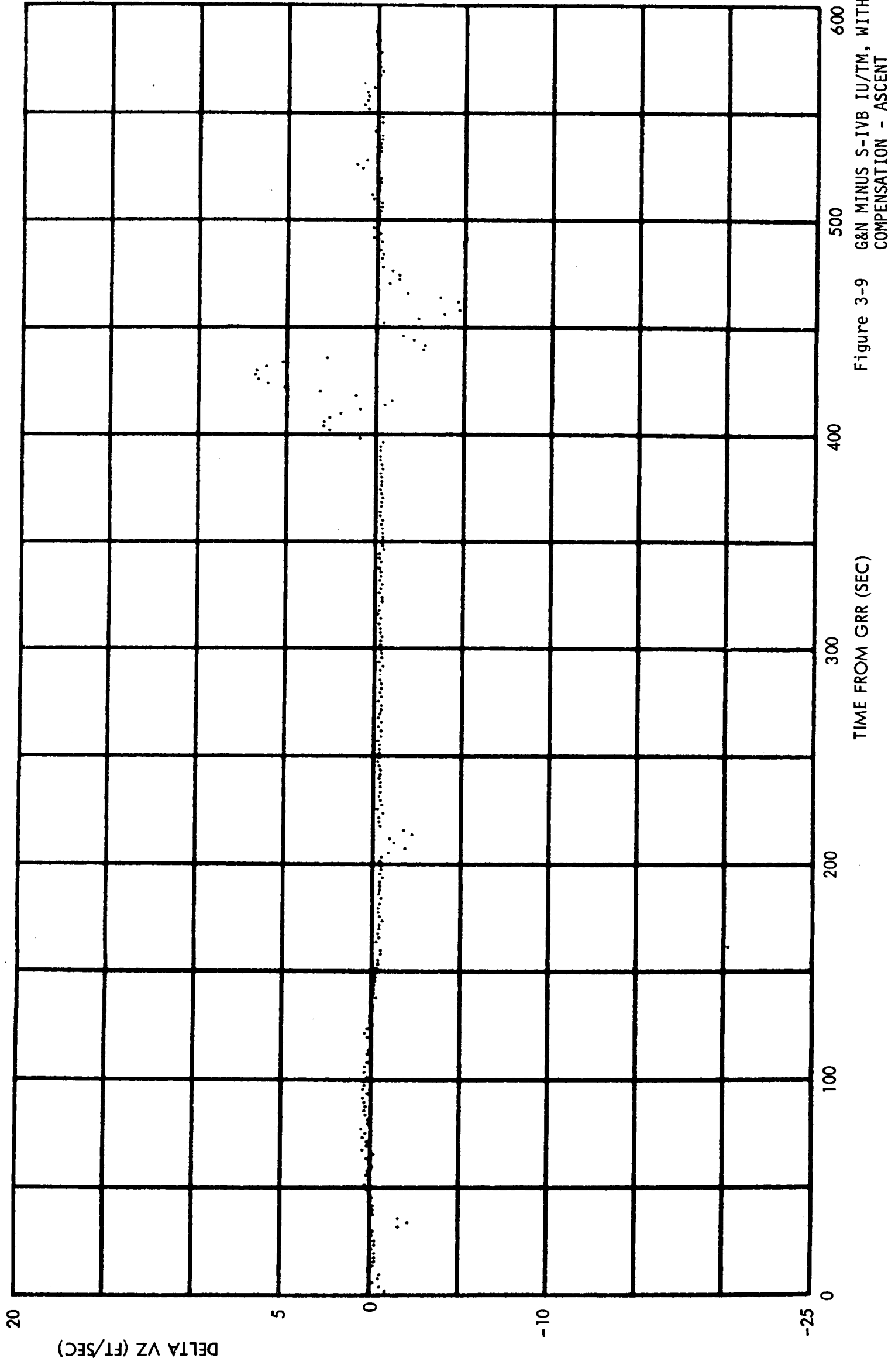


Figure 3-9 G&N MINUS S-IVB IU/TM, WITH COMPENSATION - ASCENT

Source	Data Mean*	Flight Load	Expected Error	Standard Deviation	Derived Error	Variation from Expected Error	Comments
VOX (ft/sec)	NA	NA	NA	NA	-0.066	NA	IU/TM output
VOY (ft/sec)	NA	NA	NA	NA	-1.67	NA	IU/TM output
VOZ (ft/sec)	NA	NA	NA	NA	3.52	NA	IU/TM output
DT (sec)	NA	NA	NA	NA	-0.00372	NA	
ACBX (cm/sec <sup>2</sup> )	-0.592	0.64	-1.232	0.20	-1.214	0.09σ	Measured in flight
ACBY (cm/sec <sup>2</sup> )	-0.317	-0.10	-0.217	0.20	-0.166	0.25σ	Measured in flight
ACBZ (cm/sec <sup>2</sup> )	4.384	4.4	-0.016	0.20	0.024	0.20σ	Measured in flight
SFEX (ppm)	NA	-140	0	116	-46	0.40σ	
SFEY (ppm)	NA	-330	0	116	-34	0.29σ	
SFEZ (ppm)	NA	-280	0	116	114	0.98σ	
MXAY (arc-sec)	NA	0	0	20	-17	0.85σ	
MYAX (arc-sec)	NA	0	0	20	19	0.95σ	
MZAY (arc-sec)	NA	0	0	20	4	0.20σ	
MZAX (arc-sec)	NA	0	0	20	-12	0.60σ	
NBDX (meru)	-2.27	2.4	-2.27	2	-2.808	0.27σ	Measured in flight
NBDY (meru)	-0.239	0	-0.239	2	0.0154	0.13σ	Measured in flight
NBDZ (meru)	-2.26	2.4	-2.26	2	-2.28	0.01σ	Measured in flight
ADIAX (meru/g)	NA	5.0	0	8	-3.23	0.40σ	
ADIAY (meru/g)	NA	8.0	0	8	-6.52	0.82σ	
ADIAZ (meru/g)	NA	-18.0	0	8	4.06	0.51σ	
ADSRAY (meru/g)	NA	9.0	0	5	-0.14	0.03σ	
ADOAY (meru/g)	NA	0.0	0	2-5**	3.03	0.76σ	
ADOAZ (meru/g)	NA	0.0	0	2-5**	-3.21	0.80σ	
MLMX (arc-sec)	NA	NA	0	50	30	0.6σ	
MLMY (arc-sec)	NA	NA	0	50	-21	0.42σ	
MLMZ (arc-sec)	NA	NA	0	50	-49	0.98σ	

\* Due to the small amount of preflight data available, the flight load was assumed as the correct data mean, except for those values which were measured in flight and the velocity offsets.

\*\* Recent unofficial MIT measurements. A standard deviation of + meru/g seems typical and is used in this report.

Table 3.1 IMU ERROR SOURCES, CSM - ASCENT

## 4.0 CSM DIGITAL AUTOPILOT

The major portion of the CSM and CSM/LM control activity during the mission was carried out under SCS control. Periods of G&N control were generally limited to the automatic maneuvers to the SPS and docked DPS burn attitudes, the attitude hold mode following these automatic maneuvers, and all of the SPS burns. After the SPS 6 burn, the DAP was in control during the orbit rate automatic maneuver. All of the SPS burns and most of the automatic maneuvers and periods of attitude hold were analyzed; however, most of the analysis focused on the RCS and TVC DAP operation with the CSM/LM in the docked configuration. An exception to this was the orbit rate automatic maneuver which was performed by the CSM alone.

Periods of DAP control analyzed were:

a) TVC DAP

SPS burns 1 to 8. Burns 1, 6 and 8 were not examined in as much detail as the others because of their short duration.

b) DAP Automatic Maneuvers

o Maneuvers to all of the SPS burns except SPS burns 5, 6 and 8 (deorbit). No data was available during these maneuvers.

o The maneuver to the docked DPS burn attitude.

o The orbit rate automatic maneuver.

c) DAP Attitude Hold

Attitude hold preceding each of the burns and including ullage. Only limited data were available during the ullage preceding burn 5 (last 10 seconds) and did not allow complete phase plane switching verification.

### 4.1 TVC DAP PERFORMANCE

Data summarizing the TVC DAP performance and SPS burn characteristics for each of the SPS burns are provided in Tables 4.1 to 4.5.

Plots of attitude errors, gimbal trim angles, gimbal commands and measured gimbal positions are given in Figures 4-1 to 4-14. Except for the measured gimbal positions, Ground Elapsed Time (GET) relating to the burns and peak body rates, the above data were obtained from computer words. Ignition times, ullage on-times, and burn durations are based on RCS and SPS solenoid bilevel states. Measured gimbal positions and peak body rates were obtained from time history tabulations. Autopilot performance was satisfactory during all of the SPS burns during this mission.

#### 4.1.1 Attitude Errors

Peak attitude errors in pitch and yaw for all of the burns during G&N control (the only period of SCS control during a burn were during the manual takeover near the end of burn 3) except SPS burn 5 were less than 2.5 degrees. SPS burn 5 experienced a peak yaw attitude error of 7.2 degrees; the peak pitch attitude error for this burn was 3.2 degrees. Preflight simulations indicated that this burn was more sensitive to initial condition errors and mistrims than the other burns. Initial condition errors in yaw for this burn included a 0.5 degree attitude error, a 0.3 deg/sec rate error and -0.19 degrees of yaw engine mistrim. The resultant yaw attitude deviation (Figure 4-5) was consistent with preflight analysis.

During the preliminary analysis of this burn, it was not entirely clear that the yaw gimbal actuator command was responding correctly to null the increasing yaw attitude error. For example, it can be seen from Figures 4-12 and 4-13 that there was a period of 8 seconds (54:26:39.9 to 54:26:47.9 GET) in which the attitude error increased monotonically from 5 degrees to 7 degrees and the engine command remained constant. A digital simulation of the CSM/LM DAP filter, including the switchover logic, was solved for the filter response to the measured yaw attitude error shown in Figure 4-12. The results were then compared with the measured filter response from the flight data. The measured filter response is the difference between the Yaw Actuator Command (YCMD) and the Yaw Trim Angle (YACTOFF).

Figure 4-15 presents the comparison of the measured and computed filter response to the measured attitude error. The maximum deviation between computed and measured filter output was 0.05 degrees. Some deviation is to be expected because constant mass properties (used in the calculation of the gain VARK) were assumed in the simulation.

The reason for the sudden change in the attitude error, and consequent engine response, during the last 4 seconds of the burn is due to the guidance commands being set to zero at this time. From these results it is apparent that the engine response to the yaw attitude error during SPS 5 was entirely nominal.

#### 4.1.2 Ignition Transients

The gimbal ignition transients appeared nominal in all cases. The measured gimbal command during the first 5 seconds after ignition is plotted on an expanded scale for SPS 2 in Figure 4-2a. For all burns the peak-to-peak amplitude of the initial gimbal excursion caused by gimbal compliance during the first 1/2 second of thrusting was less than 0.45 degrees for both pitch and yaw.

Gimbal oscillations reflecting propellant slosh were observed during the SPS 5 and SPS 7 burns. SPS 5 was a docked burn and followed the docked DPS burn. Oscillations during burn 5 of about 0.5 Hz were observed in both pitch and yaw and were well damped within 10 seconds after ignition. It is believed that the slosh torques were predominately due to the LM propellant during this burn. The theoretical slosh frequency of the LM propellant is approximately equal to that of the CSM at this time. Comparisons of the LM and CSM slosh dynamics in the vicinity of SPS 5 ignition are discussed in Section 6.1.2. The gimbal oscillations during burn 7 were also damped out in about 10 seconds. For both burns the measured slosh frequencies agreed with the theoretical values. Slosh induced peak-to-peak engine deflections were less than 0.25 degrees for burn 5 and 0.6 degrees for burn 7.

### 4.1.3 Manual Takeover

The rate command MTVC mode was exercised during the last 45 seconds of burn 8 and tested rate damped manual control with the LM attached. Transfer from CMC TVC to SCS MTVC occurred at 25:21:34.8 GET. Manual control is accomplished in this mode with the Rotational Hand Controller (RHC). Body rates are commanded proportional to the RHC deflection, with the pilot attempting to null the Flight Director Attitude Indicator (FDAI) displayed attitude errors. The FDAI displays the output of the attitude BMAG's which are uncaged at ignition. Roll control was accomplished using the attitude hold mode. The minimum rate, narrow deadband was selected for roll phase plane switching during MTVC. Figures 4-5 and 4-6 present plots of pitch and yaw attitude errors and rates during MTVC. In general, satisfactory control was maintained throughout the manual control. Pitch and yaw attitude errors peaked at 3.2 degrees and -4.3 degrees respectively, approximately 12 to 15 sec after manual takeover. A residual cross axis velocity of -2.5 ft/sec remained at burn termination. Neither slosh nor bending oscillations appeared to be excited during manual control. Considerably more RHC commands were issued in pitch than yaw, partially because of an initial 0.2 deg/sec body rate which was present in pitch compared to practically zero rate in yaw.

One roll RHC correction was made about 1.2 seconds after Manual Thrust Vector Control (MTVC) initiation. This command was issued to remove a roll rate which had built up to about 2.5 deg/sec by the time the RHC action was taken. A continuous 1.2 second 2-jet roll firing from the time of transfer to SCS was responsible for the rate build-up. The long jet firing was caused by the roll deadband being contracted from 5.0 degrees during G&N TVC to 0.2 degrees at SCS initiation. The roll attitude error which was present at the time of transfer to SCS was almost -4 degrees. This initial roll transient and the resulting corrective action could have been avoided had the SCS roll attitude deadband not been initially set at  $\pm 0.2$  degrees. It is recommended for future flights that preceding G&N controlled SPS burns, the SCS

deadband be set at maximum deadband ( $\pm 4$  degrees or  $\pm 4.2$  degrees, depending on whether the RATE SWITCH is set in the MAX or MIN position).

Estimated mistrims are presented in Table 4.4. These values were computed by comparing the initial trim at ignition with the single-shot trim values at switchover (ignition time + 6.42 seconds for LM ON, + 3.7 seconds for LM OFF). For short SPS burns in which there was no switchover, mistrims were not calculated. The largest value of estimated mistrim using the above method occurred on burn 7 in which the yaw mistrim was -0.486 degrees. Due to the slosh torques which had not subsided at the time of switchover, a value of YACTOFF at a later time would probably give a better trim to compare with the initial value. Four seconds after switchover, YACTOFF has a value of -0.802 and does not change for another 4 seconds. Comparing this value with the initial trim yields an estimated yaw mistrim of 0.316 degrees. In addition to initial mistrim, Table 4.4 also lists values of the MCC time updates which were communicated by voice prior to the burns, values of PACTOFF and YACTOFF at ignition, switchover, and cutoff, and measured engine position at ignition. Figures 4-3, 4-8, 4-11 and 4-14 present plots of PACTOFF and YACTOFF for SPS burns 2, 3, 4 and 5, respectively. It is clear from the plots that the cg tracker is following the migrating cg.

#### 4.1.4 Roll TVC DAP

Roll control was nominal throughout all of the burns. There were very few roll firings during any of the burns and in only one case an external roll torque was distinctly evident. During burn 4 a roll torque of about 1.25 ft-lb was observed. The roll attitude error was driven to the negative deadband, but roll control was satisfactory. Three roll firings were observed during the burn.

#### 4.1.5 Stroking Tests

The two stroking tests which were carried out during the early parts of SPS burns 2 and 3 were not analyzed in detail for this report, but

a fairly detailed time history of the gimbal actuator response during each test was included for reference. Figure 4-2a presents the response to the 40% stroking test in burn 2 and Figure 4-7a shows the 100% stroking test which was performed in burn 3.

## 4.2 RCS DAP PERFORMANCE

No anomalies were identified during the periods of RCS DAP control which were analysed. RCS DAP performance appeared nominal throughout the mission.

### 4.2.1 RCS DAP Automatic Maneuvers

Figures 4-17 to 4-22 present plots relating to three automatic maneuvers: The maneuver to burn 2 attitude; the maneuver to the docked DPS burn; and the Orbit Rate Automatic maneuver. In each case, plots of body rates and CDU angles are given with the desired body rates and desired final CDU angles dashed in. Only the last 40 seconds of data during the maneuver to burn 2 was available, as is indicated in Figures 4-17 and 4-18. However, about 160 seconds of attitude hold data following the maneuver was available and is included in the plots.

Wide deadband was used during the maneuver to burn 2 and the docked DPS burn. The orbit rate maneuver was carried out in the narrow deadband. All of the maneuvers were successfully executed, with attitude errors at the termination within the DAP deadband. The command and actual body rates were in agreement within the limits of the phase plane deadzone. No attitude overshoot was observed during any of the maneuvers. Attitude hold was properly initiated at the termination of all of the maneuvers. Bilevel data were searched to determine the frequency of RCS jet firings during the Orbit Rate Maneuver, but data were not available during that time period. Plots of the estimated body rates (Figure 4-20) indicate that an excessive number of firings did not occur. The majority of firings were minimum impulse.

#### 4.2.2 RCS DAP Attitude Hold

Figures 4-23 to 4-28 present phase plane plots of the periods of attitude hold preceding burns 3 and 4. Nominal performance was indicated in all cases. No external torques were apparent in any of the periods of attitude hold investigated except the torque due to the cg offsets during the ullages. The effect of the 20 second 4-jet +X ullage prior to burn 4 is seen in these figures. The cg offset in pitch which was present during this ullage was about 3.4 inches and resulted in a pitch disturbing acceleration of about  $0.024 \text{ deg/sec}^2$  forcing the pitch phase plane trajectory to an attitude error of about  $-0.62$  degrees. Figures 4-26 to 4-28 include the ullage maneuver as well as about 200 seconds of prior coasting flight. Predictably, there were a large number of single jet firings during this ullage to bring the phase plane trajectory back into the deadzone.

#### 4.3 ENTRY DAP PERFORMANCE

During the extra-atmosphere portion of entry, the SCS was in control of the spacecraft. Sensing of  $0.05g$  occurred at 240:42:25 GET and the Entry DAP was placed in control of the spacecraft at 240:46:47 GET. Thus, the only portions of the Entry DAP which were exercised were the 2-sec, predictive Roll DAP, and the pitch and yaw rate dampers.

Entry Roll DAP performance was found to be entirely nominal to the extent that TM data allowed analysis. On the basis of data obtained, rate damping in the pitch and yaw axes appeared nominal although complete verification was not possible due to low frequency of these data.

##### 4.3.1 Roll DAP Performance

Entry Roll DAP performance was entirely nominal. The ability of the Roll DAP to maintain the desired roll angle is shown by Figure 4-29, a time history of commanded and actual roll angles during entry.

A number of large angle, attitude maneuvers were executed during entry with little or no overshoot, supporting the assumption that jet on-times were calculated correctly. Actual verification of the jet on-time calculation could not be done due to the lack of necessary quantities on TM and the coarseness of the data.

#### 4.3.2 Pitch and Yaw Rate Damping

Every pitch firing during entry was verified to have been in accordance with the pitch rate damper design which limits pitch rate to less than two degrees per second.

Yaw damper firings are commanded by the yaw DAP to execute coordinated turns according to  $r = p \sin \alpha$  with  $\sin \alpha$  held at a constant  $-0.34202$  ( $\alpha = -20^\circ$ ). When stability-axis yaw rates exceed  $2^\circ/\text{sec}$ , yaw jets are fired to damp the rates.

During two bank angle reversals, a number of consecutive yaw axis firings occurred when the yaw rate from the SCS data was apparently well below  $2^\circ/\text{sec}$ . However, since the firings are based on the CMC rate estimates instead of the SCS data, the rate estimator data were examined in detail during these periods. The periods of high yaw thruster activity are shown in Figures 4-30 and 4-31. SCS stability axis yaw rate, CMC yaw rate calculated from PREL and RREL data, and yaw axis thruster activity are shown in these figures.

PREL and RREL were available at 200 m sec intervals (every other DAP cycle) on the TM downlist, accounting for the gaps in the plots of CMC estimated rates. Some thruster firings occurred when no rate estimator data were available. Those firings which occurred when PREL and RREL data were available on TM were according to the yaw DAP design; that is, the yaw rate had exceeded the  $2^\circ/\text{sec}$  rate deadband at the time of the firings. In some instances, the rate gyro data indicated that the yaw rate was within the deadbands.

The above analysis indicates that sufficient differences exist between the SCS data and rate estimator data to preclude use of the SCS data as a criterion for validating the yaw jet firings during periods where rate estimator data is unavailable. Several factors can contribute to this variance between the analog and CMC rate estimator data. Since the intervals of interest occurred during periods of high roll rates ( $> 10^\circ/\text{sec}$ ), the most probable cause is the CDU switching between high and low-rate sampling frequencies. This switching occurs for roll rates in excess of  $4^\circ/\text{sec}$  and can create rate errors as high as  $1^\circ/\text{sec}$ . Also,  $\dot{\gamma}$ , the rate of change of the angle between the local horizontal and the relative velocity vector, is incorporated into the rate estimator calculations when  $\dot{\gamma} > 0.5^\circ/\text{sec}$ . Another potential source of error is structural vibrations. Although the rate gyros and the IMU are subjected to the same vibration during reentry, their locations within the CM structure cause some differences in the amplitudes and frequencies of the vibrations applied to the individual pieces of equipment.

TABLE 4.1 SPS Burn Data

SPS Burn No.	Ullage			Burn		
	No. Jets	Start GET	Duration (sec)	Overlap (sec)	Start GET	Duration (sec)
1. CSM/LM	No ullage	No ullage	No ullage	No ullage	5:59:01.100	5.100
2. CSM/LM	No ullage	No ullage	No ullage	No ullage	22:12:04.103	110.283
3. CSM/LM	No ullage	No ullage	No ullage	No ullage	25:17:38.300	279.599
4. CSM/LM	4 jet	28:24:23.522	19.860	1.983	28:24:41.399	27.901
5. CSM/LM	4 jet	54:25:57*	17*	1.970	54:26:12.304	43.299
6. CSM	2 jet	123:24:49.630	19.364	1.978	123:25:07.016	1.409
7. CSM	2 jet	169:38:42.364	20.024	1.988	169:39:00.400	24.900
8. CSM (deorbit)	2 jet	240:30:58.153	18.695	1.958	240:31:14.890	11.700

\*approximate times

TABLE 4.2 Pre-Ignition Data

SPS Burn No.	Peak Ullage Rates (deg/sec)			Ignition Attitude Errors In RCS Control Axes (deg)			Ignition Rate Errors In RCS Control Axes (deg)		
	Roll	Pitch	Yaw	Roll	Pitch	Yaw	Roll	Pitch	Yaw
1	No ullage	No ullage	No ullage	-.3735	-.2747	-.3845	.0066	-.0046	-.0002
2	No ullage	No ullage	No ullage	-.4834	-.4065	-.4614	-.0048	.0012	.0024
3	No ullage	No ullage	No ullage	-.4724	.4395	-.4944	-.0009	-.0040	.0010
4	-.8789	-.0703	-.0441	.2527	-.6152	.3625	.0214	.0384	-.0384
5	-.0858	.0547	-.0485	.1978	-.6702	.4944	-.0563	.0224	.0338
6	-.1108	.0812	.0602	-.4395	-.6042	-.2087	.0016	.0452	.0026
7	-.1246	-.2418	-.2300	-.3845	-.6372	.2637	-.0867	.0767	.1780
8	-.1011	-.1205	.2431	-.4285	-.6152	.1868	.0594	.0121	.1245

TABLE 4.3 Rates and Attitude Errors During SPS Burns

SPS Burn No.	Burn Peak Attitude Errors In Body Axes (deg)			Burn Peak Rates In Body Axes (deg/sec)			Final Attitude Error In Body Axes (deg)		
	Roll	Pitch	Yaw	Roll	Pitch	Yaw	Roll	Pitch	Yaw
1	-.54	-.16	.48	-.27	.27	.14	-.54	-.16	.48
2	-5.05	2.31	-1.30	.31	-.77	-.29	-.30	.189	-1.12
3	5.01	-3.12	4.36	2.45	-.72	-.55	-.52	-1.74	4.03
4	1.99	2.48	2.77	-.15	.55	-.34	1.99	-1.45	2.45
5	5.09	-3.18	7.21	.53	.64	.90	4.06	-1.32	4.43
6	.10*	.25*	.41*	-.47	-.13	1.06	.10	.25	.41
7	4.89	.35	-1.85	2.06	.81	1.81	4.99	-.04	.45
8	3.80	1.35	-.71	-.52	-1.08	1.36	3.80	.21	.48

\* Only one data point was available due to the short burn duration (1.4 sec).

TABLE 4.4 ENGINE GLOBAL TRIMS

SPS Burn No.	MCC Trim Update	Pitch Angle (deg)			Single - Shot Change	Final Value YACTOFF	Mistrim
		Initial Trim YACTOFF	Engine Position	PACTOFF			
1	1.00	1.0206	.975	-	.9720	-	
2	1.00	1.0206	1.019	.9720	1.215	0.0486	
3	1.18	1.215	1.195	1.215	*1.458	0.0	
4	1.50	1.531	1.549	1.288	1.264	0.243	
5	1.10	1.1178	1.063	1.069	1.094	0.0488	
6	-0.89	-0.923	-0.814	-	-0.923	-	
7	-0.70	-0.923	-0.814	-0.972	-0.948	0.0486	
8	-0.64	-0.656	X	-0.948	-0.826	0.292	

- No switchover due to short burn X - No data \* PACTOFF, YACTOFF = 1.4094 and -0.5346 at MVC initiation (ignition + 236.5 sec)

SPS Burn No.	MCC Trim Update	Yaw Angle (deg)			Single - Shot Change	Final Value YACTOFF	Mistrim
		Initial Trim YACTOFF	Engine Position	PACTOFF			
1	-0.20	-0.194	-0.175	-	-0.122	-	
2	-0.20	-0.194	-0.175	-0.146	-0.170	-0.048	
3	-0.17	-0.170	-0.175	-0.1701	*-0.632	0.0	
4	-0.69	-0.705	-0.644	-0.608	-0.608	-0.007	
5	-0.80	-0.8262	-0.772	-0.632	-0.704	-0.194	
6	-1.13	-1.160	-1.07	-	-1.166	-	
7	-1.10	-1.118	-1.028	-0.632	-0.923	-0.486	
8	-0.94	-0.972	X	-0.826	-0.899	-0.146	

TABLE 4.5 Velocity-to-be-gained and Velocity Residuals for SPS Burns

SPS Burn No.	Noun 85 DSKY Display (Control Axes)				Noun 40 Display			
	V <sub>gx</sub> Residual		V <sub>gy</sub> Residual		V <sub>gz</sub> Residual		V <sub>g</sub> Magnitude	
	Initial	Trimmed	Initial	Trimmed	Initial	Trimmed	Initial	Final
1	1.6	-	.5	-	-.2	-	36.8	1.5
2	0.0	-	1.0	-	.2	-	850.6	.7
3	2.7	-	-2.5	-	-2.3	-	2570.7	4.4
4	.2	-	3.9	-	2.7	-	299.1	4.7
5	1.9	-	11.4	-	1.7	-	571.8	11.7
6	1.1	-	-.6	-	-.3	-	38.8	1.2
7	-1.3	-	1.0	-	-.2	-	653.3	1.8
8	7.5	-1.6	.63	.7	-2.0	-2.5	321.4	3.1

- No velocity trimming performed

FIGURE 4-1

SPS 2 - Attitude Errors

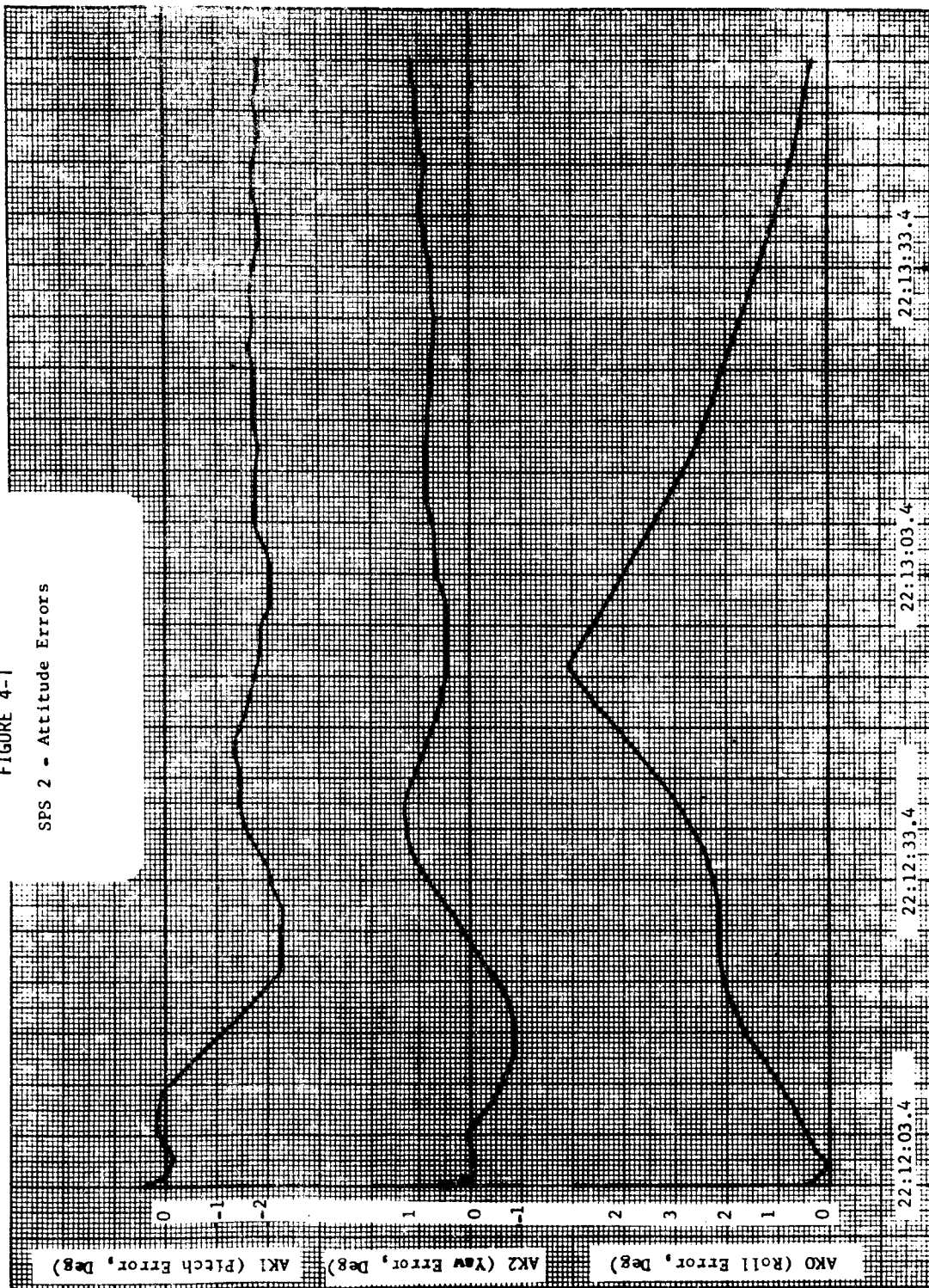
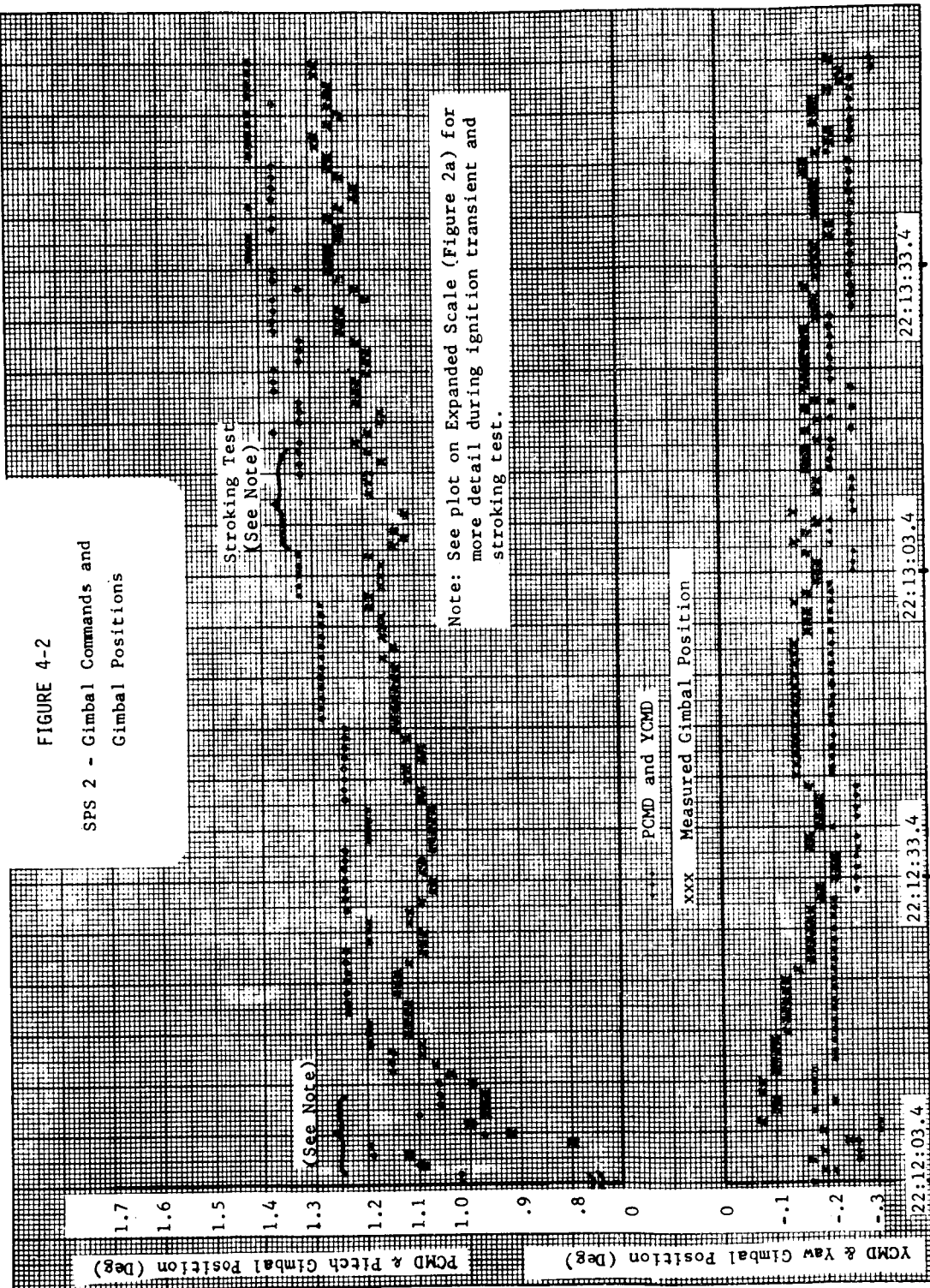


FIGURE 4-2

SPS 2 - Gimbal Commands and  
Gimbal Positions



GET (HR:MIN:SEC)

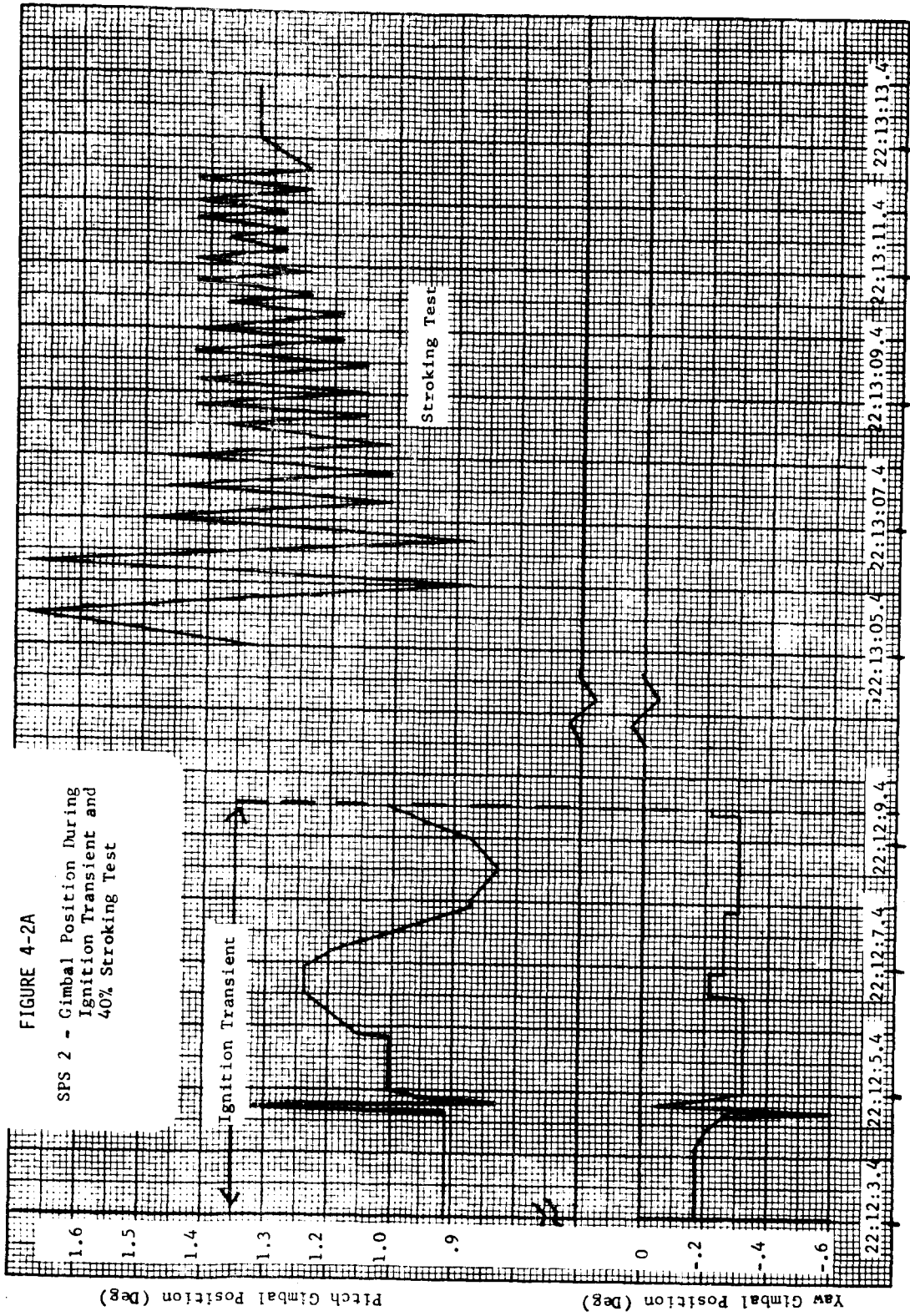


FIGURE 4-2A

SPS 2 - Gimbal Position During Ignition Transient and 40% Stroking Test

GET (HR:MIN:SEC)

FIGURE 4-3

SPS 2 - Trim Angles  
(PACTOFF and YACTOFF)

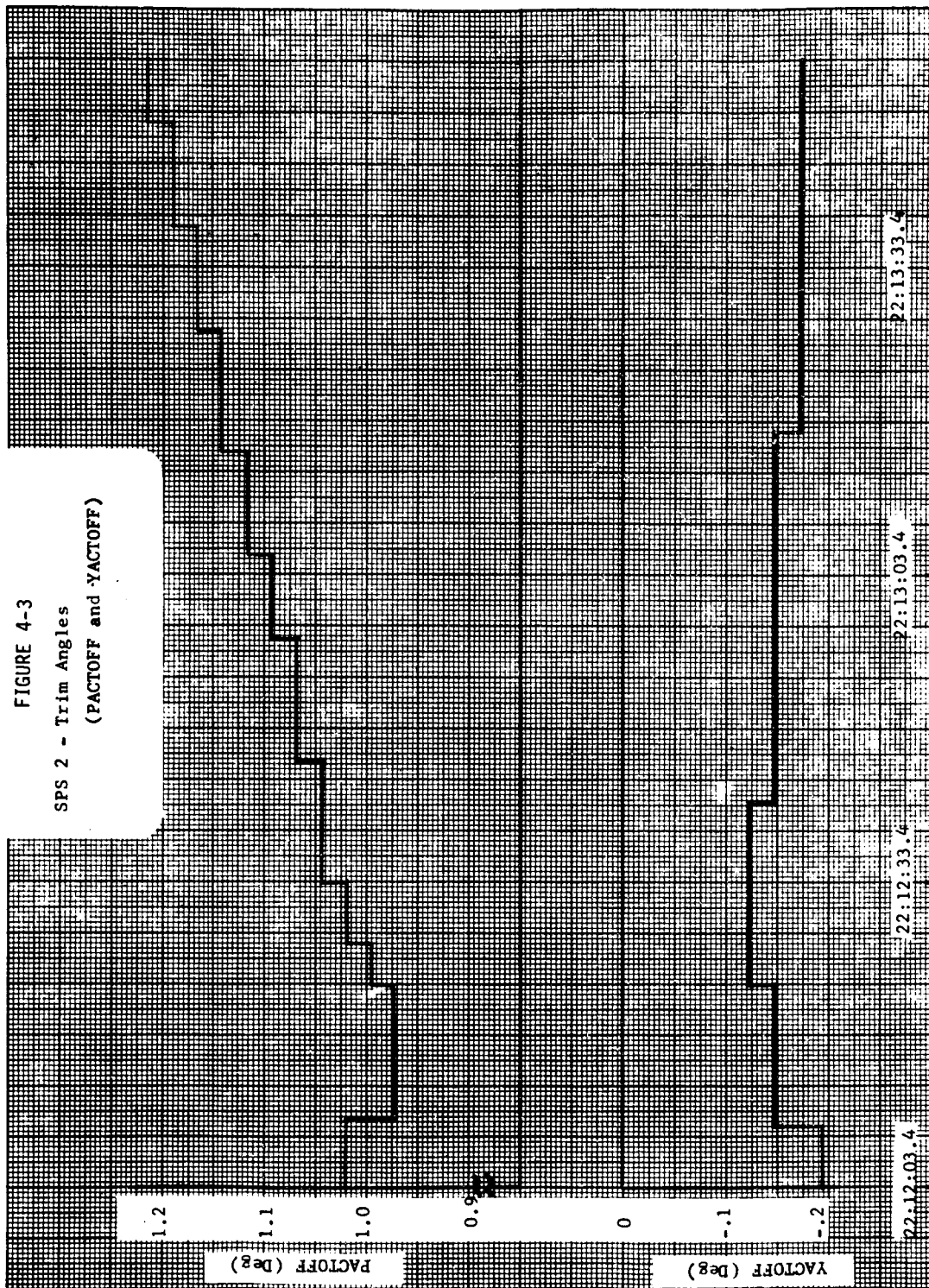


FIGURE 4-4

SPS 3 - Attitude Errors

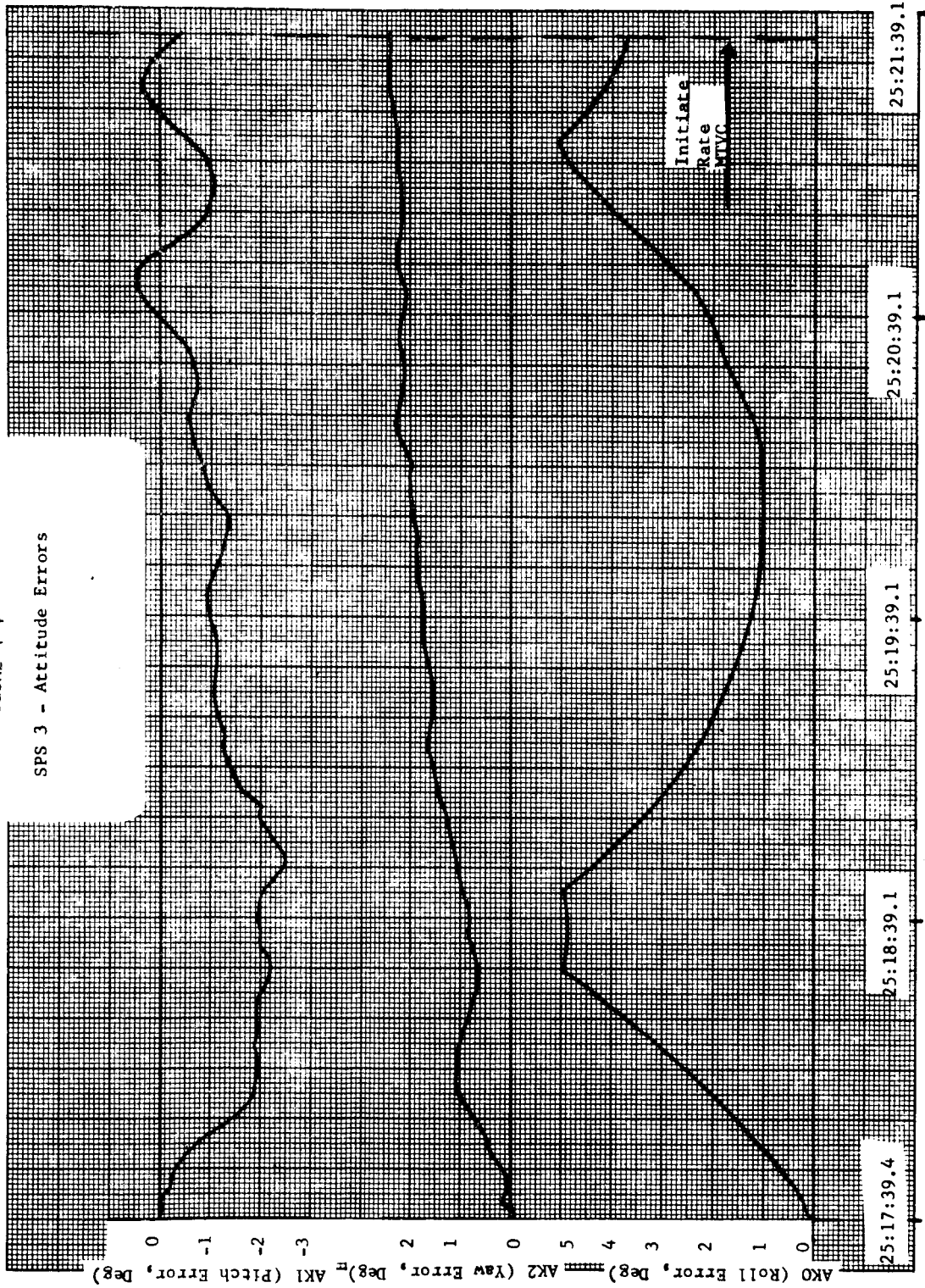
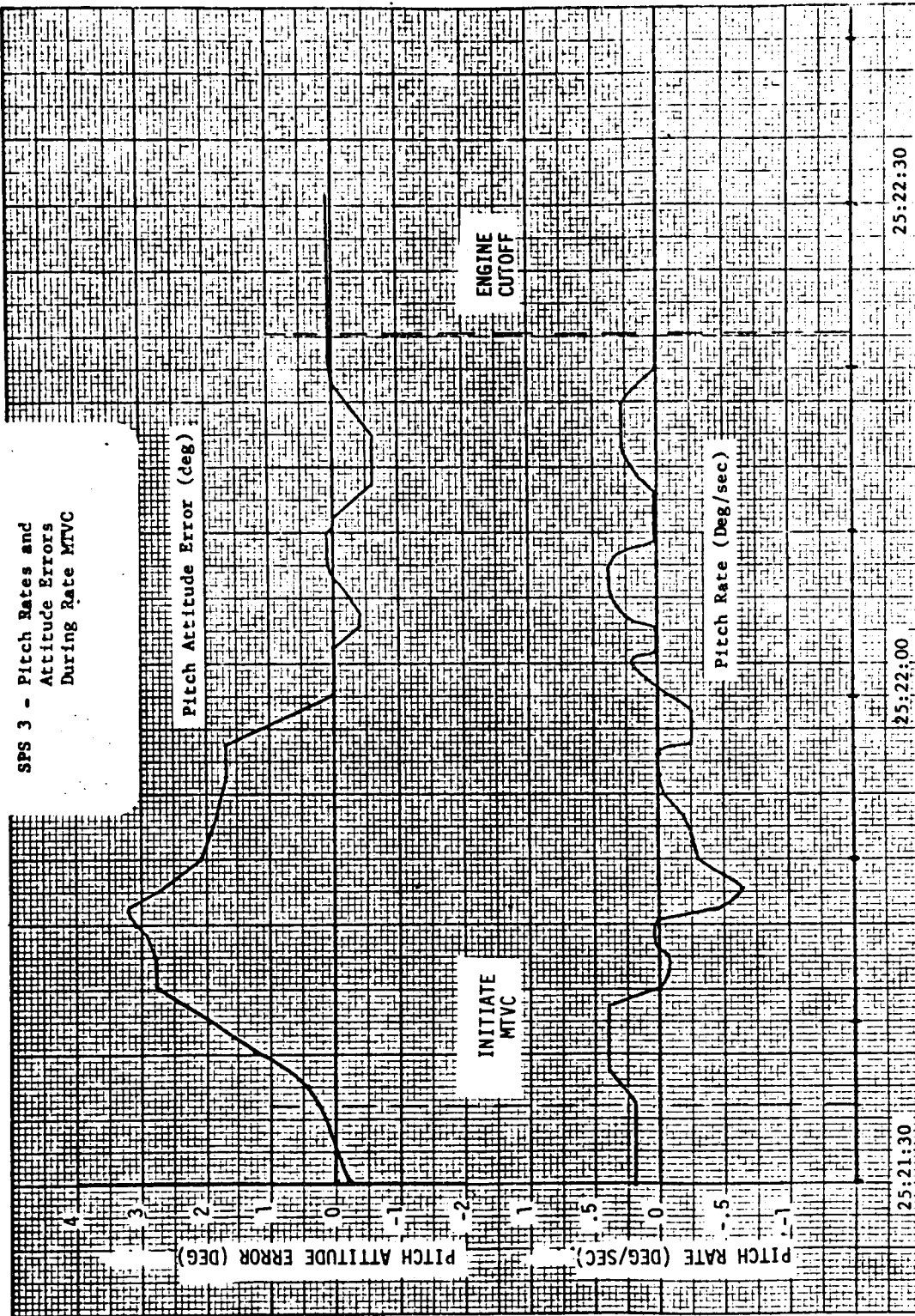


FIGURE 4-5

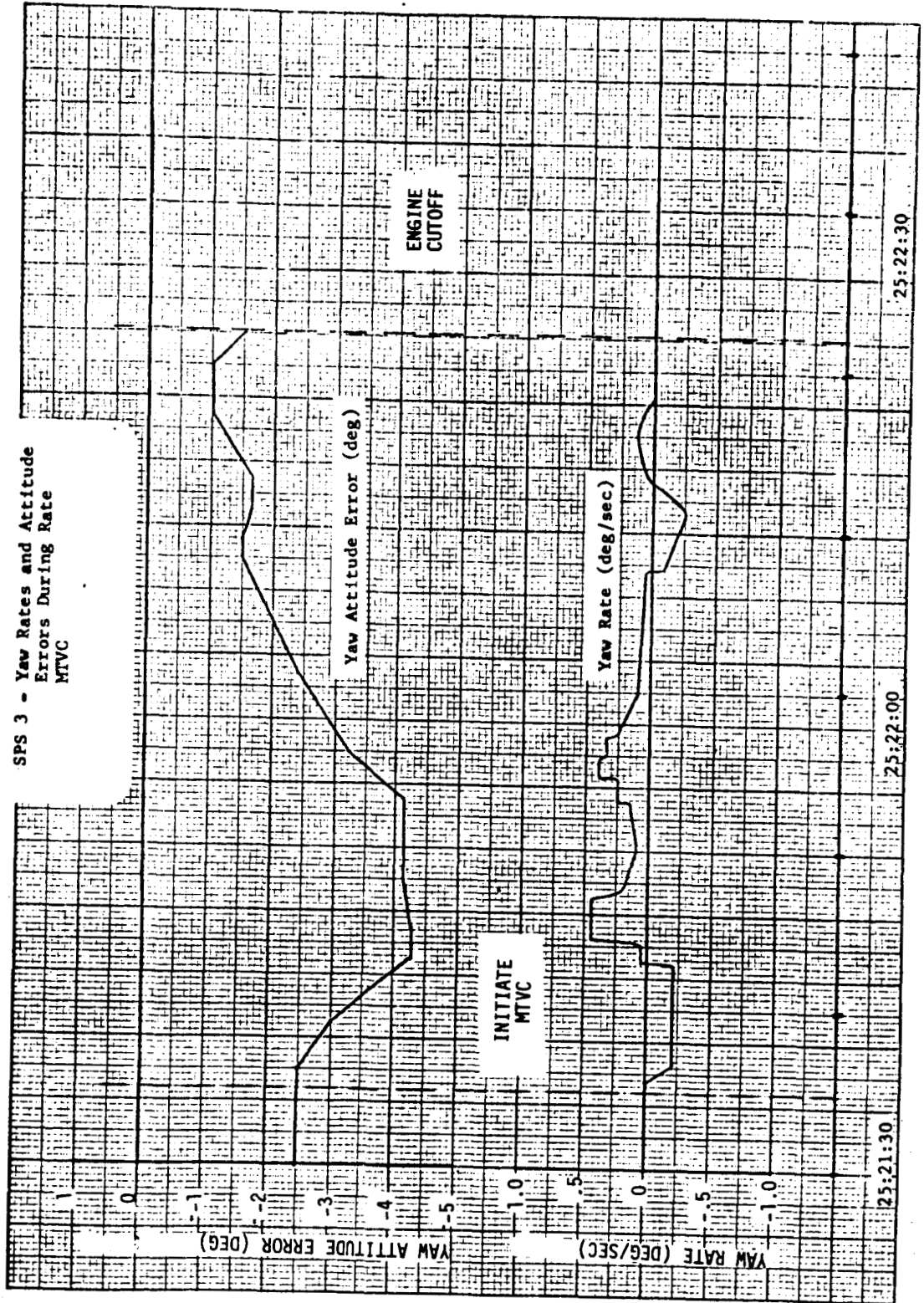
SPS 3 - Pitch Rates and Attitude Errors During Rate MTVC



GET (HR:MIN:SEC)

FIGURE 4-6

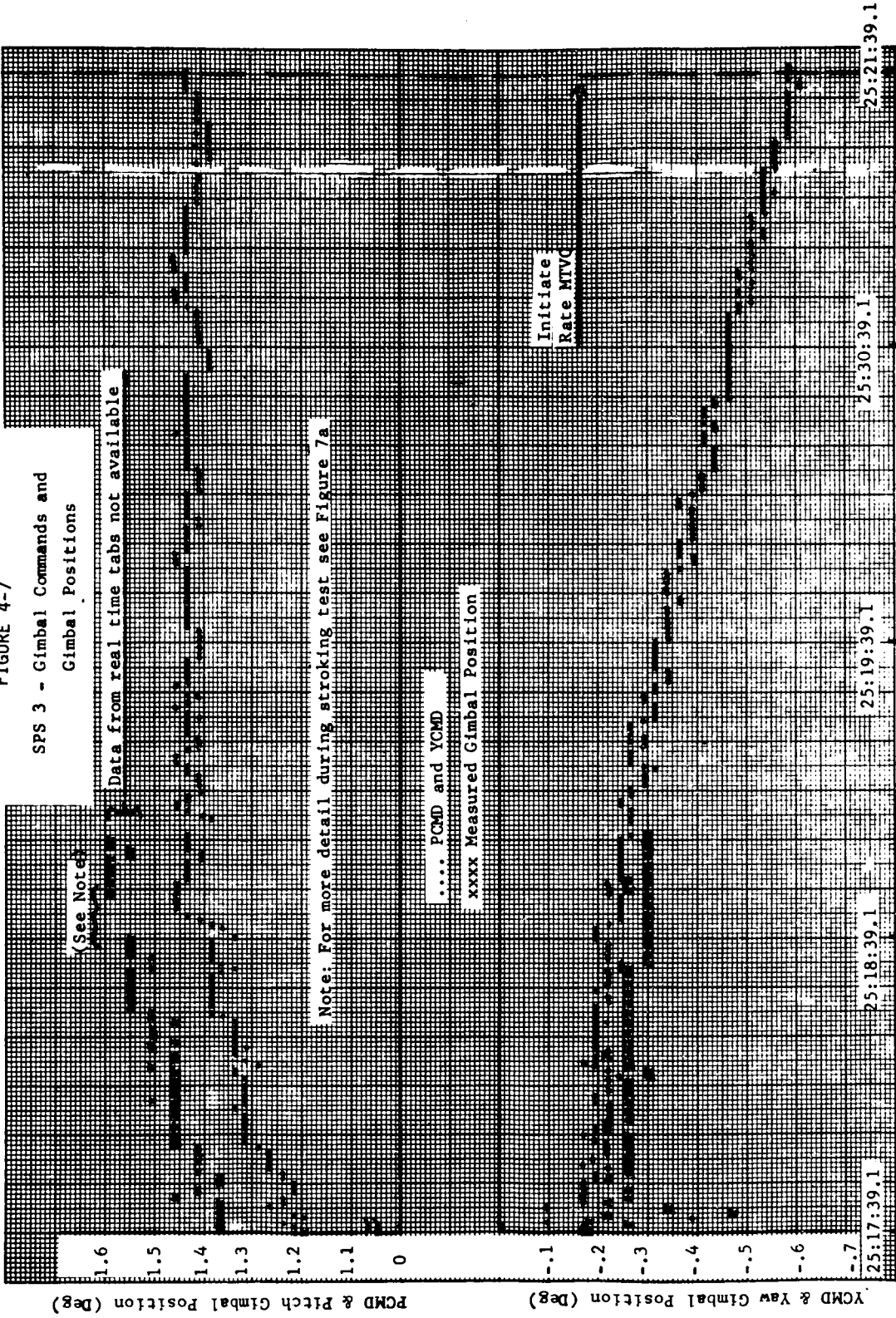
SPS 3 - Yaw Rates and Attitude Errors During Rate MTVC



GET (HR:MIN:SEC)

FIGURE 4-7

SPS 3 - Gimbal Commands and  
Gimbal Positions



GET (HR:MIN:SEC)

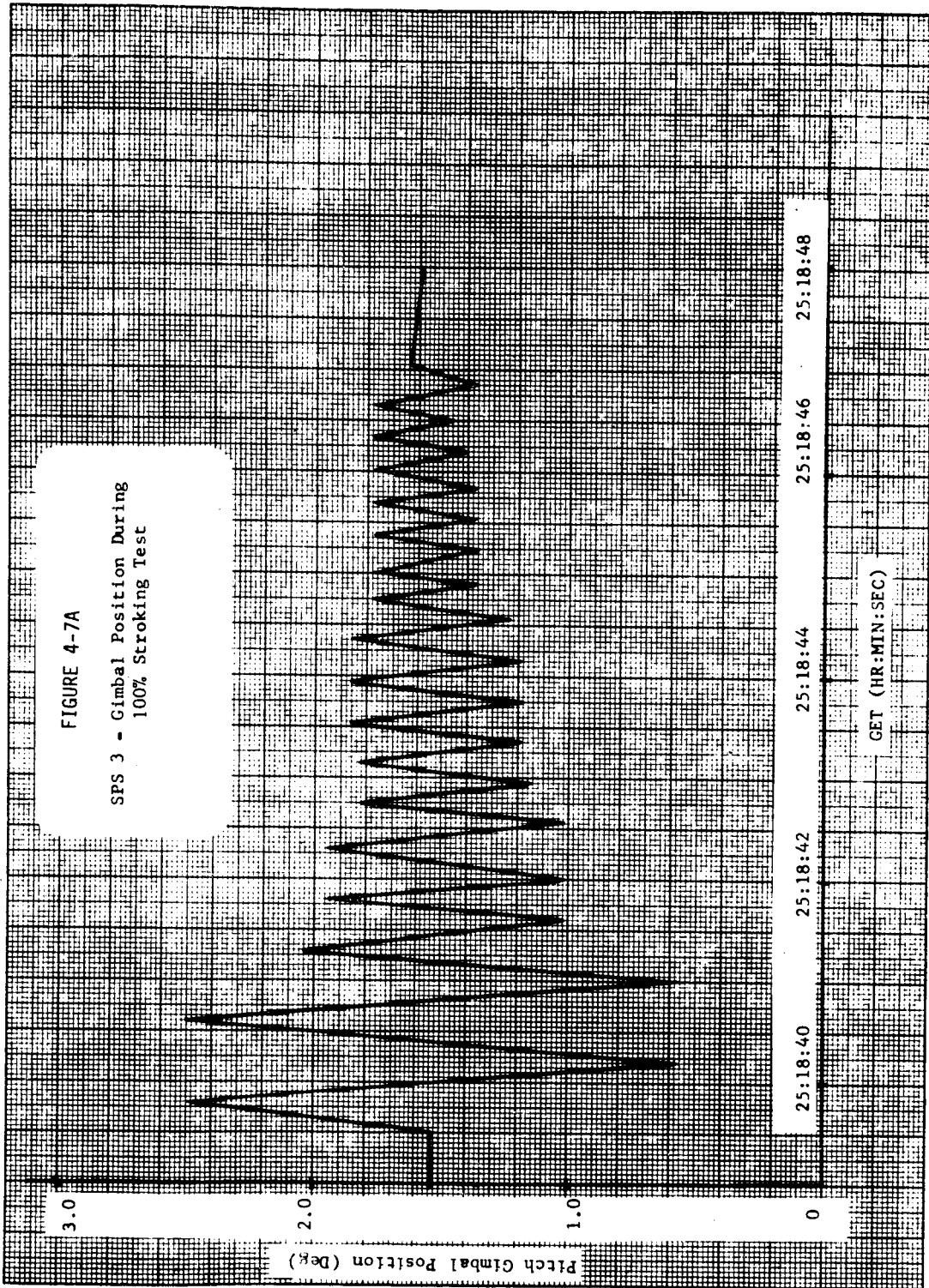




FIGURE 4-9

SPS 4 - Attitude Errors

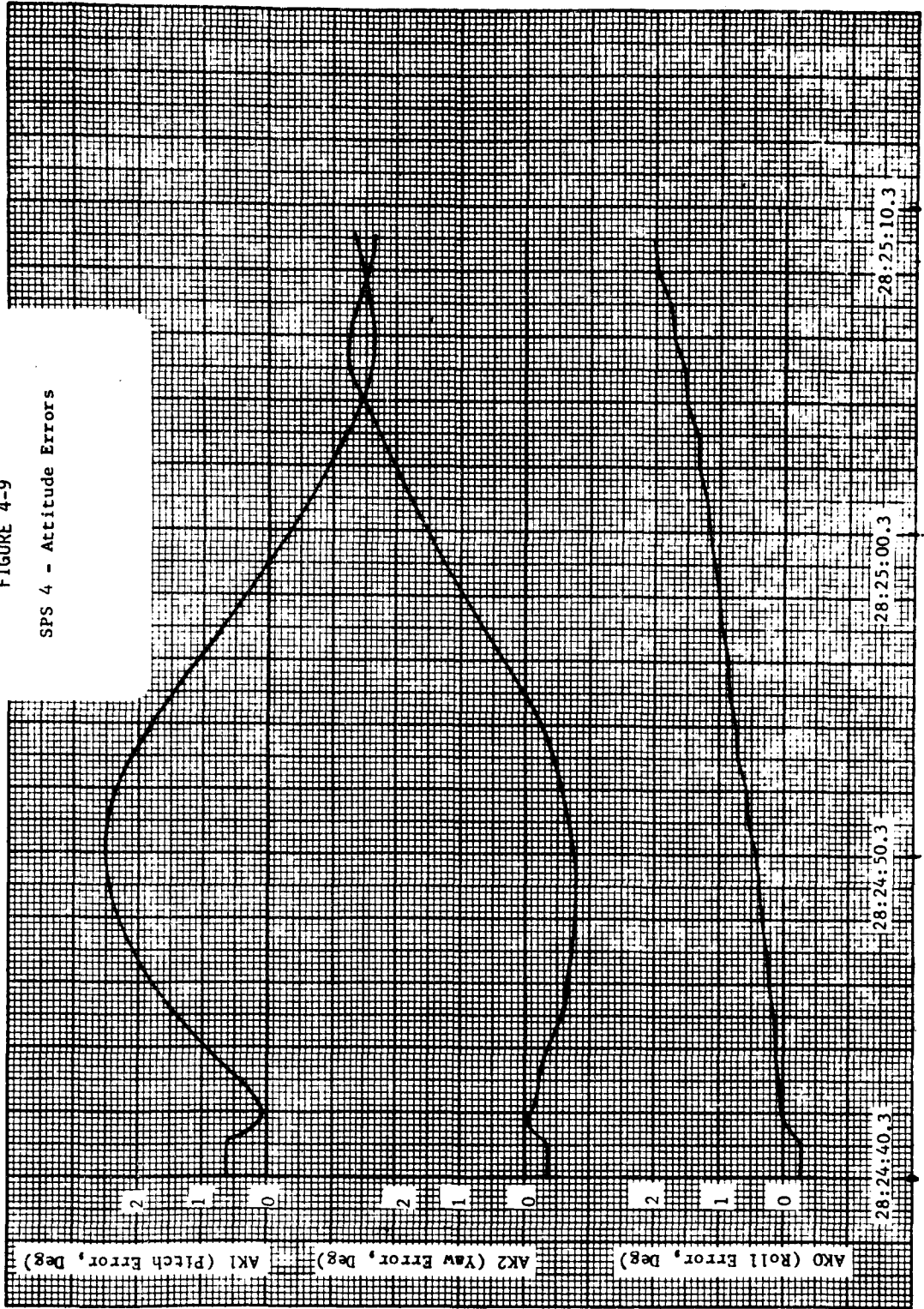
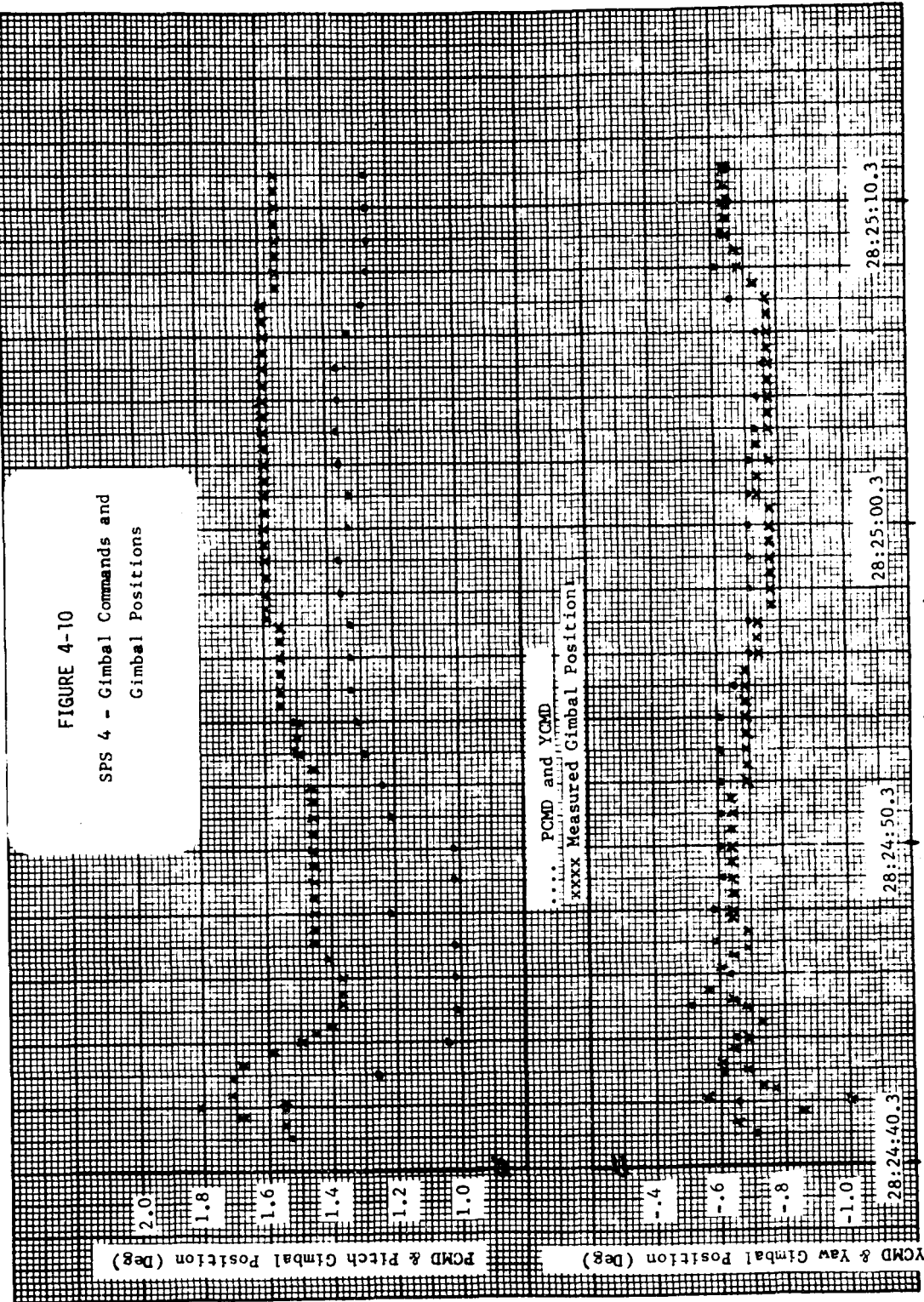


FIGURE 4-10

SPS 4 - Gimbal Commands and  
Gimbal Positions



GET (HR:MIN:SEC)

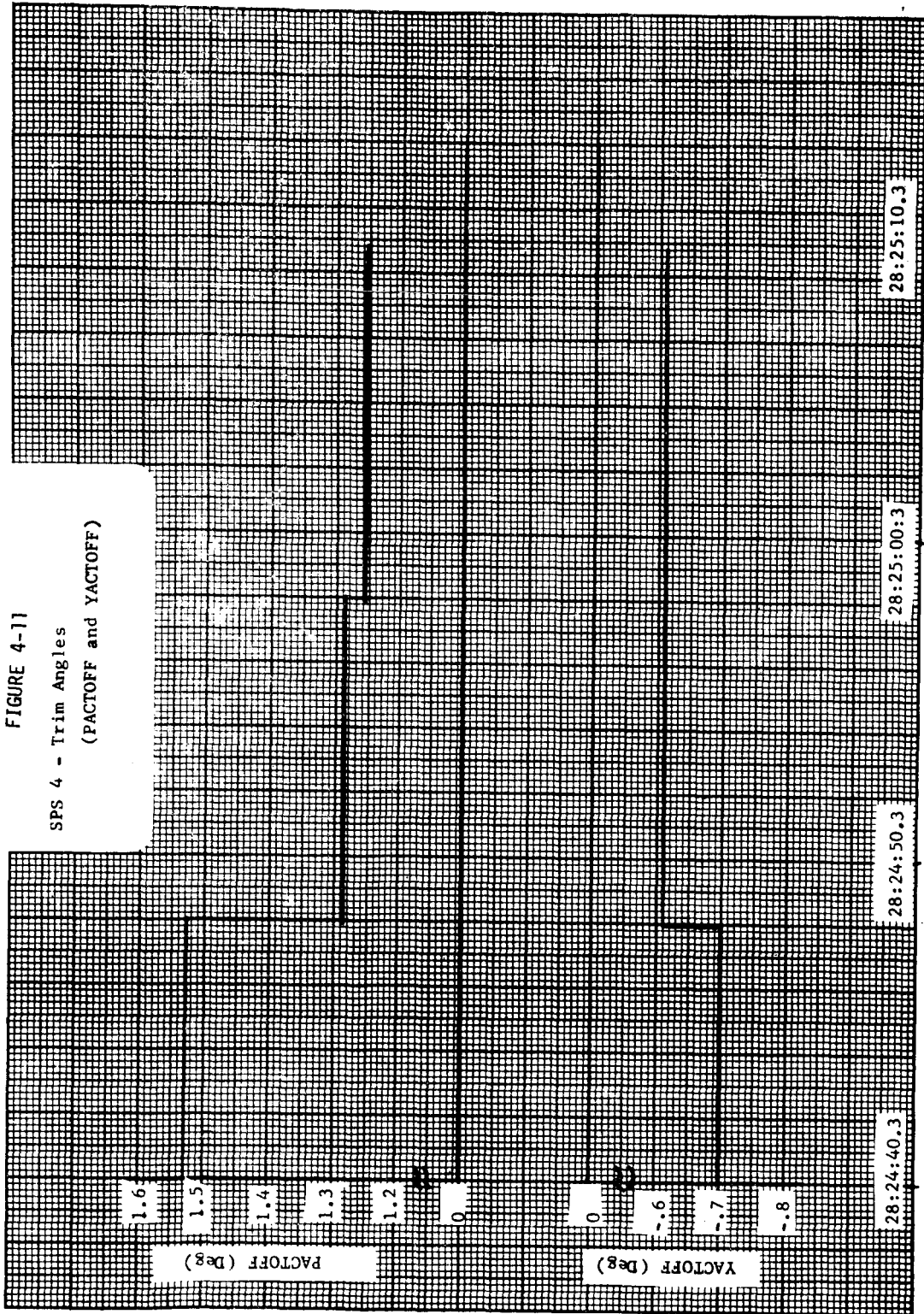
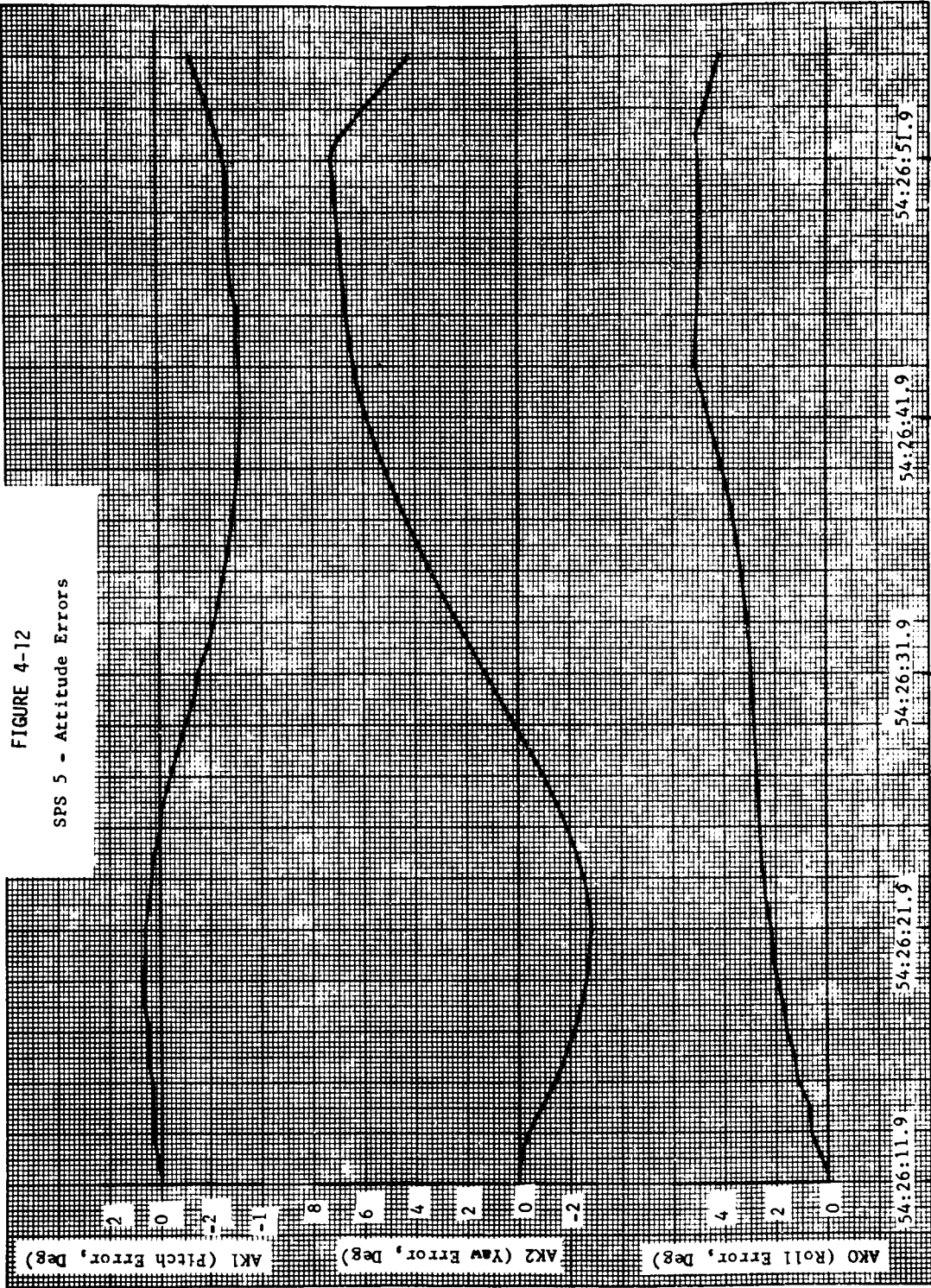


FIGURE 4-11  
 SPS 4 - Trim Angles  
 (PACTOFF and YACTOFF)

GET (HR: MIN: SEC)

FIGURE 4-12

SPS 5 - Attitude Errors



GET (HR:MIN:SEC)

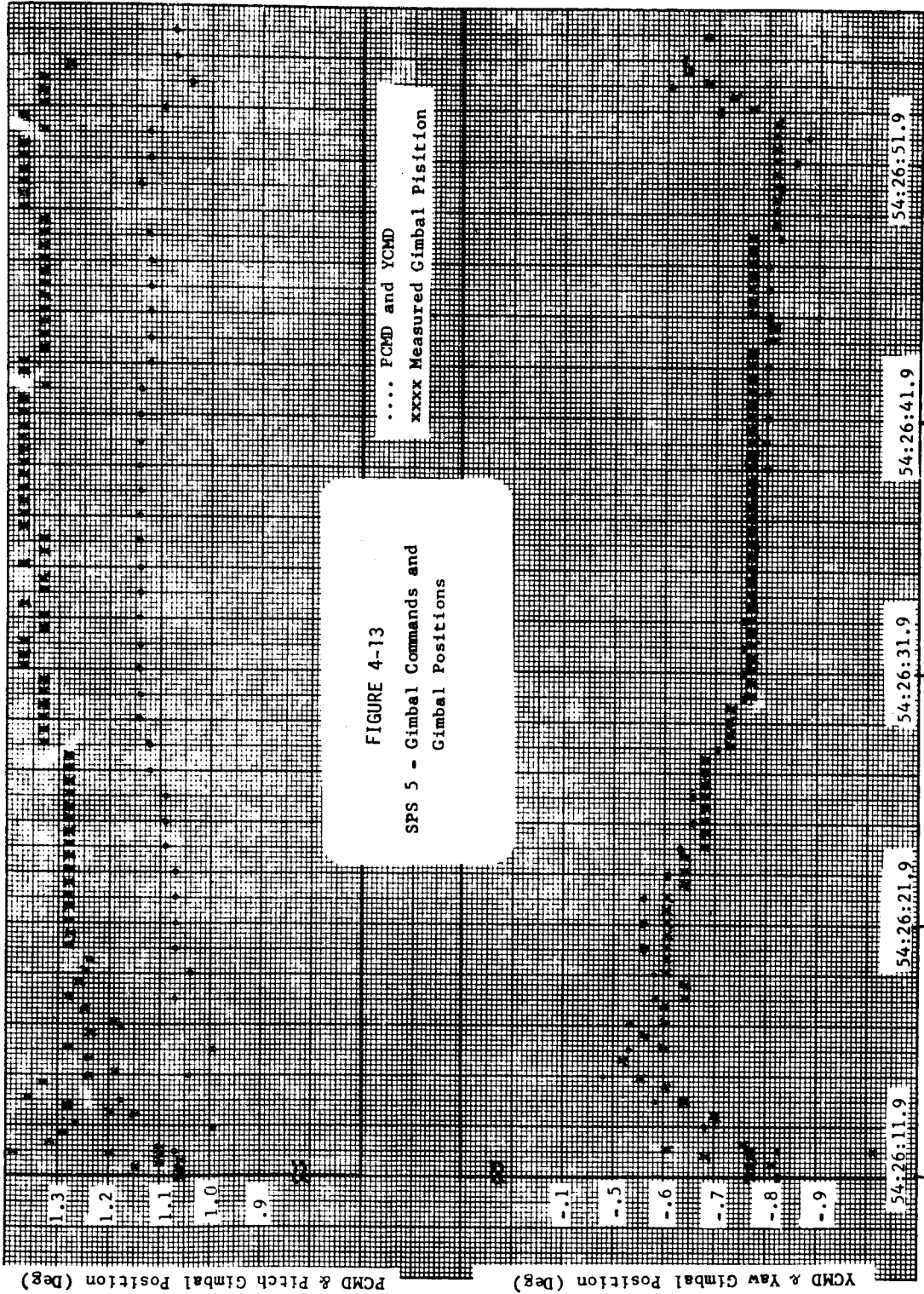
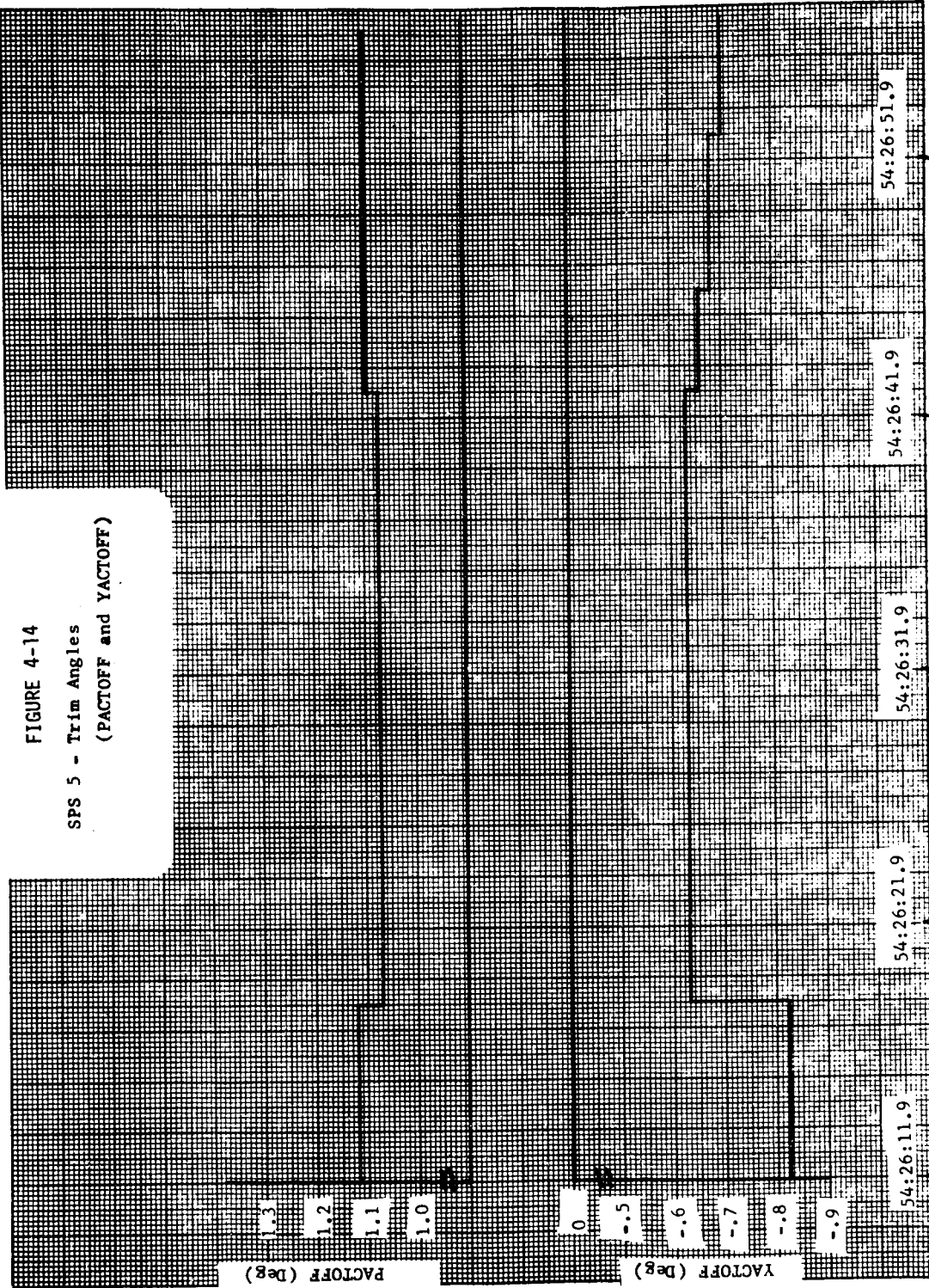


FIGURE 4-13  
 SPS 5 - Gimbal Commands and  
 Gimbal Positions

GET (HR:MIN:SEC)

FIGURE 4-14

SPS 5 - Trim Angles  
(PACTOFF and YACTOFF)



GET (HR:MIN:SEC)

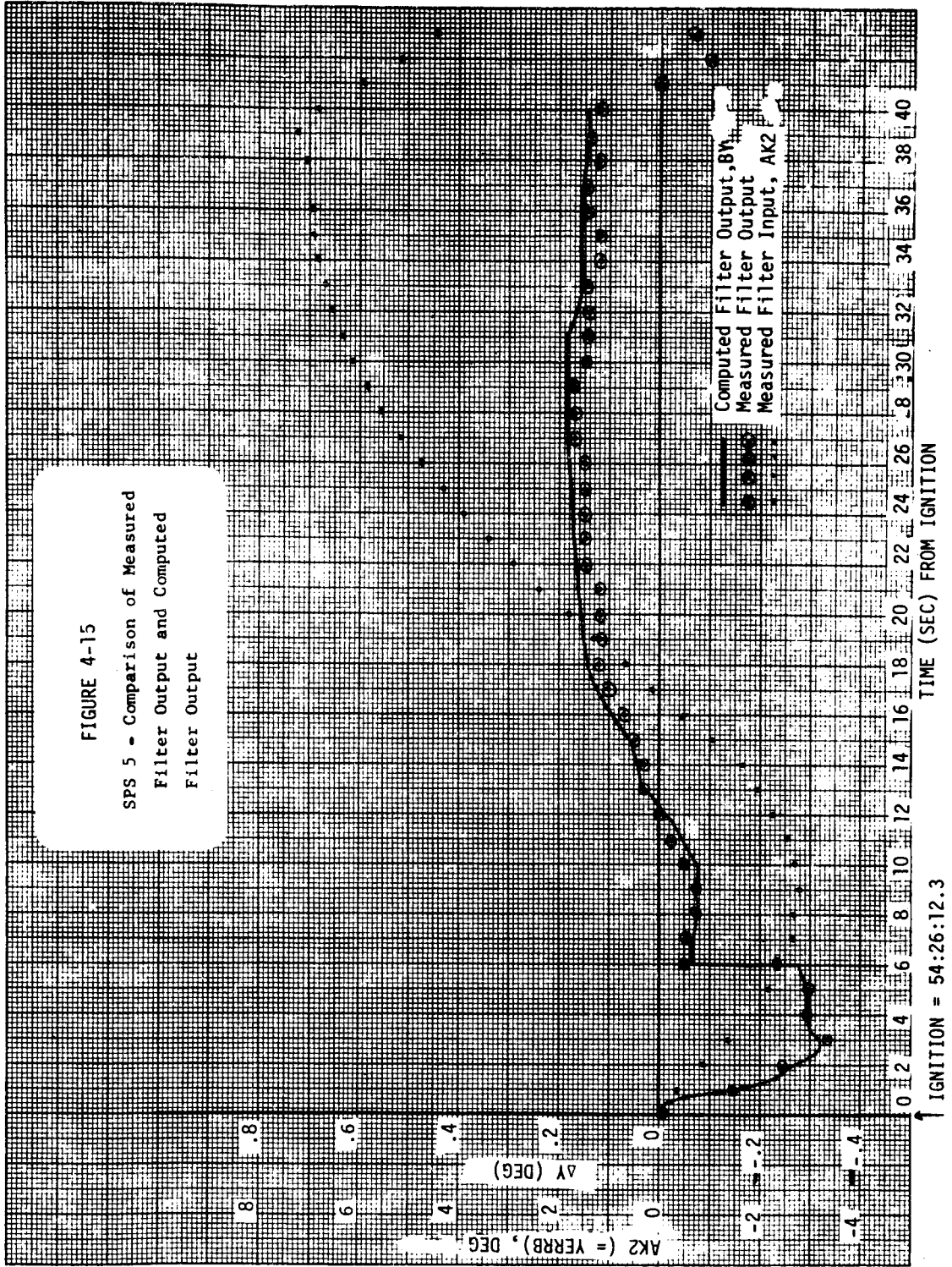
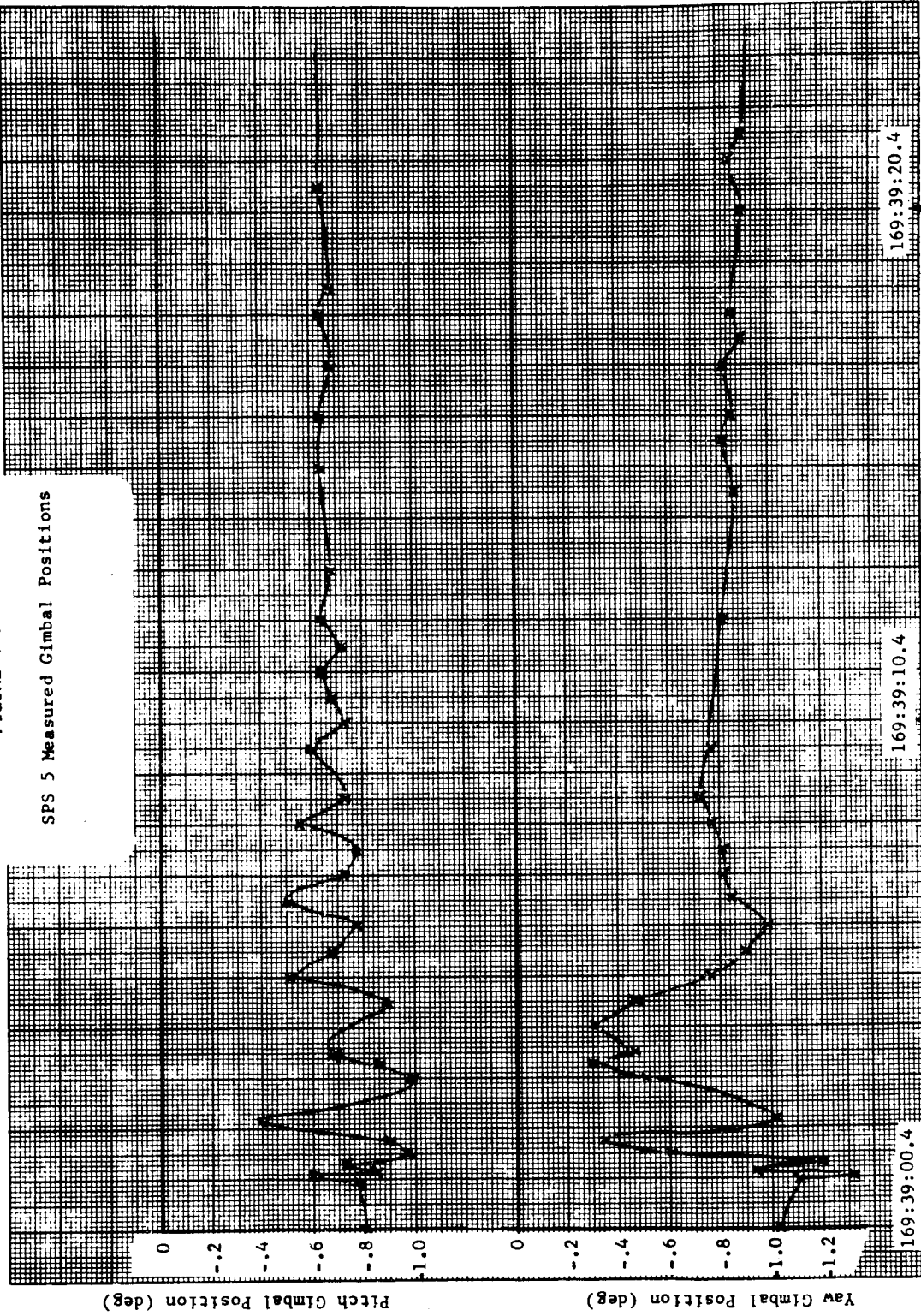


FIGURE 4-16

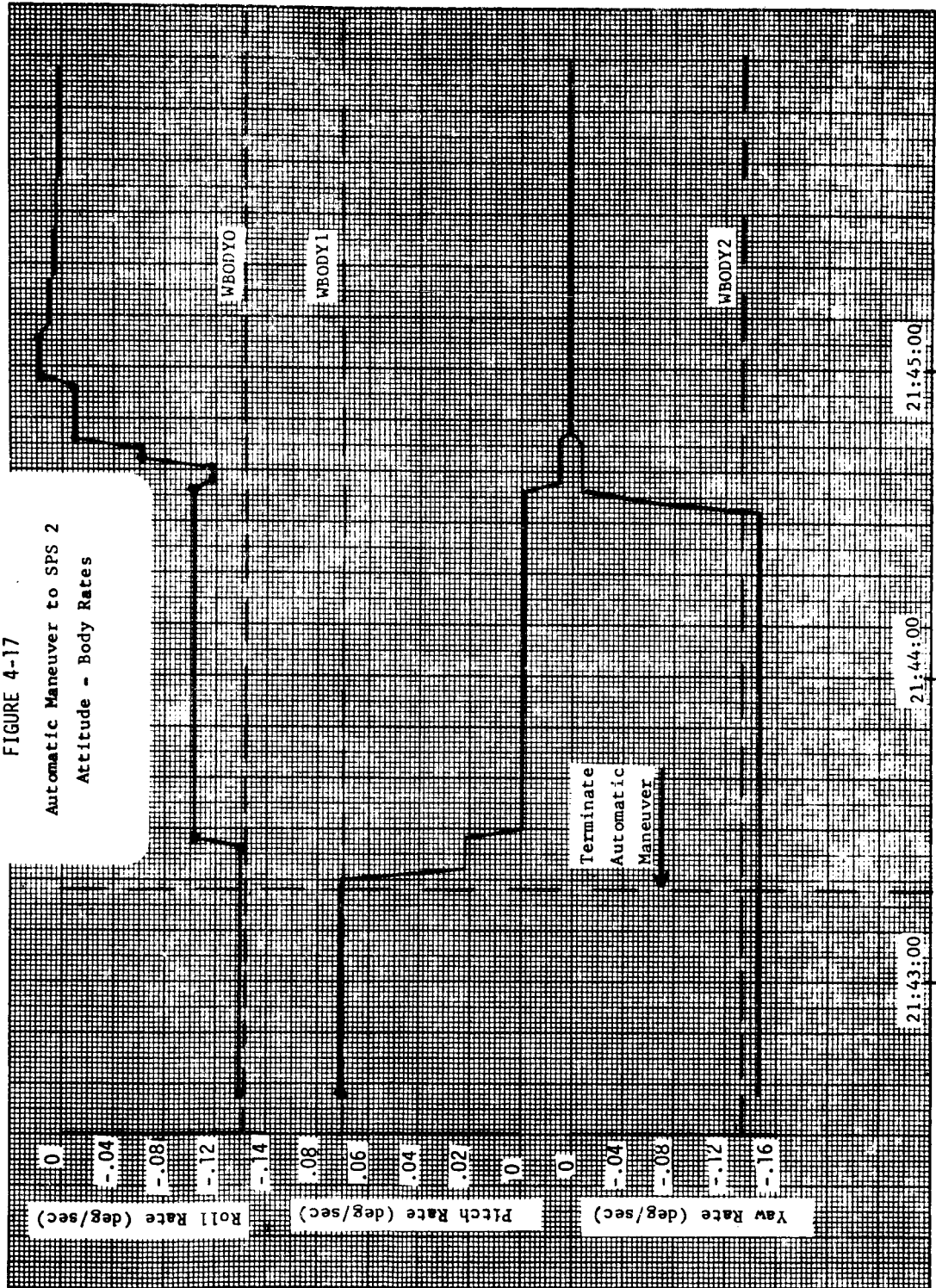
SPS 5 Measured Gimbal Positions



GET (HR:MIN:SEC)

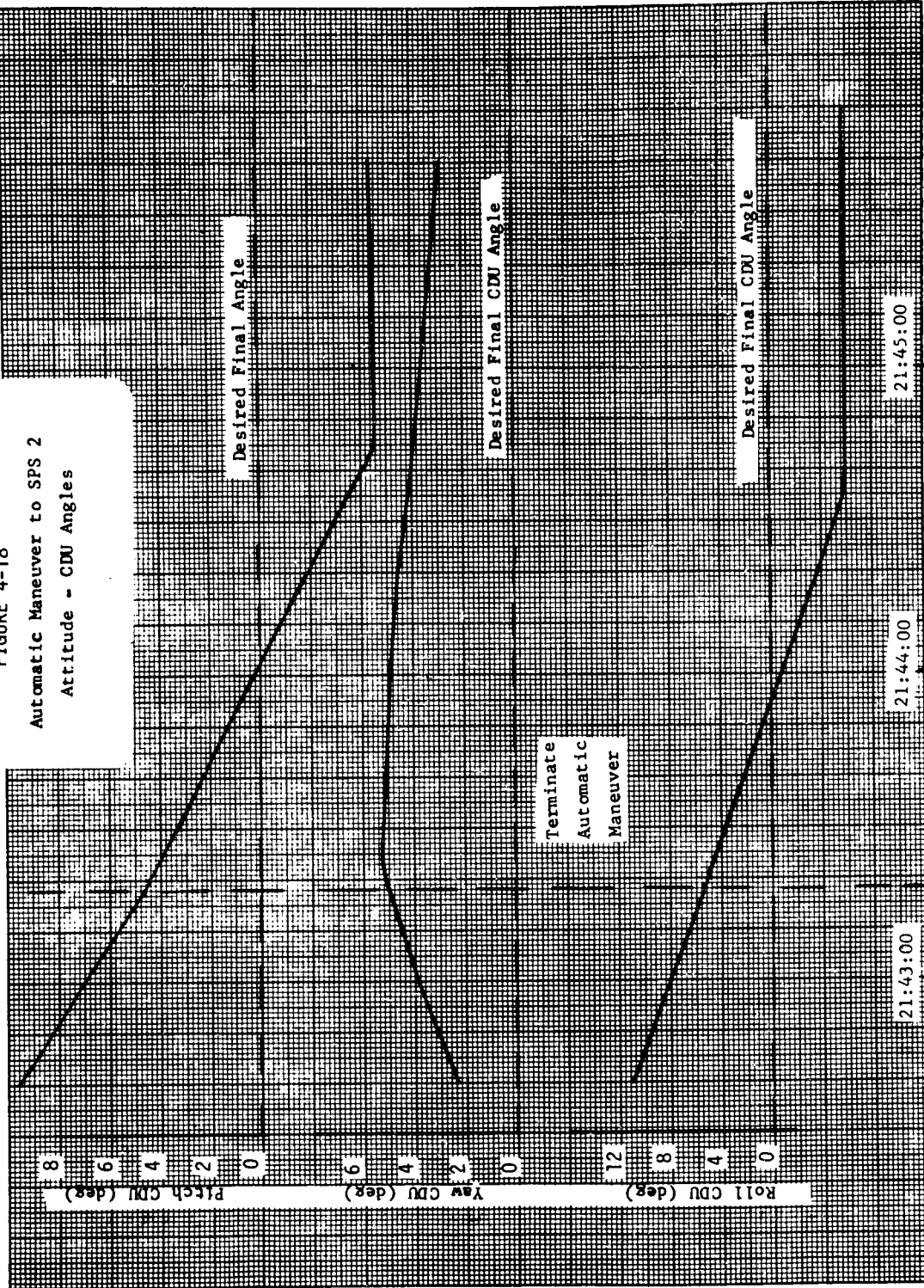
FIGURE 4-17

Automatic Maneuver to SPS 2  
Attitude - Body Rates



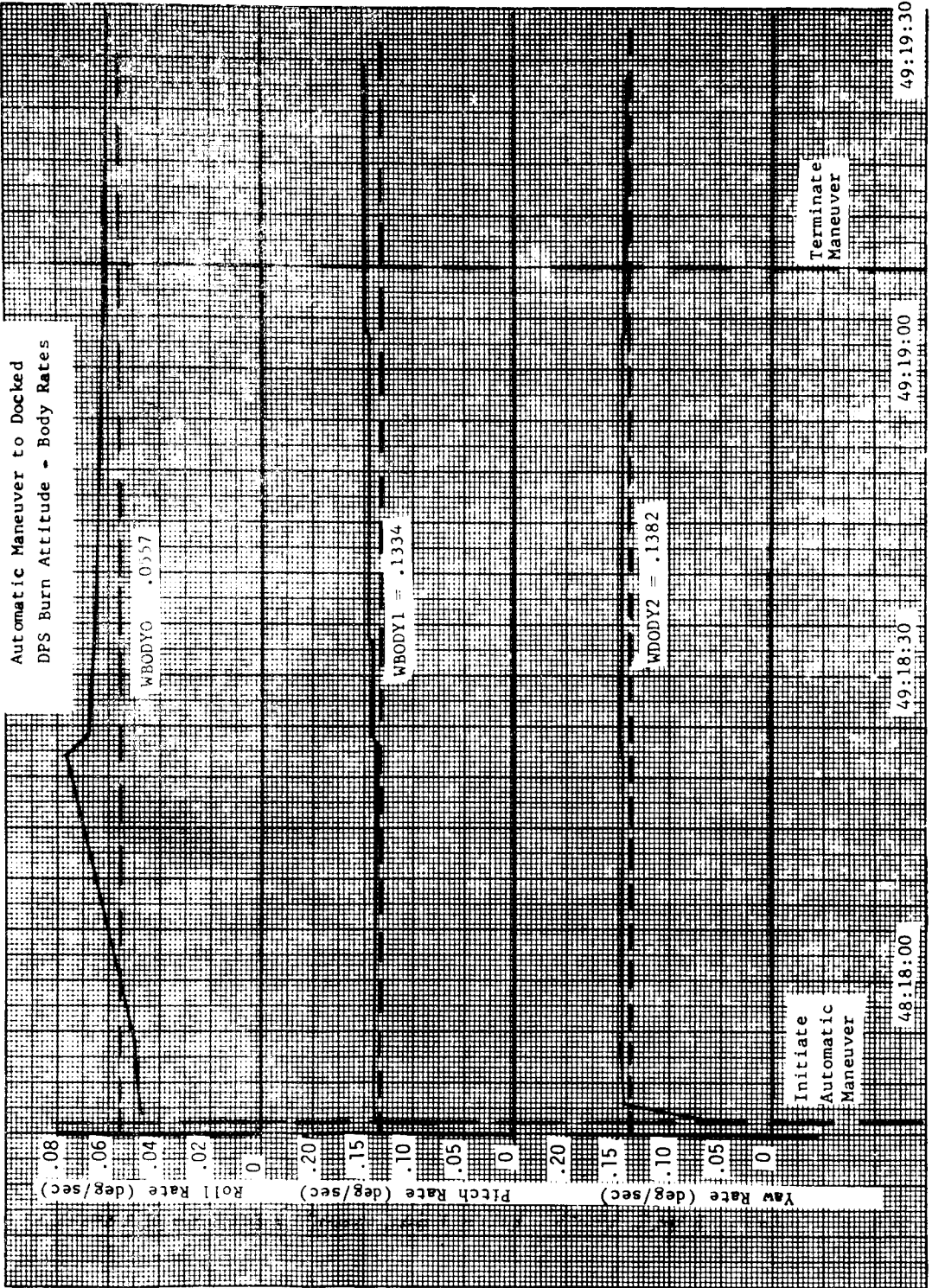
GET (HR:MIN:SEC)

FIGURE 4-18  
Automatic Maneuver to SPS 2  
Attitude - CDU Angles



GET (HR:MIN:SEC)

FIGURE 4-19



GET (H:MIN:SEC)

FIGURE 4-20

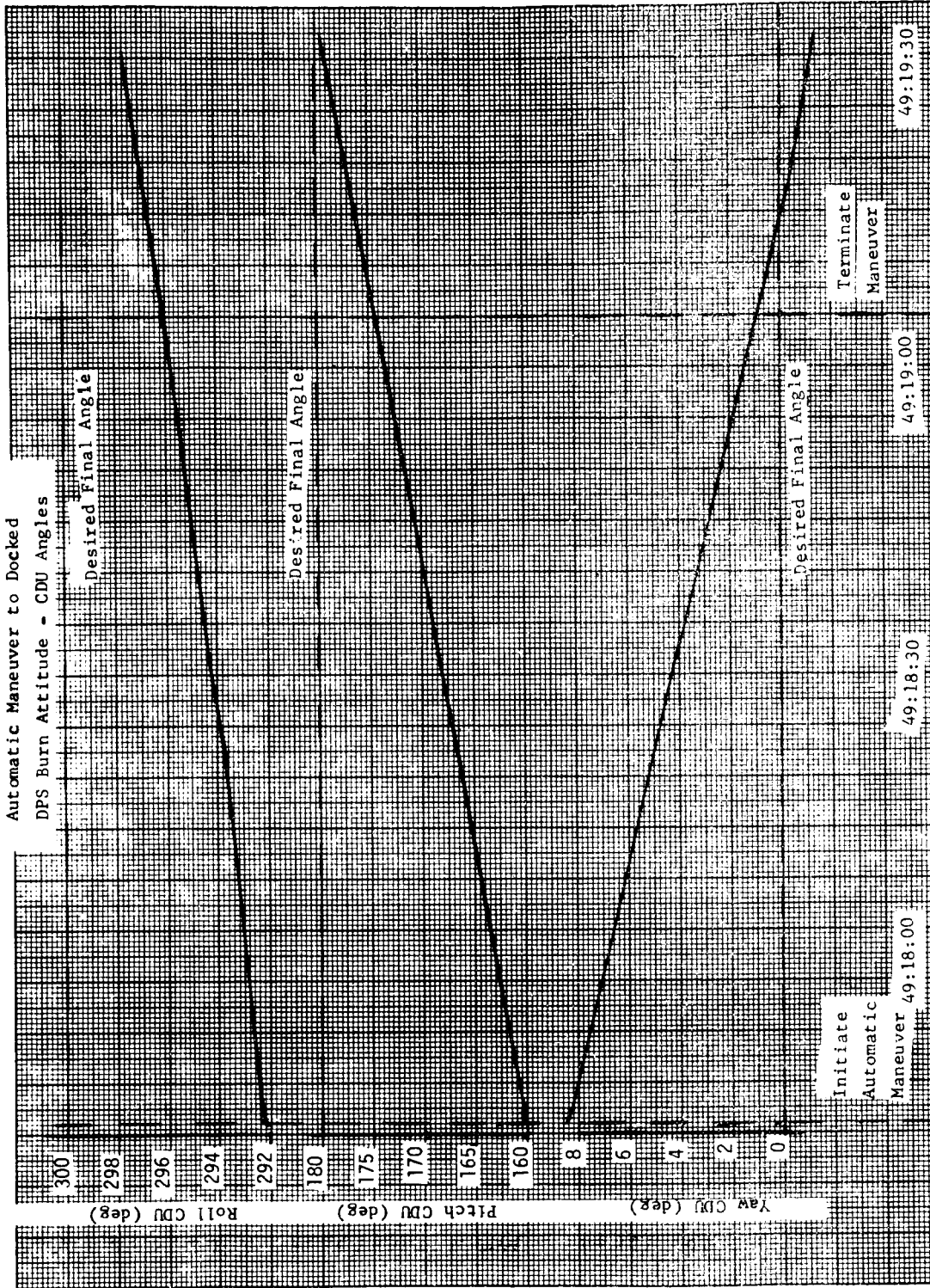


FIGURE 4-21

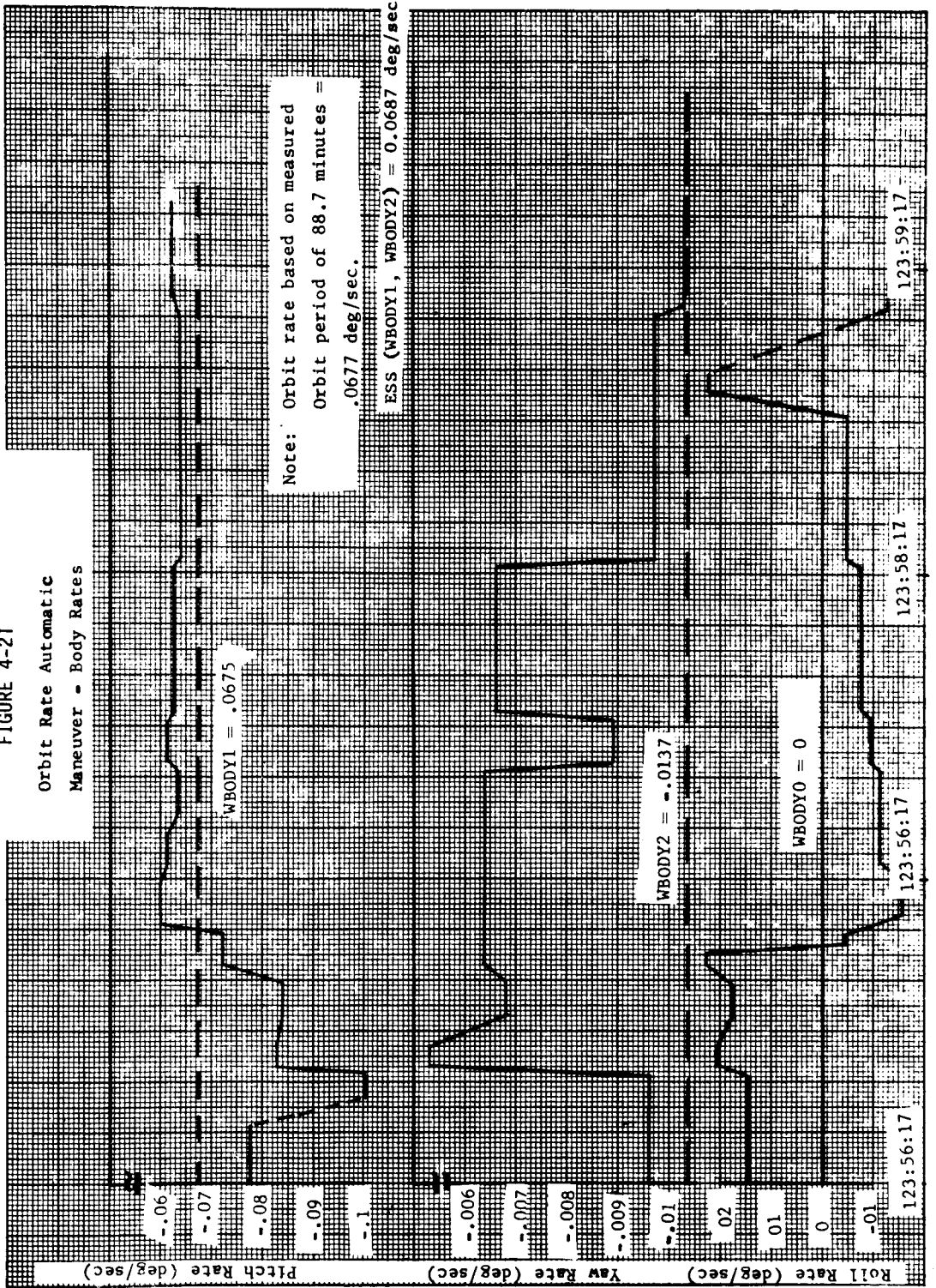
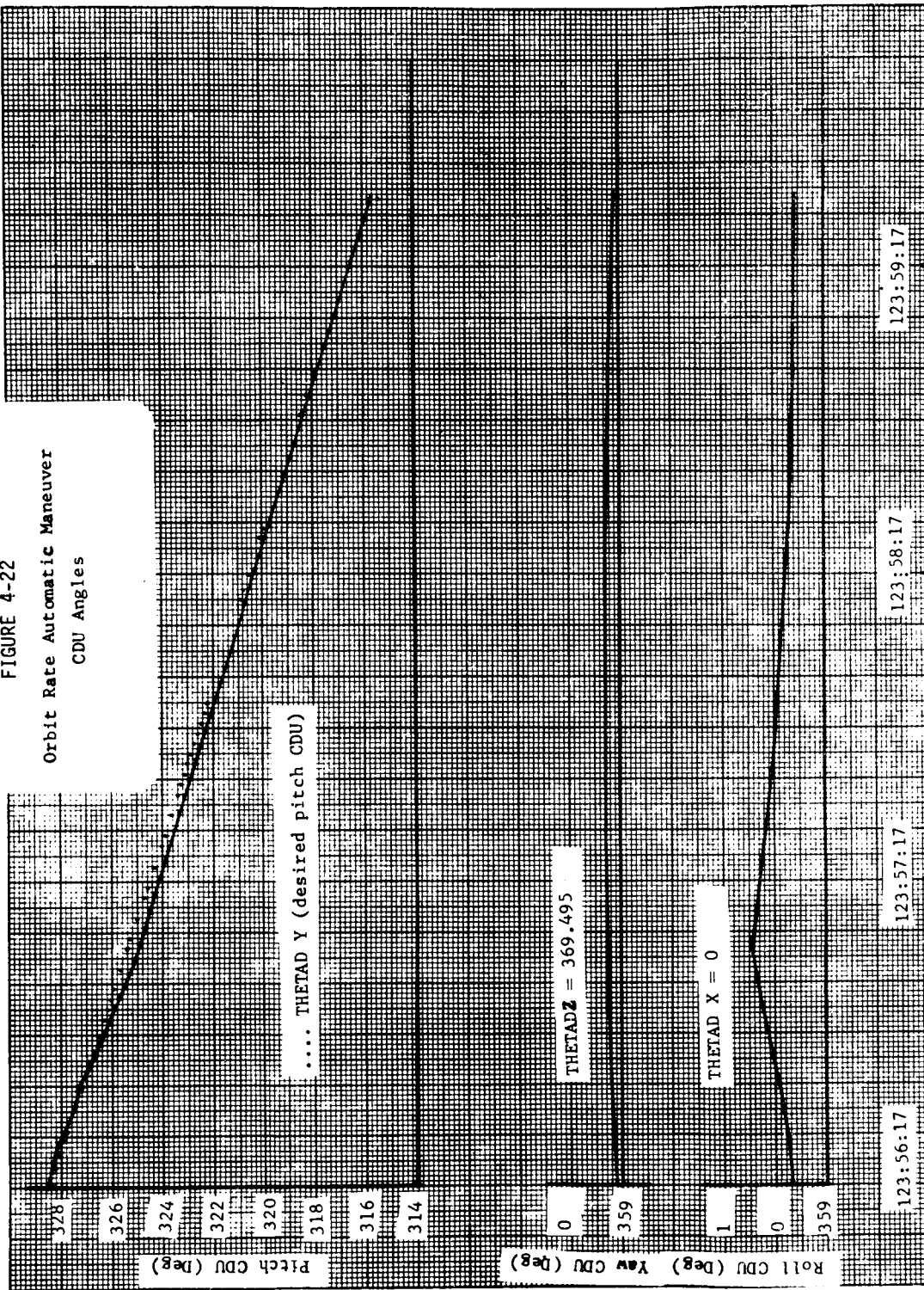


FIGURE 4-22

Orbit Rate Automatic Maneuver  
CDU Angles



GET (HR:MIN:SEC)

FIGURE 4-23

Attitude Hold Prior to SPS 3 -

Roll Phase Plane

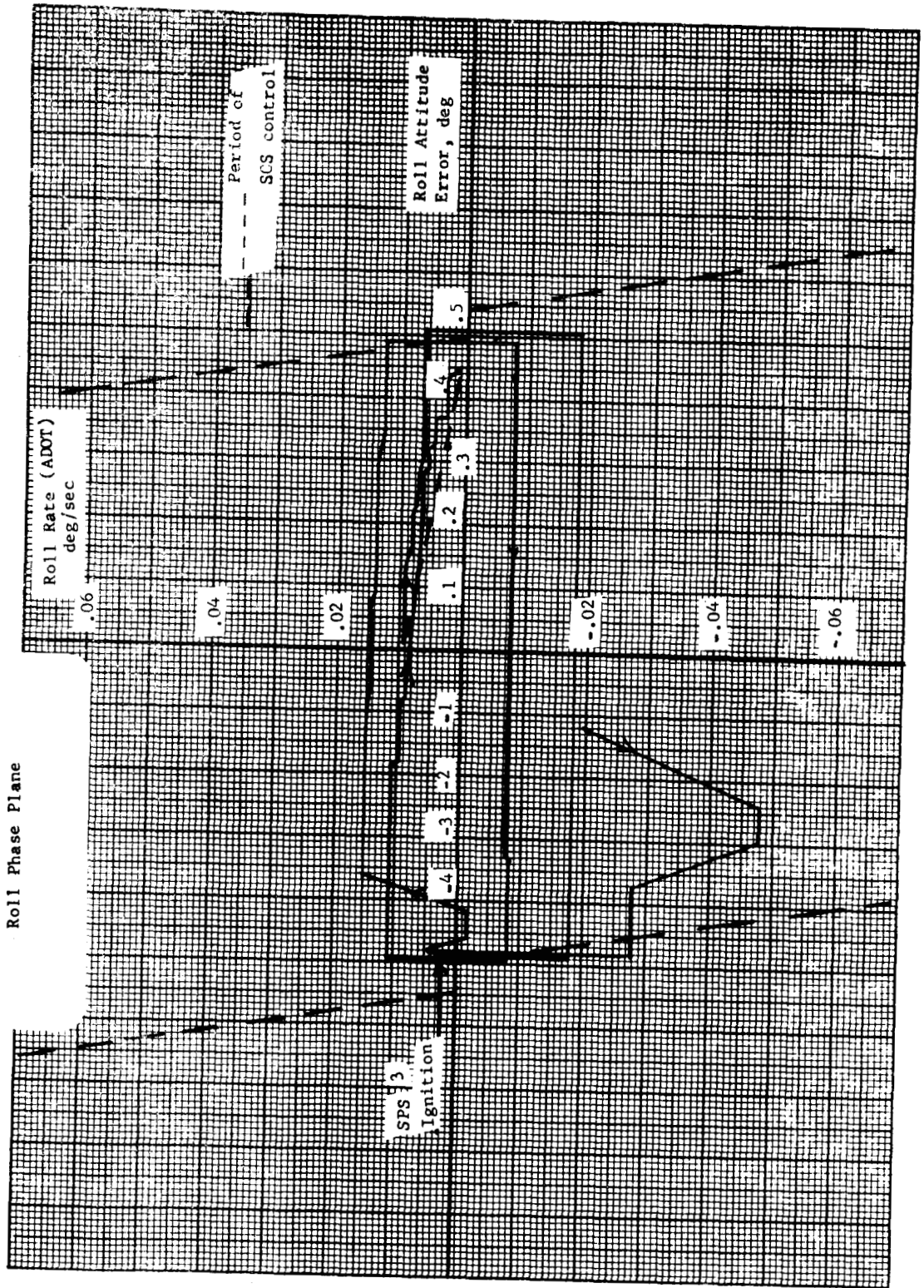


FIGURE 4-24

Attitude Hold Prior to SPS 3 -  
Pitch Phase Plane

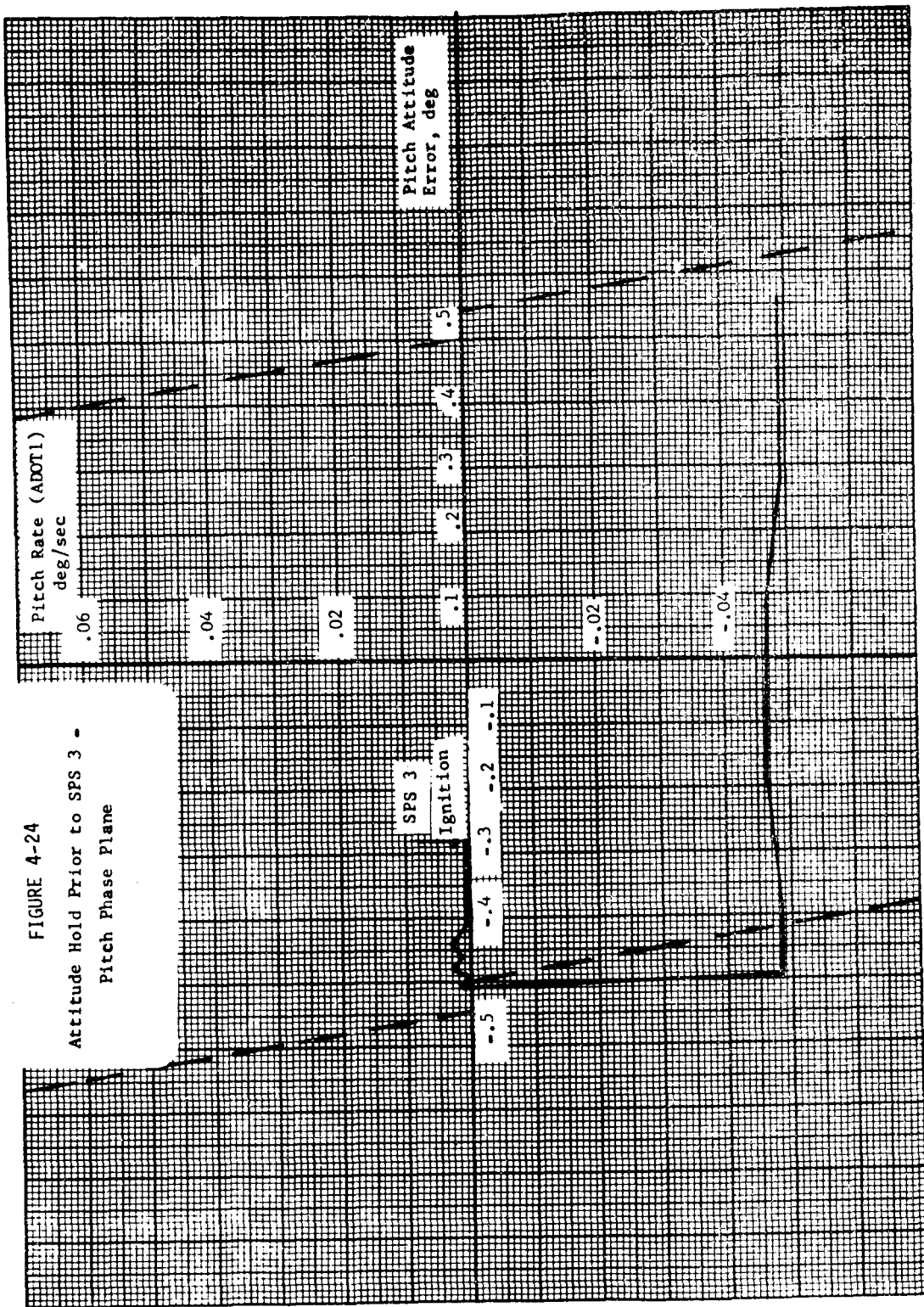
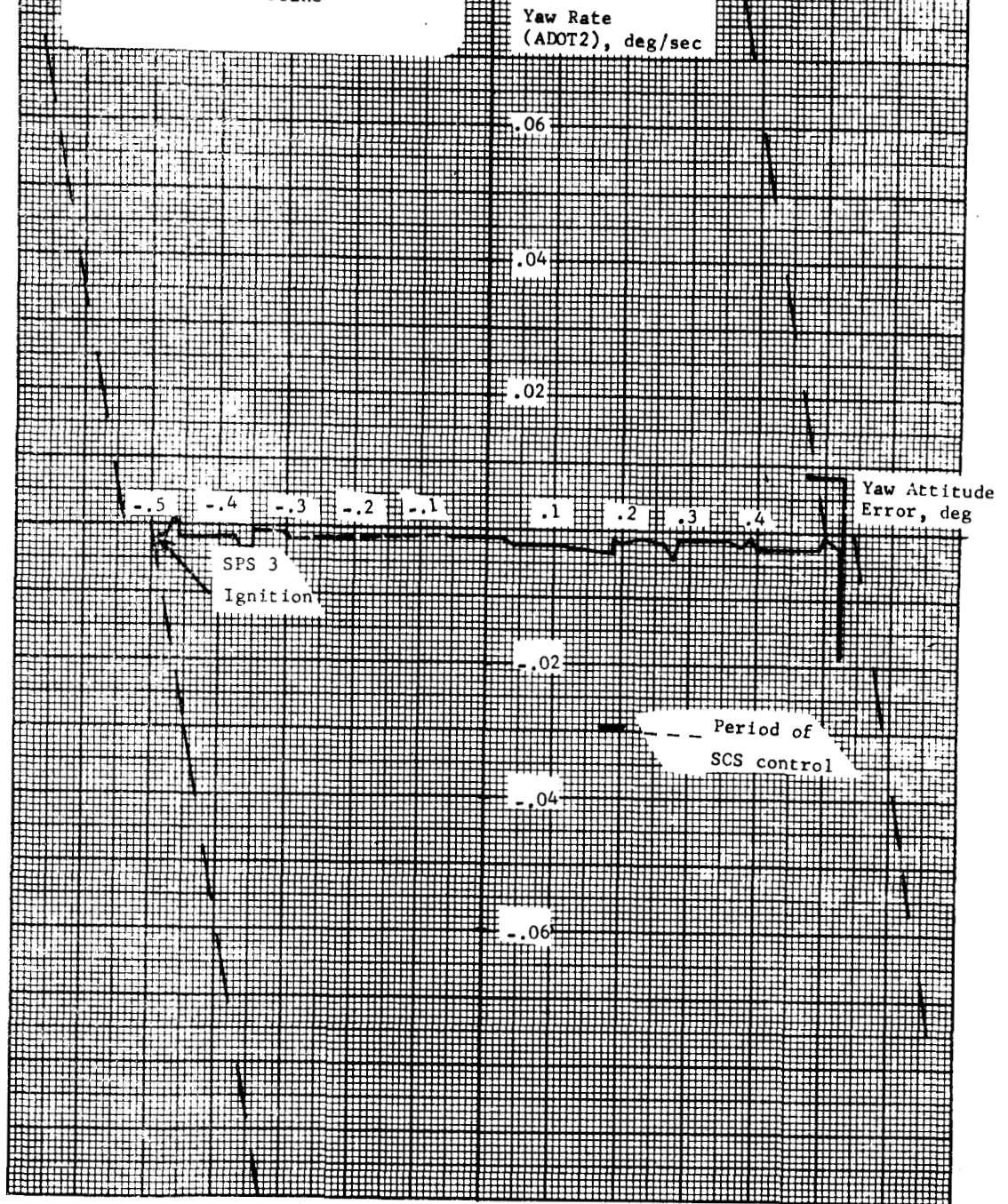


FIGURE 4-25  
Attitude Hold Prior to SPS 3 -  
Yaw Phase Plane



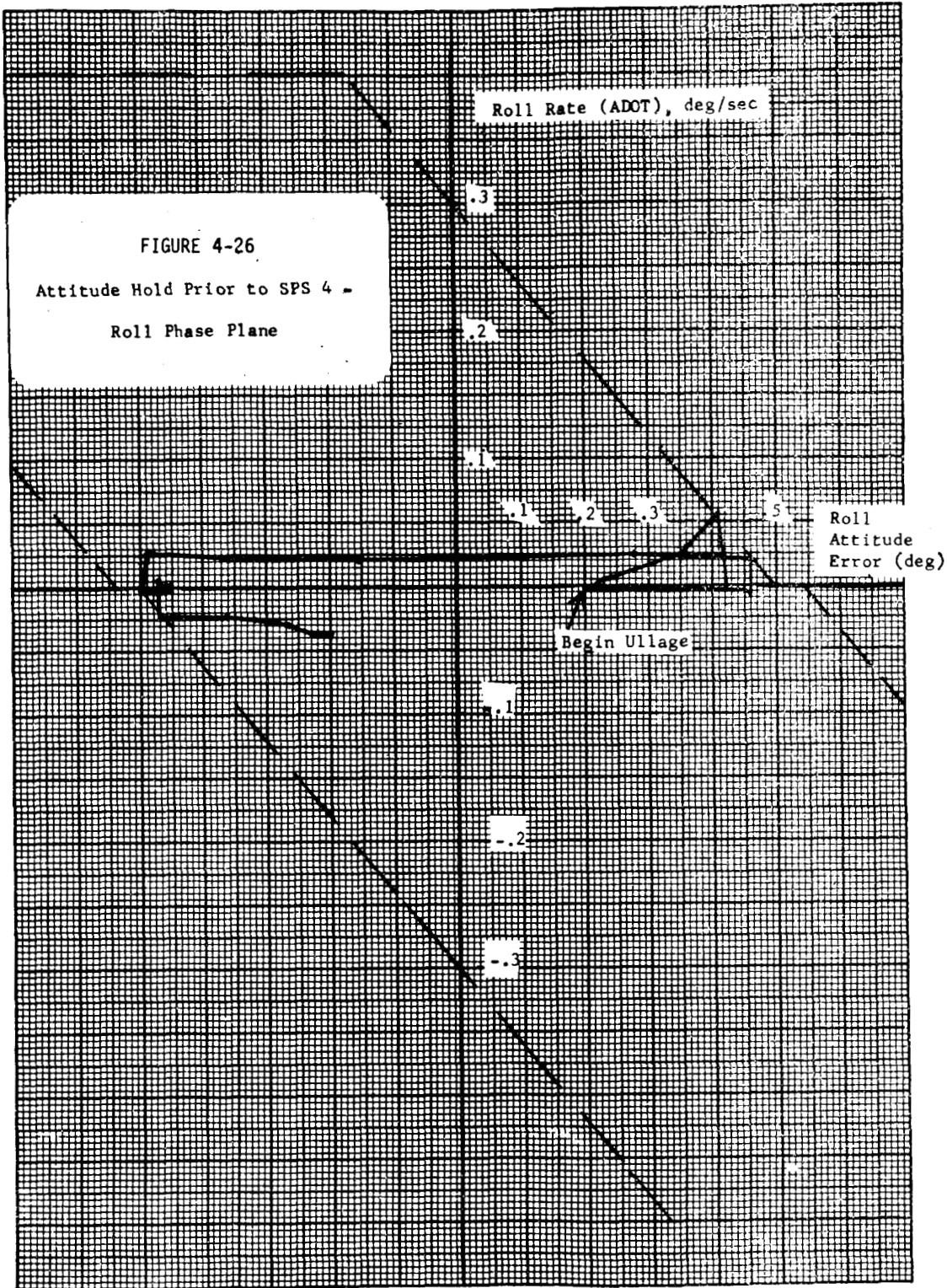


FIGURE 4-26  
 Attitude Hold Prior to SPS 4 -  
 Roll Phase Plane

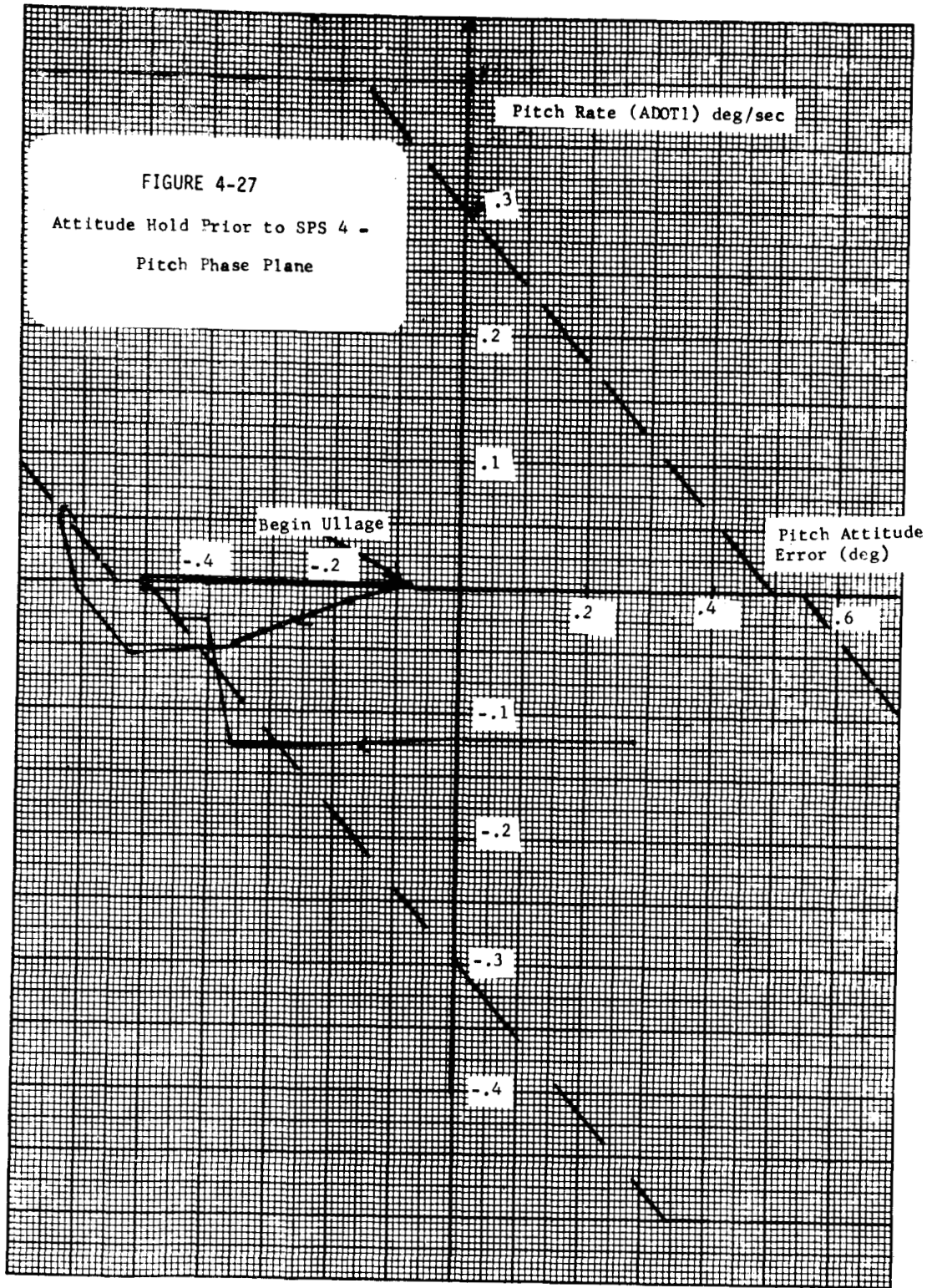
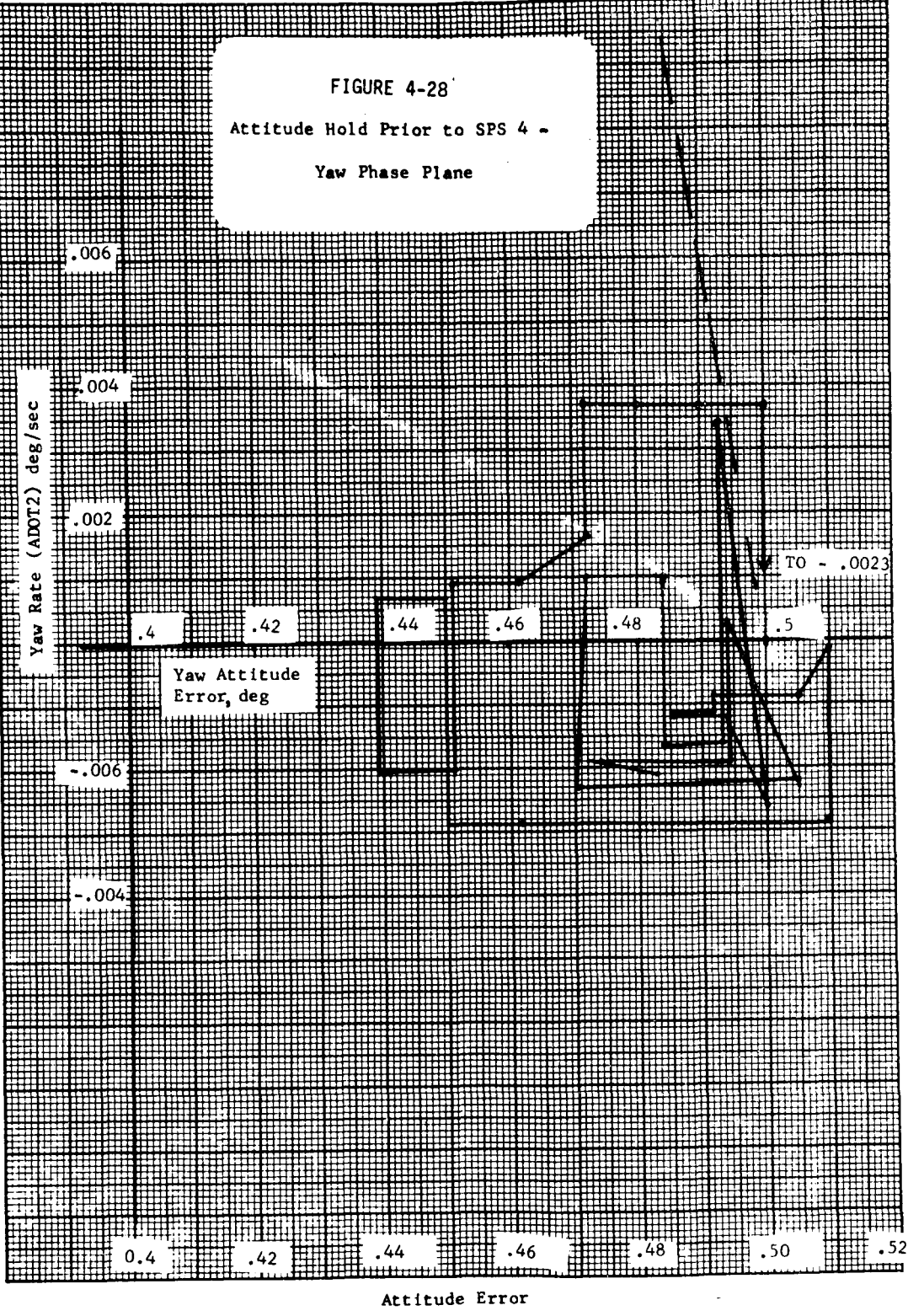


FIGURE 4-28  
 Attitude Hold Prior to SPS 4 -  
 Yaw Phase Plane



## 5.0 LM IMU PERFORMANCE

### 5.1 DPS 1 VELOCITY COMPARISON

Analysis of the LM system was based on the CSM as a standard. The LM errors were not corrected for CSM errors as determined from the ascent data for two reasons. First, in the CM/S-IVB comparison, the S-IVB errors are unknown and are thereby attributed to the CSM. Second, for the DPS burn, the average acceleration over the burn was only 0.13 g's on the LM X-axis. These two conditions lend to low confidence levels in the derived LM solution, since combinations of extremely small error sources could give a reasonable solution to the small residuals involved. Table 5.1 lists what are believed to be the major LM errors with respect to the CM for this burn. If a CSM corrected set is desired, it can be obtained by merely subtracting the CM errors from the LM errors. The exception to the above is that between ascent and DPS 1, ACBX was changed from  $-1.214 \text{ cm/sec}^2$  to zero due to an updated compensation load between the two flight phases.

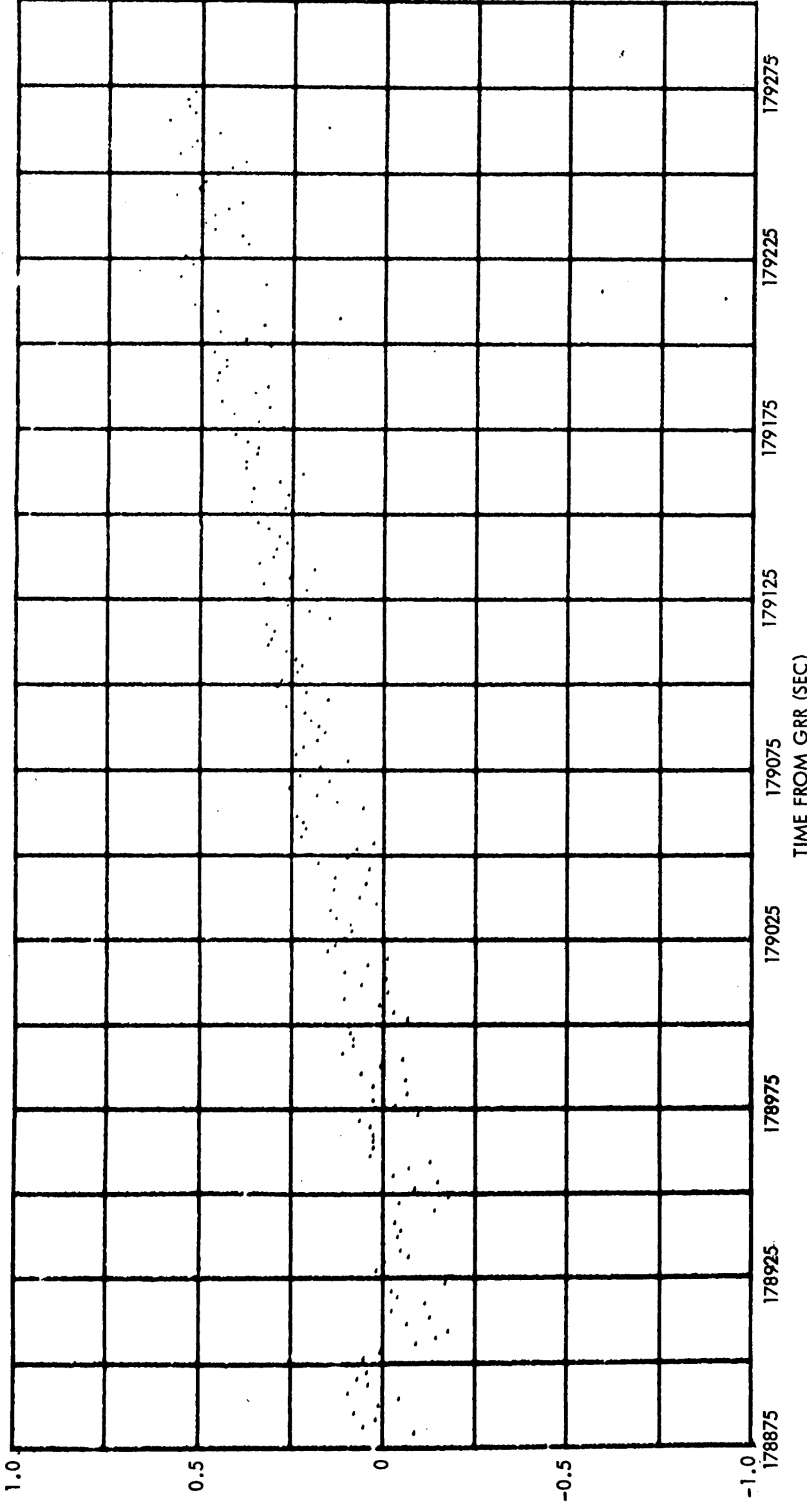
The uncompensated velocity comparisons for DPS-1 are shown in Figures 5-1 through 5-3 and the compensated residuals are shown in Figures 5-4 through 5-6, respectively.

Due to the exceptionally good fit of the derived data with respect to the expected errors, no discussion of the individual errors is necessary.

<u>Source</u>	<u>Data Mean*</u>	<u>Flight Load</u>	<u>Expected Error</u>	<u>Standard Deviation</u>	<u>Derived Error</u>	<u>Variation from Expected Error</u>	<u>Comments</u>
VOX (ft/sec)	NA	NA	NA	NA	-0.09	NA	
VOY (ft/sec)	NA	NA	NA	NA	0.44	NA	
VOZ (ft/sec)	NA	NA	NA	NA	0.06	NA	
DT (sec)	NA	NA	NA	NA	-0.013	NA	
ACBX (cm/sec <sup>2</sup> )	0.33	0.31	-0.02	0.2	0.049	0.25σ	Measured in flight
ACBY (cm/sec <sup>2</sup> )	0.037	0.10	0.063	0.2	0.043	0.22σ	Measured in flight
ACBZ (cm/sec <sup>2</sup> )	0	0	0	0.2	0.032	0.16σ	Measured in flight
SFEX (PPM)	NA	-968	0	116	17	0.15σ	
MYAZ (arc-sec)	NA	0	0	20	12	0.06σ	
MLMY (arc-sec)	NA	NA	0	65	-12	0.18σ	
MLMZ (arc-sec)	NA	NA	0	65	28	0.60σ	

\* Due to the small amount of preflight data available, the flight load was assumed as the correct data mean, except for those values which were measured in flight and the velocity offsets

Table 5.1 IMU ERROR SOURCES, LM - DPS-1



DELTA VX (FT/SEC)

Figure 5-1 LM-CSM WITHOUT  
COMPENSATION - DPS-1

TIME FROM GRR (SEC)

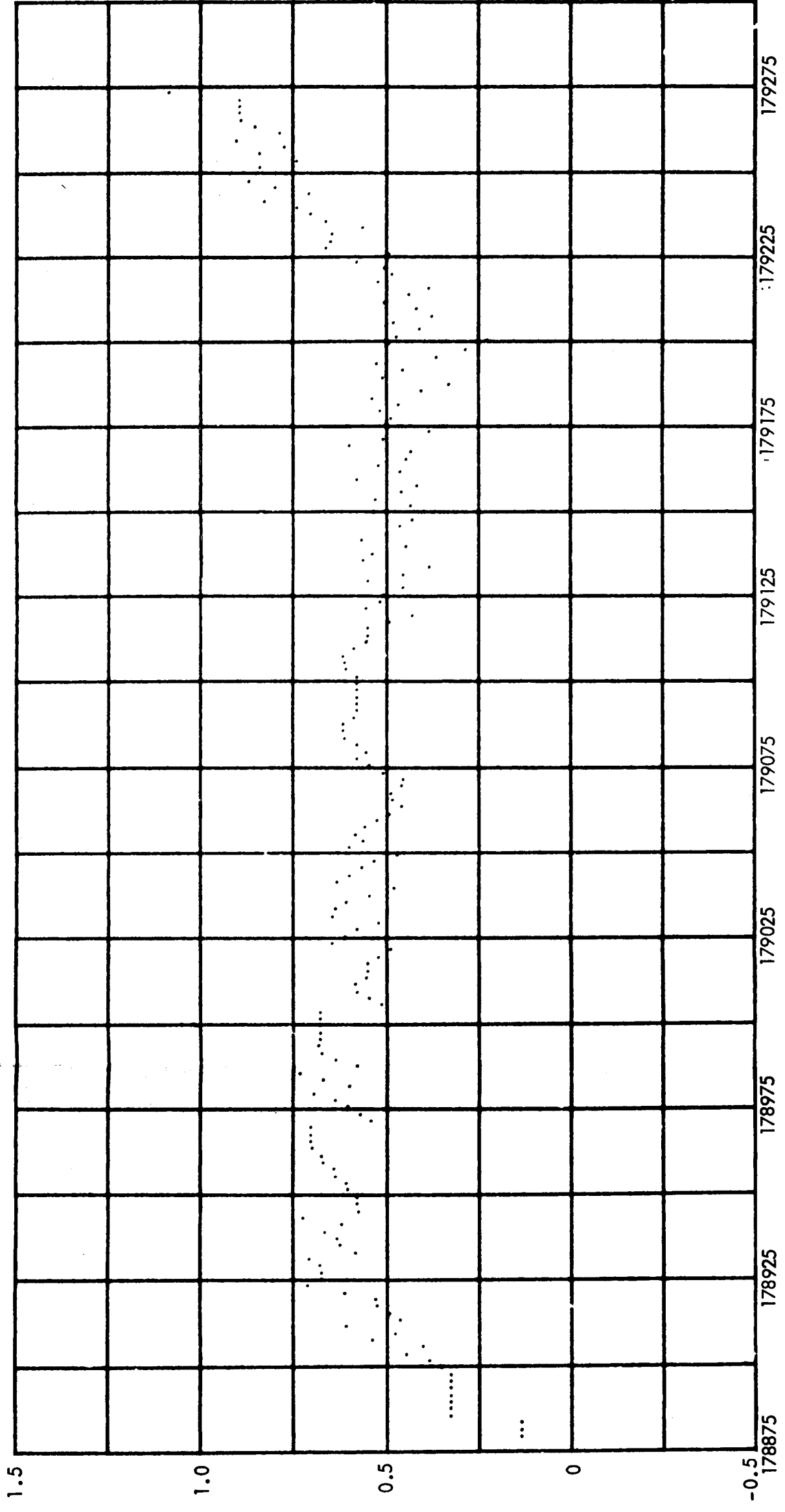


Figure 5-2 LM-CSM WITHOUT COMPENSATION - DPS-1

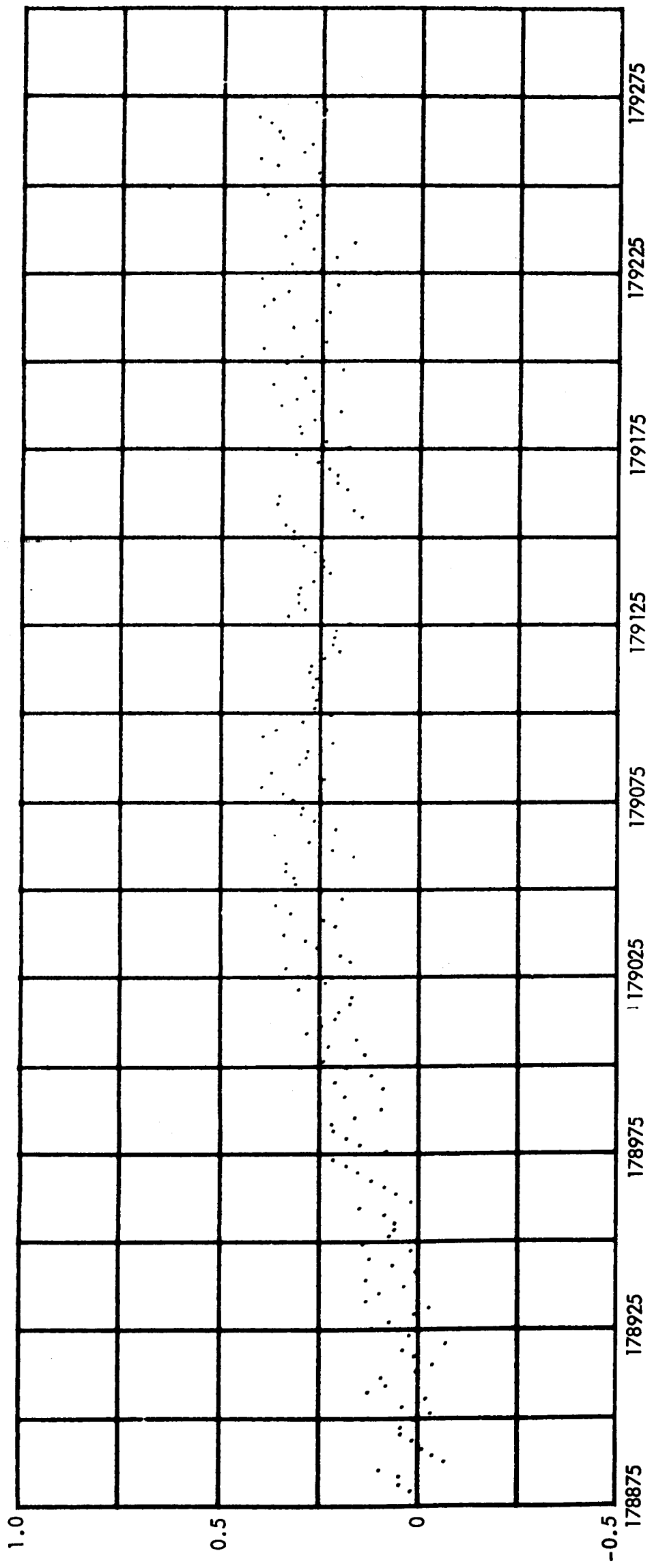
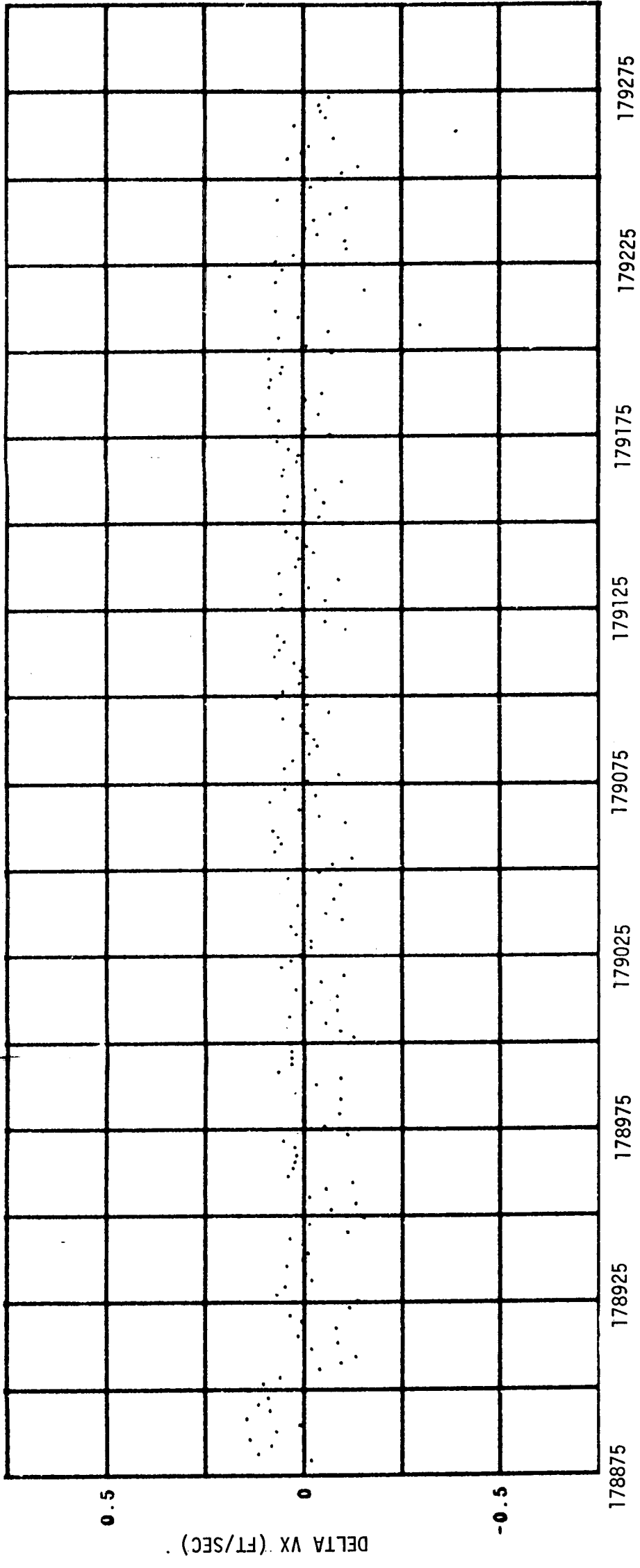


Figure 5-3 LM-CSM WITHOUT COMPENSATION - DPS-1





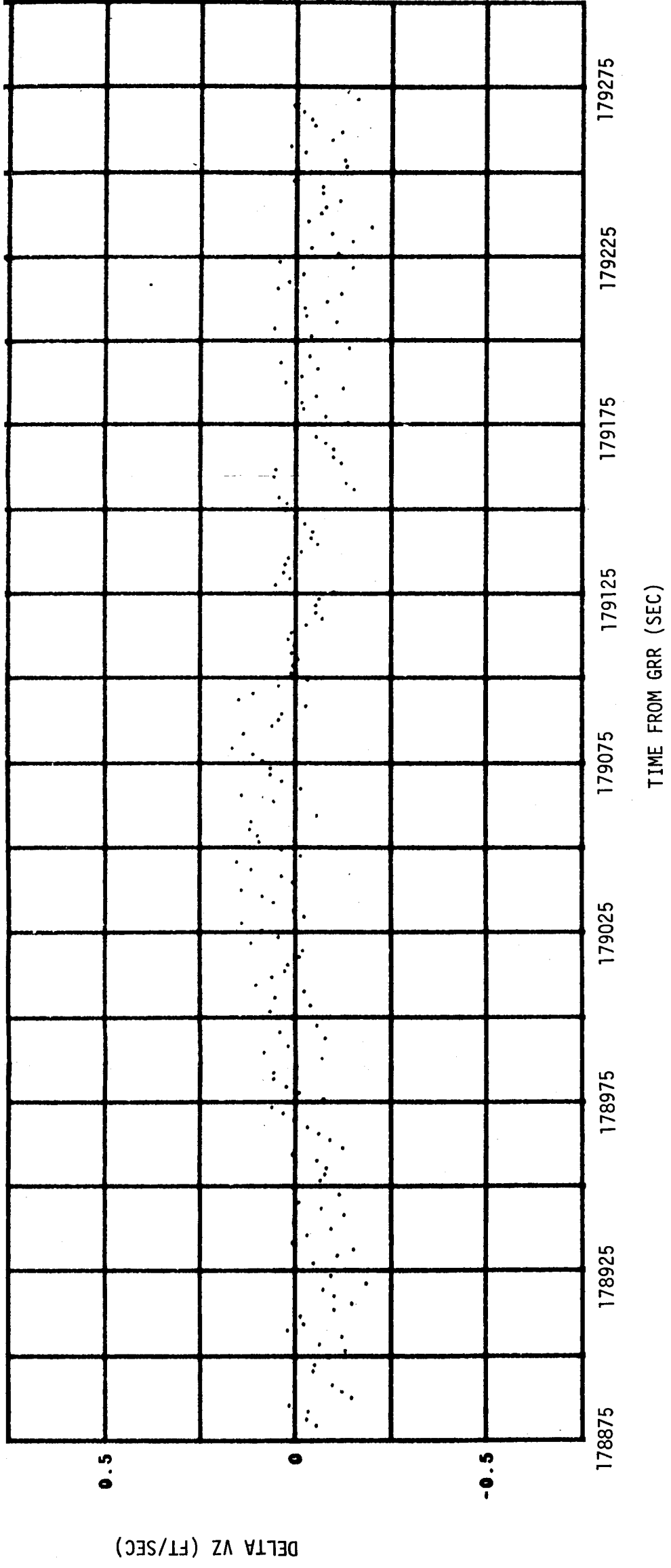


Figure 5-6 LM-CSM WITH COMPENSATION  
DPS - 1

## 6.0 LM DIGITAL AUTOPILOT

The degree of detail and accuracy of the post flight analysis of the LM DAP was dependent on the available telemetry (TM) data. An accurate analysis was not always obtained since the majority of the LGC downlink parameters used were sampled once per two second TM cycle. In some cases, maneuvers and burns were performed over areas where coverage was not available. This section discusses the three distinct configurations which the LM DAP must control, i.e.

- a) LM/CSM Docked Configuration
- b) Descent Configuration
- c) Ascent Configuration.

Automatic maneuvers, PGNCs controlled burns and periods of attitude hold were investigated for each configuration. The various modes which were analyzed were:

- a) Attitude Hold (coasting and powered flight)
- b) Manual Rate Command
- c) Automatic Maneuvers
- d) Automatic Steering.

### 6.1 LM/CSM DOCKED CONFIGURATION

The data used in the analysis of this configuration were taken from the computer words downlinked and the associated oscillograph records. The maneuver to the burn attitude and the attitude hold before and after the burn were performed by the CSM and are not included under the LM analysis.

#### 6.1.1 Docked DPS Burn

A 2-jet ullage (jets 6 and 14) was started at 49:41:25.6 and continued until 49:41:35.2. Ignition occurred at 49:41:33.0 with the manual throttle set at 11.37% of maximum throttle setting. At 49:41:45 the manual

throttle had been placed at 38% maximum setting and the automatic throttle started building up to the fixed throttle point at 49:42:0.75.

V65E was keyed in prior to ignition to inhibit the X-axis RCS jets from firing during the Docked DPS Burn. The flight directors reported during realtime monitoring the appearance of 8 or 9 rapid RCS pulses at ignition. A review of the oscillograph records and bilevel tabulations did not substantiate this observation. The observed firings must have been real time telemetry noise. One firing did occur at 59:41:31.3 which was during the period of ullage. Jets 1 and 10 (4U and 1D) came on for 0.1 sec to provide +V rotation. This firing was in accordance with the phase plane logic. Exclusive of ullage, no X-axis RCS jets were fired throughout the burn. The only RCS activity was balanced coupled 2-jet firings which produced rotations about the P-axis. All firings were 0.1 sec in duration which is a minimum impulse for the LM/CSM docked configuration. A sample of the P-axis phase plane is shown in Figure 6-1 and indicates that the firings occurred at the switching lines as planned.

Peak angular rates following the throttle-up to the fixed throttle position were quite low (0.14 deg/sec about the Q-axis and 0.2 deg/sec about the R-axis). The angular rates and attitude excursions obtained during the steady-state portion of the burn were low and less than the values predicted by preflight simulations. The peak angular rates which occurred during the throttling profile near the end of the burn were -0.35 deg/sec for the Q-axis and 0.53 deg/sec for the R-axis. Both peaks occurred at 49:47:12. These rates were within the range of 0.5 to 0.6 deg/sec which was predicted by preflight simulation. A plot of the LGC estimated rates during the throttling profile is contained in Figure 6-2. For comparison, the rates obtained from the CSM BMAG's are shown in Figure 6-3. The general agreement of the shape of the curves is very good in the two figures. The effect of slosh, which will be discussed in Section 6.1.2, very evident in Figure 6-3. This effect is not as pronounced in the estimated rates because of the filtering action of the rate estimator and the low visibility afforded

by the 1 sec TM data. Figure 6-4 contains the plots of velocities-to-be-gained in body coordinates for this burn. The burn was terminated at 49:47:45, the velocity error in the Y-axis was 3.5 ft/sec and the velocity error in the Z-axis was -1.9 ft/sec at cutoff.

### 6.1.2 Slosh

Slosh, or an effect which appeared to be slosh, was quite evident during the docked DPS burn. The Pitch, Roll and Yaw Logic Error traces (Channels GH1248, GH1249 and GH1247) oscillated quite noticeably during various portions of the burn. The oscillations were not always sustained and would appear and disappear at various times during the burn. The following table summarizes some of the more noticeable oscillations.

<u>TIME</u>	<u>AXIS</u>	<u>VEHICLE WEIGHT</u>	<u>FREQUENCY</u>
49:44:29	Roll	57579 1b	0.39 H <sub>Z</sub>
49:44:40	Yaw	57227 1b	0.37 H <sub>Z</sub>
49:46:7.5	Pitch	54411 1b	0.41 H <sub>Z</sub>
49:46:7.5	Roll	54411 1b	0.40 H <sub>Z</sub>
49:46:20.0	Pitch	53990 1b	0.41 H <sub>Z</sub>
49:46:20.0	Roll	53990 1b	0.41 H <sub>Z</sub>
49:46:20.0	Yaw	53990 1b	0.40 H <sub>Z</sub>

The above mentioned oscillations did not show up in the LM analog rate traced on the oscillograph records, but this is probably due to the scaling. The oscillations are very noticeable in the CSM rate traces contained in Figure 6-3. The frequency of the oscillations in Figure 6-3 is 0.4 H<sub>Z</sub> before the throttling profile was started. Very slight oscillations were observed in the Gimbal Drive Actuators (Channels GH1313 - Pitch and GH1314 - Roll) during the periods in which the logic error traces oscillated. For instance, the frequency of oscillation of the Roll GDA at 49:46:7.5 was 0.4 H<sub>Z</sub>. The oscillations of the Roll GDA were in phase with the pitch logic oscillations and were 180 degrees out of phase with the roll logic oscillations.

Theoretical calculations were made in an attempt to identify the presence of slosh. Based on the acceleration of the vehicle and the percentage of fuel left, the calculated frequency of slosh for the DPS tanks varied between 0.355 Hz and 0.358 Hz. The theoretical frequency of slosh for the APS tanks was 0.6 Hz, but at this time the APS tanks were full and would not cause the oscillations. The theoretical slosh frequency for the CSM fuel and oxidizer tanks was 0.36 Hz based on the amount of fuel remaining after SPS 4 and the acceleration obtained during the Docked DPS burn. The theoretical slosh masses were calculated and are tabulated below.

	<u>Fuel</u>	<u>Oxidizer</u>
CSM after SPS 4	150.0 kg	237.0 kg
LM with 0.714% fuel left	336.9 kg	536.2 kg
LM with 0.690% fuel left	336.9 kg	536.2 kg
LM with 0.53% fuel left	331.3 kg	527.3 kg
LM with 0.509% fuel left	328.9 kg	523.4 kg

A review of the first four SPS burns did not show any strong evidence of slosh. However, the SPS 5 burn which followed the Docked DPS burn did show evidence of an oscillation of 0.5 Hz. This turns out to be the theoretical slosh frequency of the DPS tanks at this time.

In the SUNDANCE preflight software verification testing, runs were made for the docked DPS burn with and without slosh modeling. For the cases in which slosh was modeled, the gimbals were observed to oscillate with a frequency of 0.357 Hz. The frequency of oscillation of the gimbals for the cases without slosh were roughly 0.22Hz. Thus, it seems safe to assume that the oscillations of the rate and logic error traces were caused by slosh and not by the Gimbal Trim System. The maximum peak-to-peak amplitude of 0.4 deg/sec of the rate oscillations in Figure 6-3 agreed with preflight simulation results.

### 6.1.3 Compliance

The Pitch and Roll Gimbal Drive Actuator positions (Channels GH1313 and GH1314) along with the engine throttle profile are plotted in Figure 6-5 for the beginning and end of the docked DPS burn. At about 49:42:09 the GDA's appeared to have reached steady-state positions. Using the formulas in Reference 1 which relates GDA position in inches to equivalent engine bell rotation, one obtains the following steady-state trim positions:

Pitch = -0.0276 deg

Roll = -1.525 deg

The theoretical trim values based on the mass property data contained in Reference 2 are:

Pitch = -0.421 deg

Roll = -1.218 deg

This amounts to an average difference between actual and theoretical trim of about 0.35 deg.

It was very noticeable that the gimbal drive actuators did not show significant activity following the automatic throttle-up to the fixed throttle position (FTP), i.e., the majority of compliance effects occurred between zero and 40% of FTP. Compliance is presently being modeled as a linear thrust misalignment and the above mentioned fact does not correlate with this model. Also, the peak-to-peak excursions of the GDA's, obtained during the throttling profile at the end of the burn, were approximately midway between the corresponding values obtained from preflight simulations in which compliance was and was not modeled. Further investigations should be conducted to determine the exact nature of compliance.

## 6.2 DESCENT CONFIGURATION

Two burns were performed in the descent configuration during the Apollo 9 mission. The first, the DPS Phasing Burn, was performed under AGS control and is discussed in Section 7. The second burn which was the

DPS Insertion Burn is discussed below. No TM coverage was available for the automatic maneuvers to the burn attitudes.

#### 6.2.1 DPS Insertion Burn

Ullage was initiated at 95:39:0.628 for the insertion burn and continued until 95:39:9.138. During this period, several U, V jet firings occurred for attitude control as required by the phase plane logic. Numerous 1 and 2-jet firings occurred throughout the burn which were required for attitude control. The angular rates and attitude errors throughout the burn were of the order expected based on pre-flight simulations. The peak angular rates about the U and V axes were 1.18 deg/sec and -0.67 deg/sec, respectively. The peak attitude errors for both axes were less than 11.7 degrees. Figure 6-6 contains a plot of the U-axis attitude error and the associated U-axis RCS jet firings. The deadband for the Insertion Burn is one degree and it can be observed that the firings generally occur during the periods in which the attitude error exceeds  $\pm 1$  degree. The lack of high frequency data prevents an exact investigation of the P and V-axes respectively. The time period covered by plots 6-7 and 6-8 includes ullage, the Insertion Burn and a portion of the nulling of the residual velocities. A plot of the velocity-to-be-gained from the Insertion Burn is contained in Figure 6-9.

Figure 6-10 presents a time history of the gimbal drive actuators for the Insertion Burn. The frequency of oscillation of both of the GDA's is 0.2 Hz. The theoretical slosh frequency for the conditions existing during this burn is 0.18 Hz. A review of the LM rate traces on the oscillograph records revealed oscillations in the pitch and roll axes of 0.2Hz. As before, there seems to be a good correlation between the calculated slosh frequency and the observed rate oscillations.

Preliminary analysis indicated that the thrust buildup for the Insertion Burn had been very slow and that the change in velocity over a two second period just managed to exceed the threshold value on the last pass through the  $\Delta V$  Monitor. A detailed review of the TM data revealed that the  $\Delta V$  for the first pass through the  $\Delta V$  Monitor was 11 cm/sec, 12 cm/sec for the second pass, and 105 cm/sec for the fourth pass. Due to a data dropout, the information on the third pass was not available. The required threshold of 36 cm/sec after four passes was therefore certainly exceeded with ease after the fourth pass. Whether or not the threshold was exceeded on the third pass cannot be determined due to the lack of data.

### 6.2.2 Attitude Hold

Figures 6-11, 6-12 and 6-13 contain phase plane plots for the P, U and V-axes for a period of attitude hold for the unstaged configuration just prior to the DPS Insertion Burn. At this point, the deadband was set to one degree which is the powered flight deadband. The digital autopilot functioned properly in the attitude hold mode and the phase planes were as expected. The presence of an external disturbing torque about the V-axis is evident in Figure 6-13. The exact nature of the disturbing torque is not known at this time. Further investigations will be carried out in this area.

## 6.3 ASCENT CONFIGURATION

The LM was staged at the beginning of the CSI Burn and the remaining rendezvous sequence was performed with the ascent configuration. After docking with the CSM, the crew transferred to the CSM and an unmanned APS Burn to depletion was performed. The analysis of the ascent configuration includes two burns, an automatic maneuver, a period of attitude hold and a period during which manual control was exercised.

### 6.3.1 Automatic Maneuver

Data covering the automatic maneuver to the CDH Burn attitude was received by the HTV Station on Rev 61. The maneuver was performed at 2.0 deg/sec with commanded rates about the Q and R axes. Figure 6-14 is a plot of the commanded and LGC vehicle rates about the P, Q and R-axes.

The figure shows a slight rate overshoot in the Q and R-axes, but the overall rate performance was satisfactory. The rate overshoot is characteristic of the rate estimator and was anticipated based on preflight simulations. Figure 6-15 illustrates the CDU angles during the maneuver. The CDUXD, CDUYD and CDUZD are the final desired ball angles and the plots indicate that the automatic maneuver provided the appropriate vehicle rotation.

### 6.3.2 Attitude Hold

Figures 6-16, 6-17 and 6-18 contain phase plane plots of a period of attitude hold for the ascent configuration immediately following the APS Burn to depletion. The APS Burn was terminated by the  $\Delta V$  Monitor when low thrust was detected. The programmed guidance equations reset the deadband to the astronaut specified value (5 degrees in this case) and automatically requested an ullage. The burn programs were recycled back to the TIG-5 program and remained there in a 5 degree deadband until an "ENTER" was received (i.e., ullage was terminated and re-ignition was not requested). After receiving a "PROCEED", the attitude errors were zeroed and the deadband was set to 0.3 deg by the APS burn program P42. Exit from P42 placed the deadband back at 5 deg. The DAP functioned properly during this period and the phase planes were as expected. The transition from the 5 deg deadband to the 0.3 deg deadband was very smooth and can be observed in the above mentioned figures.

### 6.3.3 Manual Control

Eight minutes of data received by BDA Rev 63 were analyzed during a period just prior to docking. The DAP was in a 0.3 degree deadband attitude hold mode, but there was a profusion of RHC and TTCA activity at this time. Figures 6-19, 6-20 and 6-21 present phase plane plots during this period of the docking sequence. The figures indicate that the DAP was nulling the rates and maintaining a 0.3 degree attitude deadband after the release of the RHC or TTCA. The dashed lines in the figures indicate rate and attitude errors induced by RHC activity.

The other attitude excursions were caused by TTCA activity. The theoretical rate changes for each axis (P, U, V) during a minimum impulse limit cycle are 0.1 deg/sec for this configuration. The observed rate changes were of this order of magnitude whenever there was no RHC or TTCA activity.

#### 6.3.4 CSI Burn

+0.5  
The data for the CSI Burn was received by TAN on Rev 61. This was a 4-jet RCS PGNCS controlled burn. The 4-jets (jets 2, 6, 10 and 14) were turned on at 96:16:6.5 and the burn was terminated at 96:16:38.2. The phase planes presented in Figures 6-22, 6-23 and 6-24 include the periods of attitude hold prior to the CSI burn, the burn, and the nulling of residual Vg's following the burn. The phase planes show that, in general, the DAP was holding the appropriate deadband (1.1 deg = 0.3 narrow deadband + 0.8 deg "FLAT"). The spikes in rates are a result of the X and Z axes translations following the burn. Shortly after the burn started, jets 6 and 10 began toggling on and off to provide attitude control about the U and V-axes (jet 6 turning off produced a +U rotation and jet 10 turning off produced a -V rotation). Due to the position of the cg, the angular errors remained at the deadband limits for the duration of the burn.

Figure 6-25 presents a time history of the velocity-to-be-gained for the CSI burn. The velocity errors at cutoff in the X, Y and Z-axes were 1.003, 0.04 and -1.361 ft/sec respectively.

#### 6.3.5 APS Burn to Depletion

The APS Burn to depletion was investigated based on downlinked computer words received by Texas on Rev 64. Once again, the burn was very much as expected based on preflight simulations. The ullage before this burn was about 32 sec long. The normal sequence is for ullage to come on 3.5 sec before ignition. The crew, after observing

a buildup of velocity, would key in "Proceed" sometime during this 3.5 sec period and ignition would occur as planned. In this case, the "Proceed" (V33E) had to be keyed in by telemetry and was somewhat delayed. Once the V33E was received, ignition occurred and the burn proceeded as planned.

During the burn, the peak angular rates about the Q and R-axes were of the order of  $\pm 5.0$  deg/sec. This compares favorably with the predicted rates of 5.0 to 6.0 deg/sec. The larger angular error excursions were of the order of  $\pm 2.5$  deg which again agrees with preflight simulations. The limit cycle frequency was calculated during a steady state portion of the burn (101:57:43). The observed limit cycle frequency was  $0.37 \text{ Hz}$  for the pitch axis (Q-axis) and  $0.375 \text{ Hz}$  for the roll axis (R-axis). Theoretical calculations based on the existing offset accelerations predict a limit cycle frequency of  $0.35 \text{ Hz}$  for the Q-axis and  $0.38 \text{ Hz}$  for the R-axis. Early in the flight (101:53:30), the limit cycle frequency was  $0.36 \text{ Hz}$  for the pitch axis and  $0.75 \text{ Hz}$  for the roll axis.

Figure 6-26 is a phase plane plot of a steady state portion of the APS burn. The original intent of the plot was to trace out the shape of the limit cycle trajectory by plotting a sufficient number of points. However, due to the limit cycle frequency and low data sampling frequency, a good outline of the limit cycle shape could not be obtained. The dashed line of this figure shows an approximate limit cycle trajectory. The plot does show that, on a qualitative basis, the results lie within a range consistent with preflight simulation results.

Figures 6-27 and 6-38 are plots of short segments of the UERROR and VERROR, respectively, during the APS burn to depletion. Also plotted are the U-jet and V-jet firings. The jet-firing history is available at 10 msec intervals while the LGC attitude error data is available only at one-second intervals. In general, the attitude errors corroborate the jet firings. It should be noted that the attitude deadband (one degree) is not a constant, but is a function of angular rate (see the switching curves in Figure 6-26).

The cross-coupling between the control axes described in Section 2.1.1 of Reference 3 was evident during this burn. A long firing of jet 10 would be followed by a firing of jet 6, during which there would be another short firing of jet 10. This extra firing of jet 10 resulted from the acceleration coupled into the V-axis from jet 6 (which produces a U-axis torque) during the period when the V-axis limit cycle was in its "coast" phase. It should be noted that these extra firings were against the offset acceleration and did not represent an inefficient use of fuel.

The termination of the burn and subsequent coasting phase of this burn were covered in Section 6.3.2 of this report.

-0.5

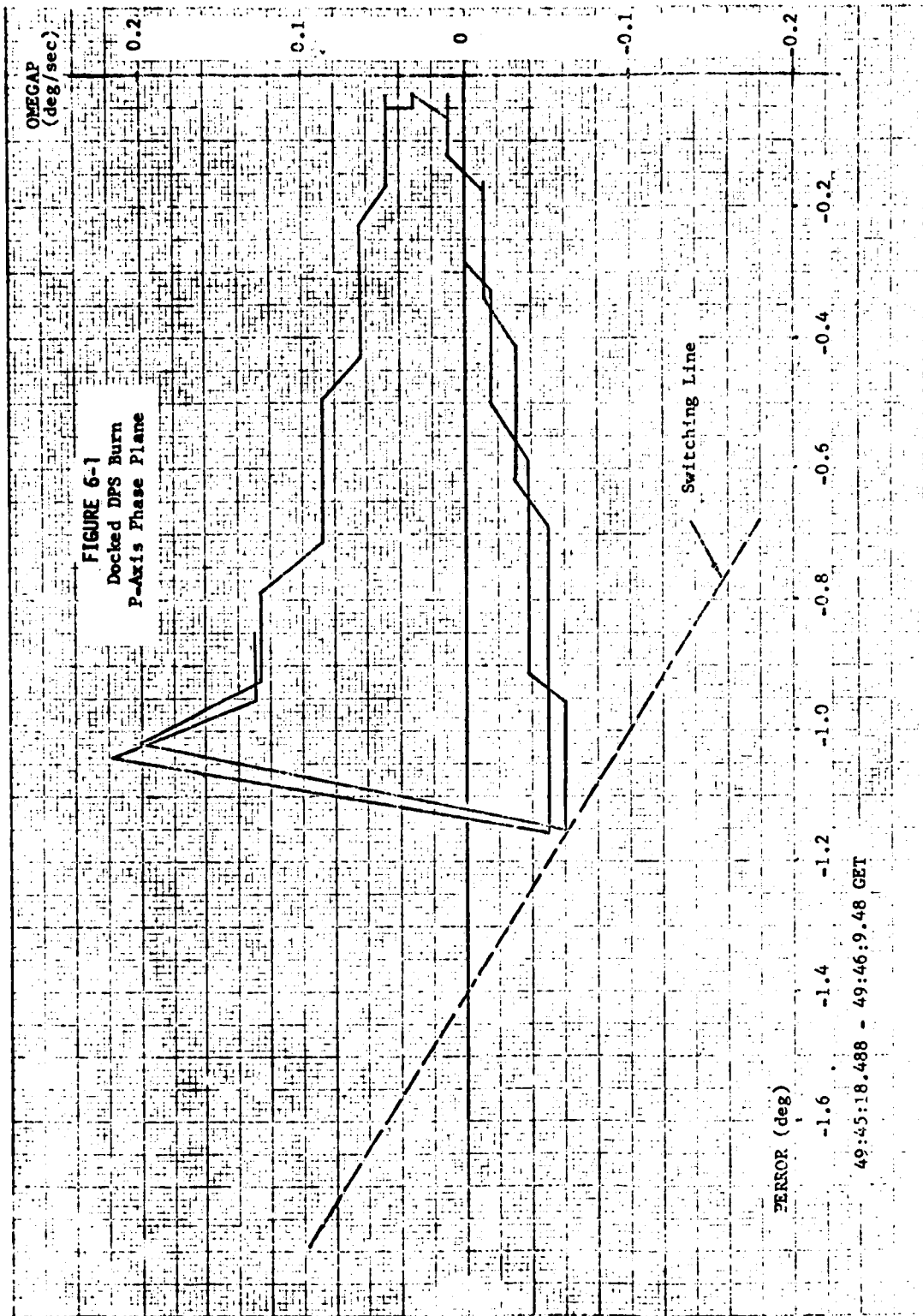
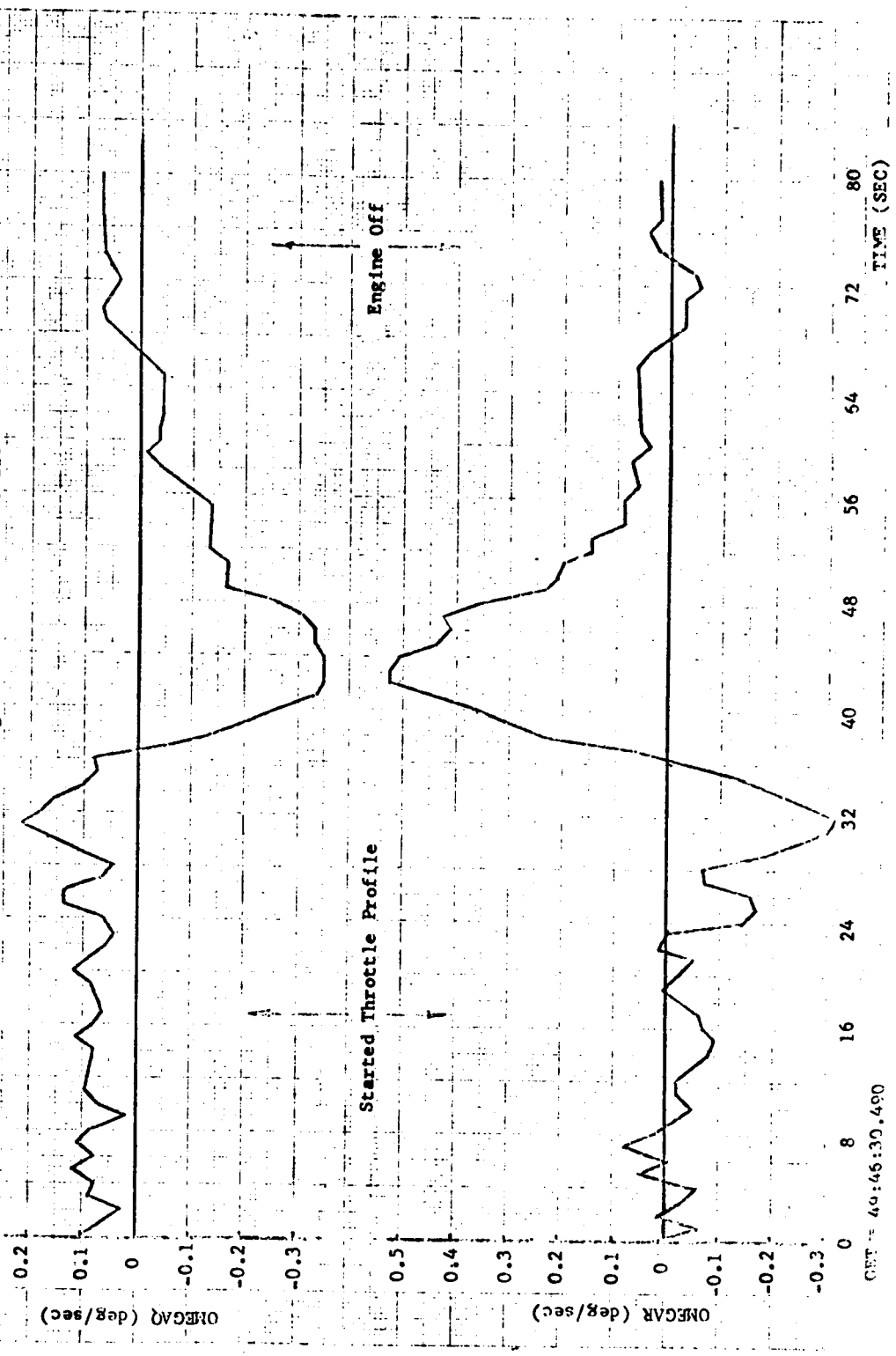


FIGURE 6-2  
LCC Angular Rates vs Time During Manual Throttle Profile



CET 46:46:30.480

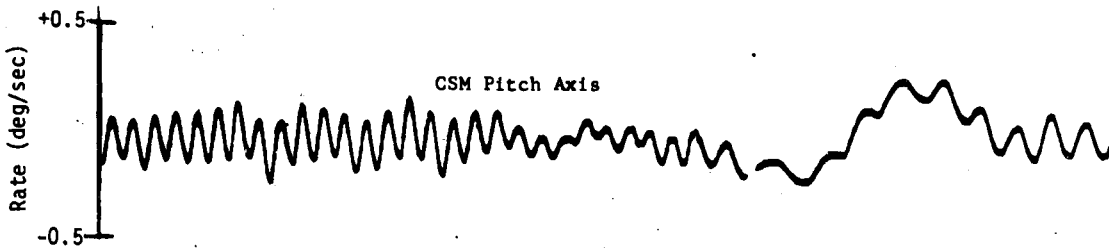
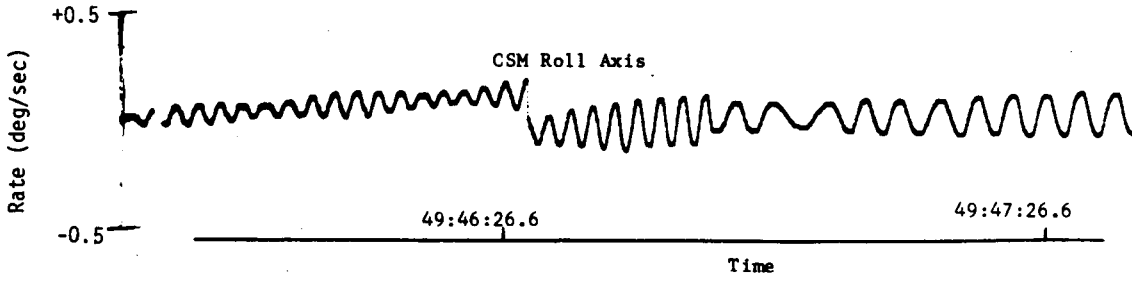
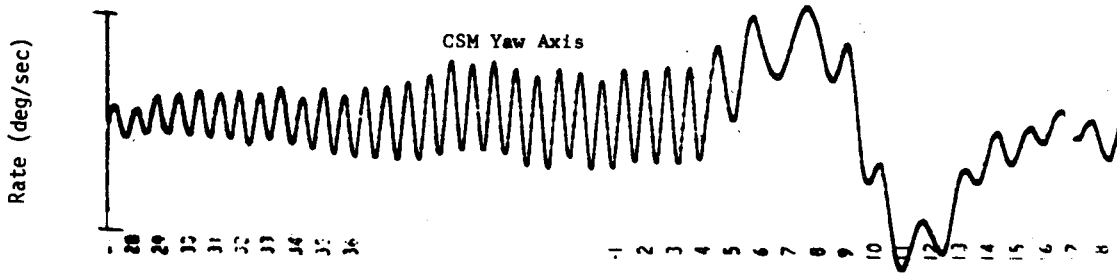
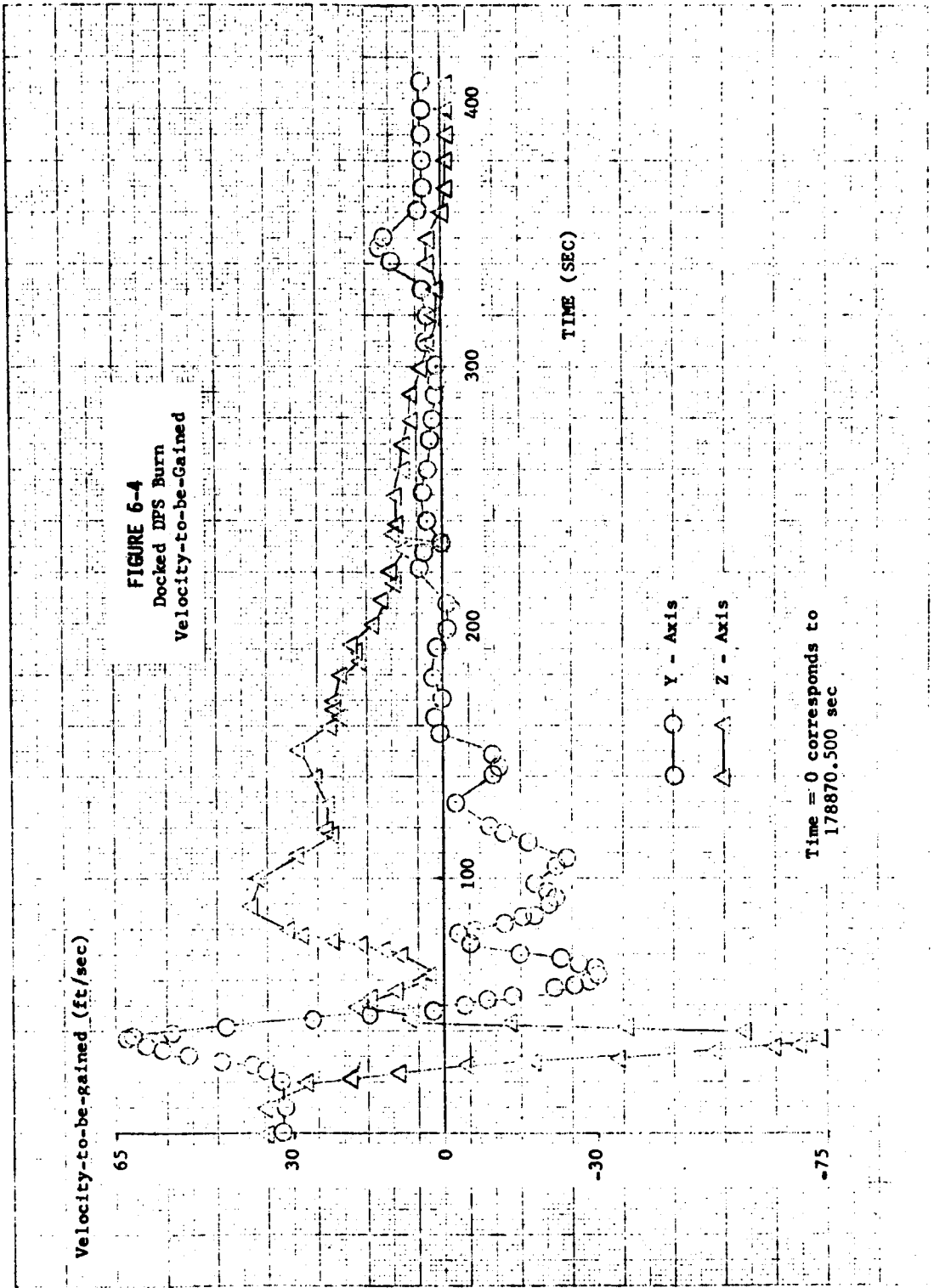
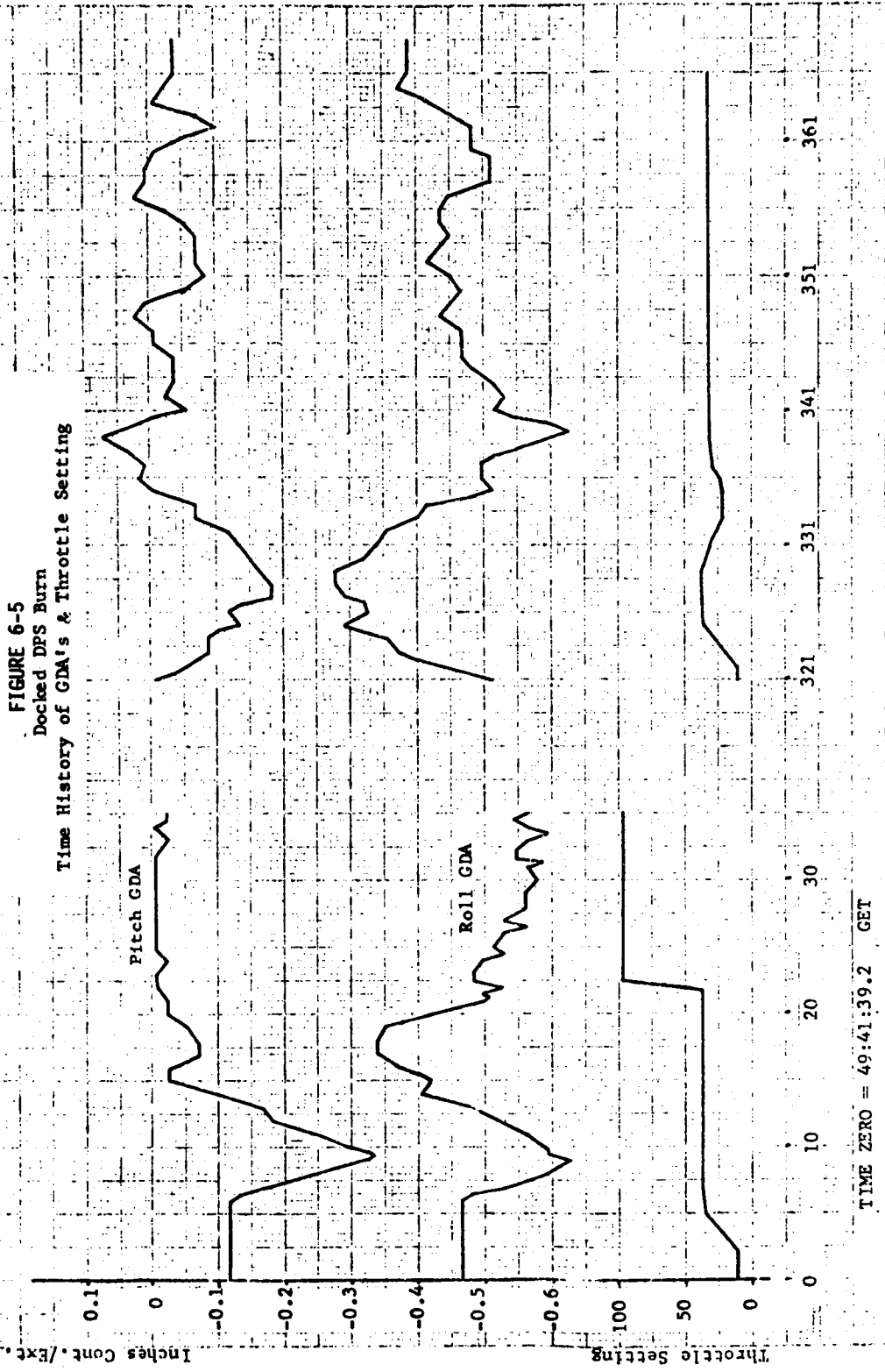


Figure 6-3  
 Docked DPS Burn  
 CSM BMAG Rates



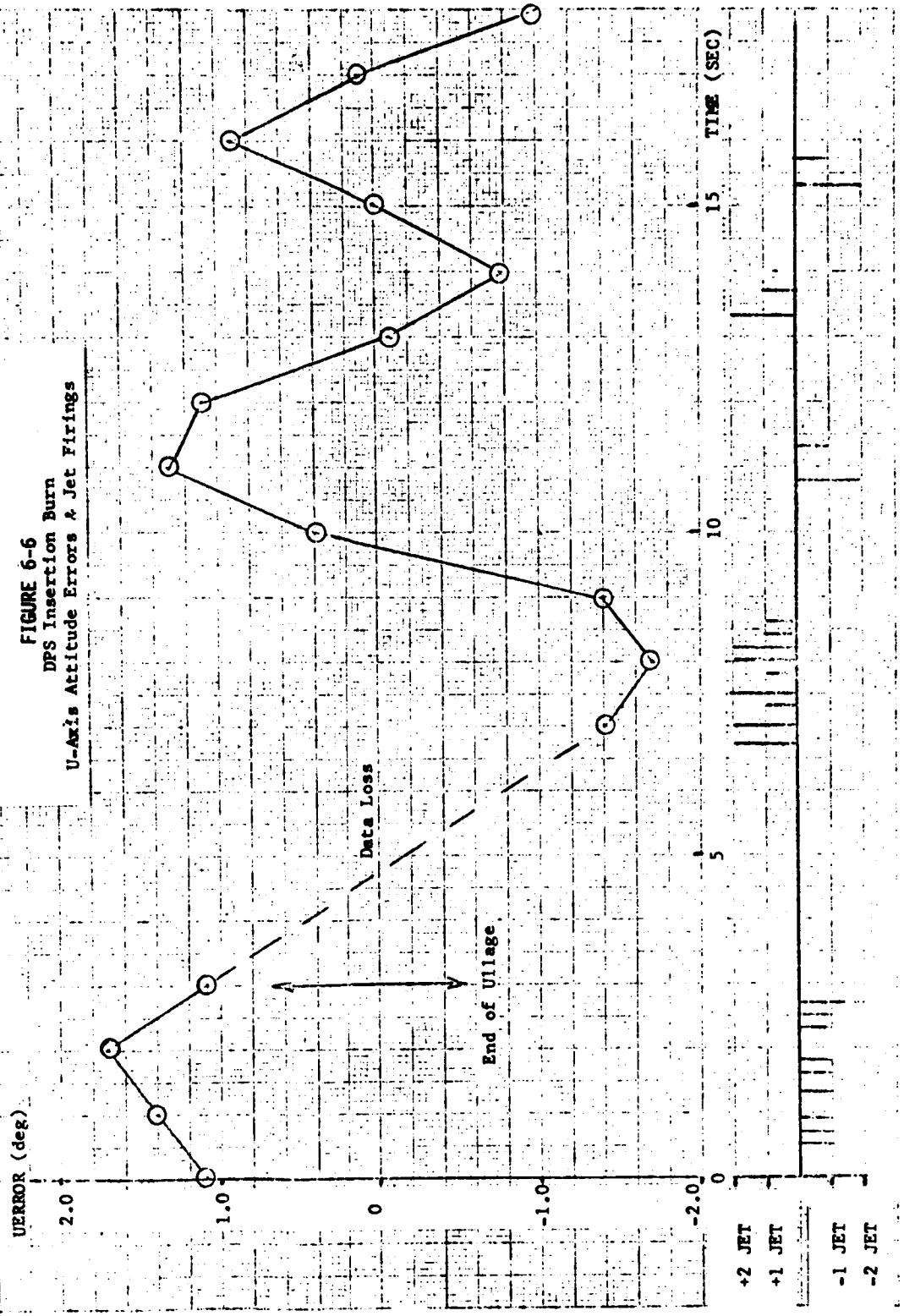


**FIGURE 6-5**  
**Docked DPS Burn**  
**Time History of GDA's & Throttle Setting**



TIME ZERO = 49:41:39.2 GET

**FIGURE 6-6**  
**DPS Insertion Burn**  
**U-Axis Attitude Errors & Jet Firings**



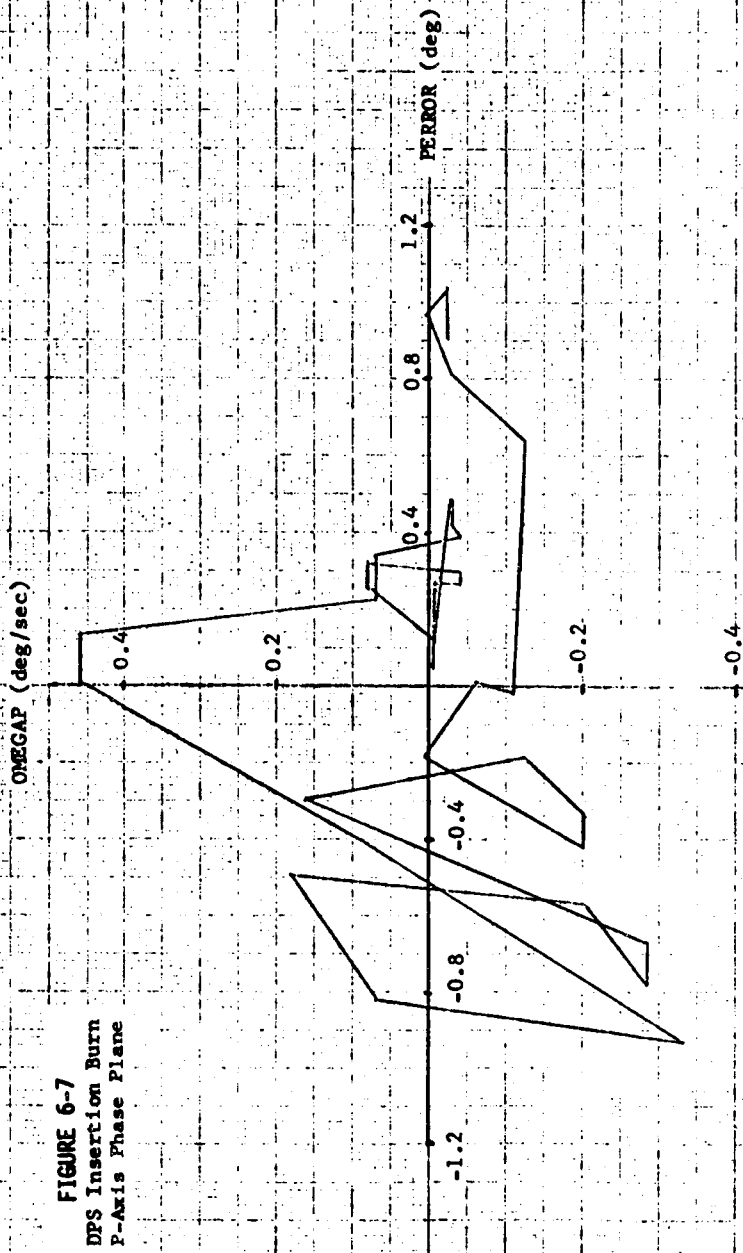


**FIGURE 6-7**  
 DPS Insertion Burn  
 P-Axis Phase Plane

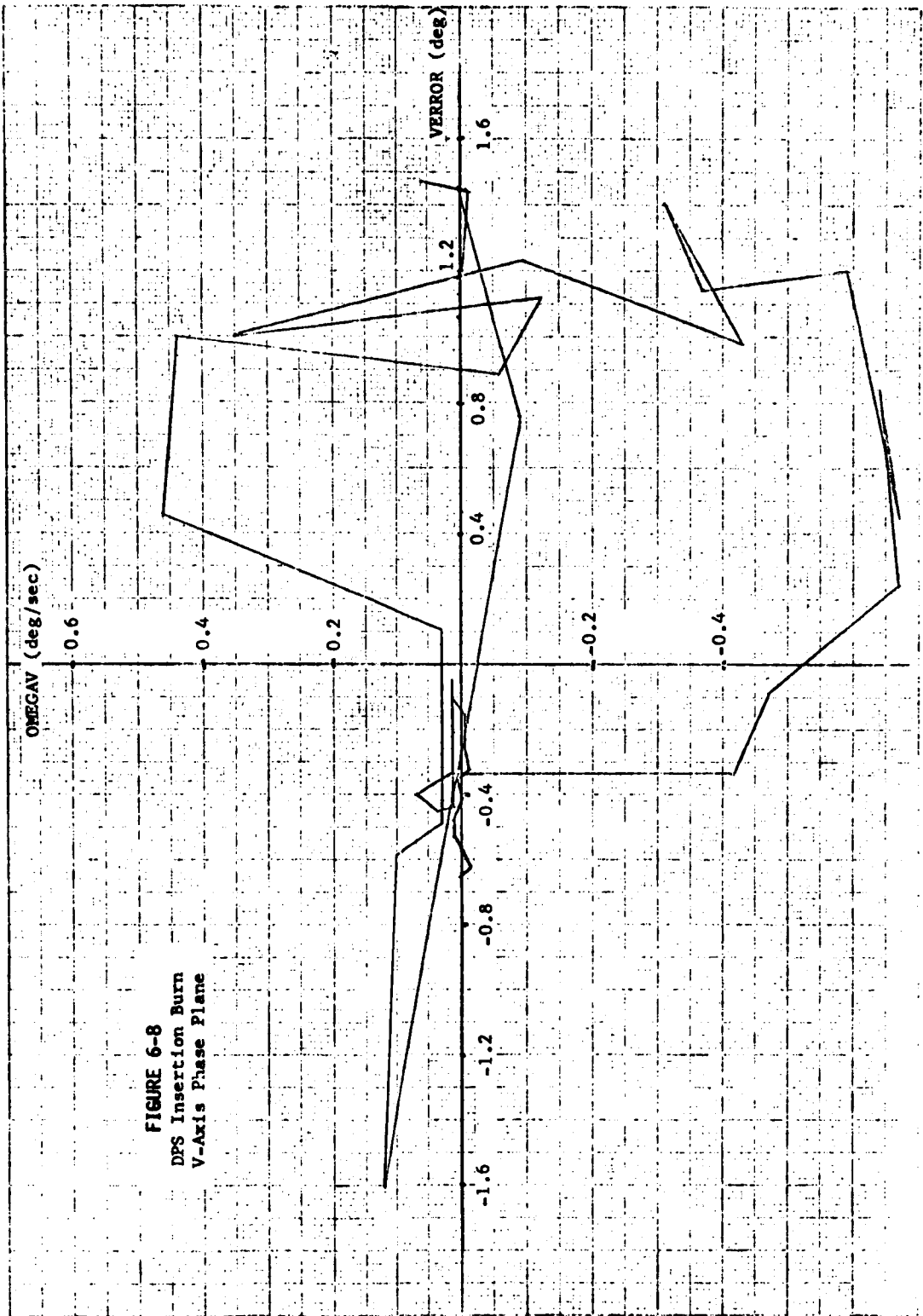


**FIGURE 6-8**  
 DFS Insertion Burn  
 V-Axis Phase Plane

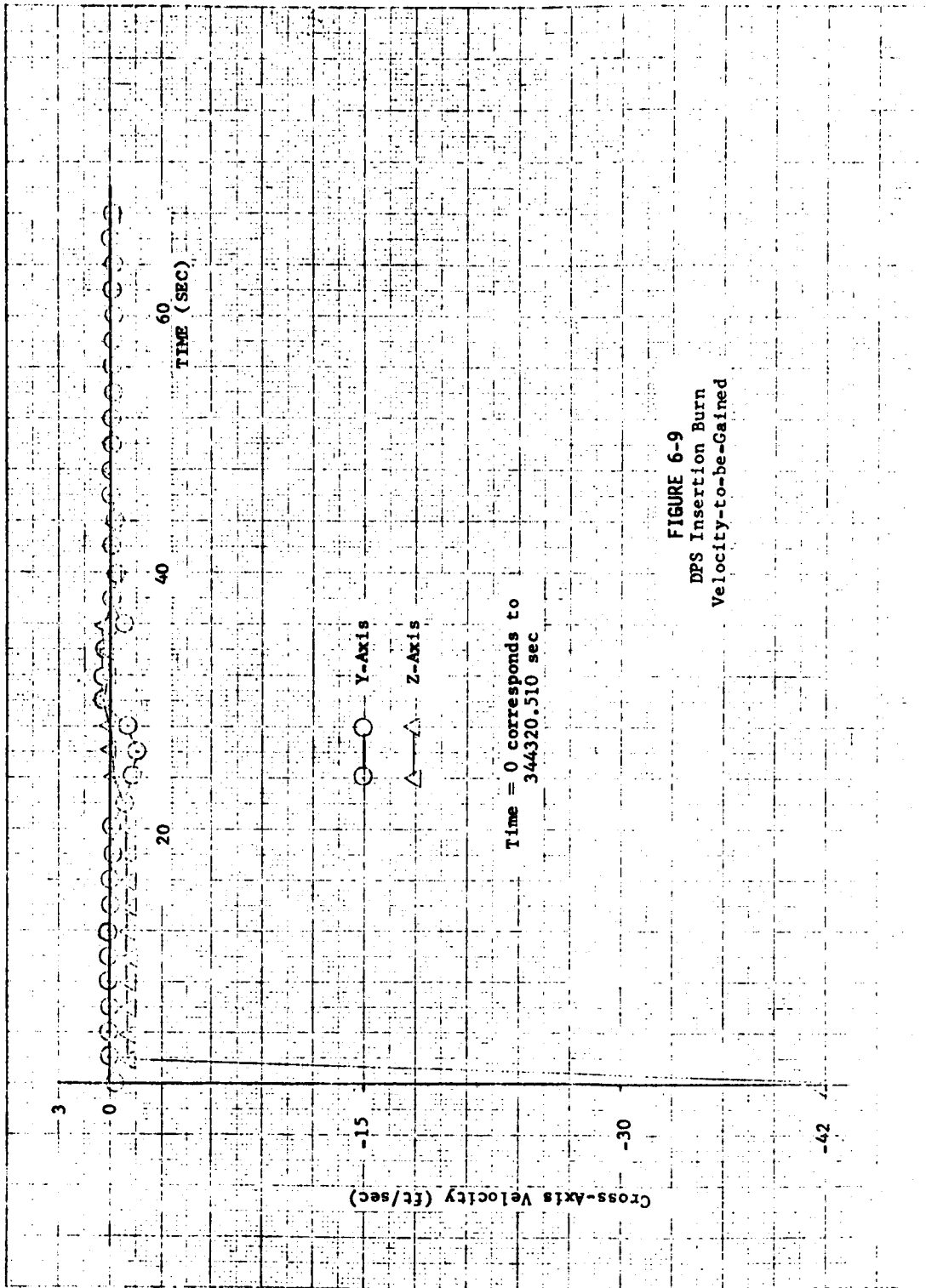


FIGURE 6-9  
DFS Insertion Burn  
Velocity-to-be-Gained

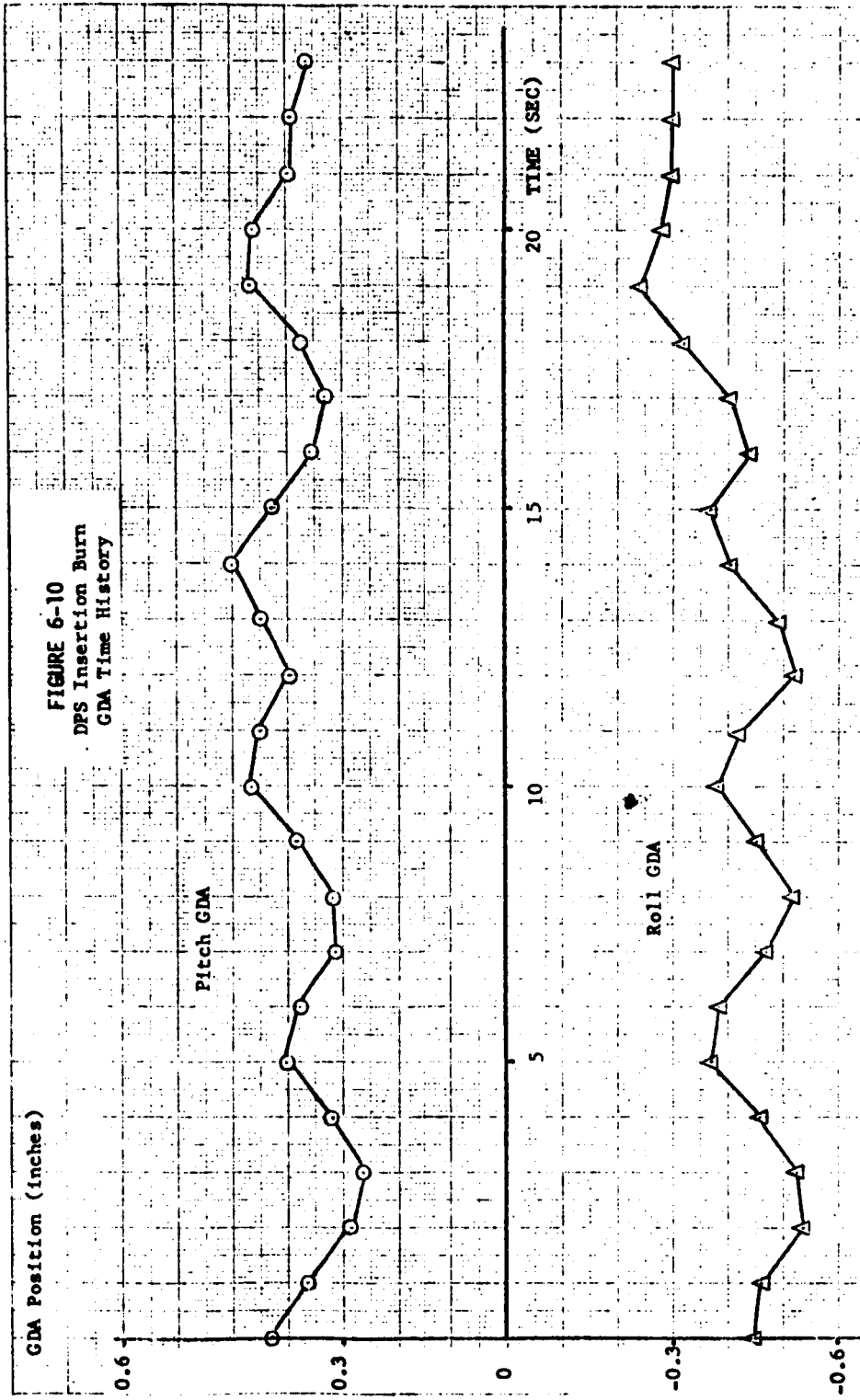


FIGURE 6-11  
Descent Configuration-Att. Hold  
P-Axis Phase Plane

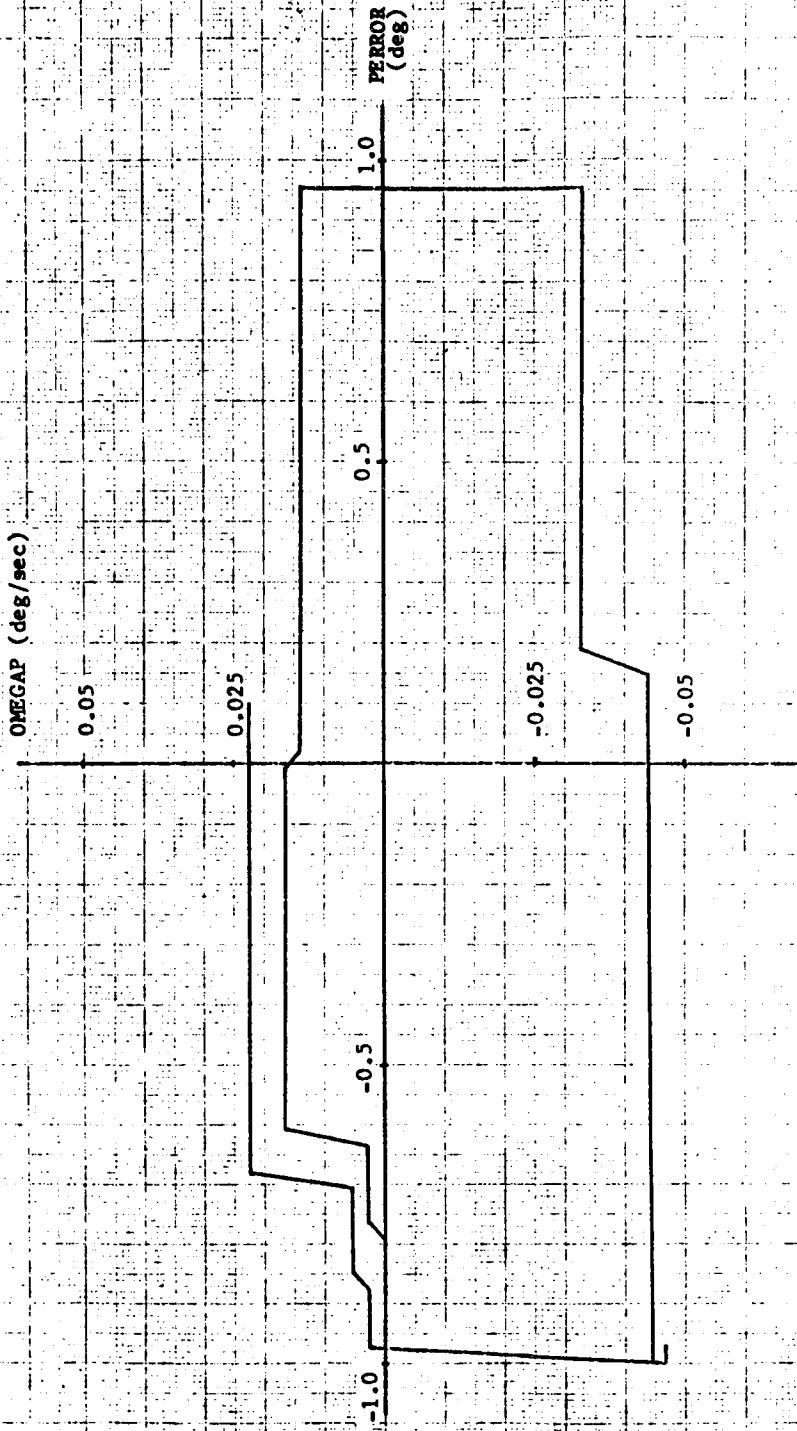




FIGURE 6-13  
 Descent: Configuration-Att. Hold  
 V-Axis Phase Plane

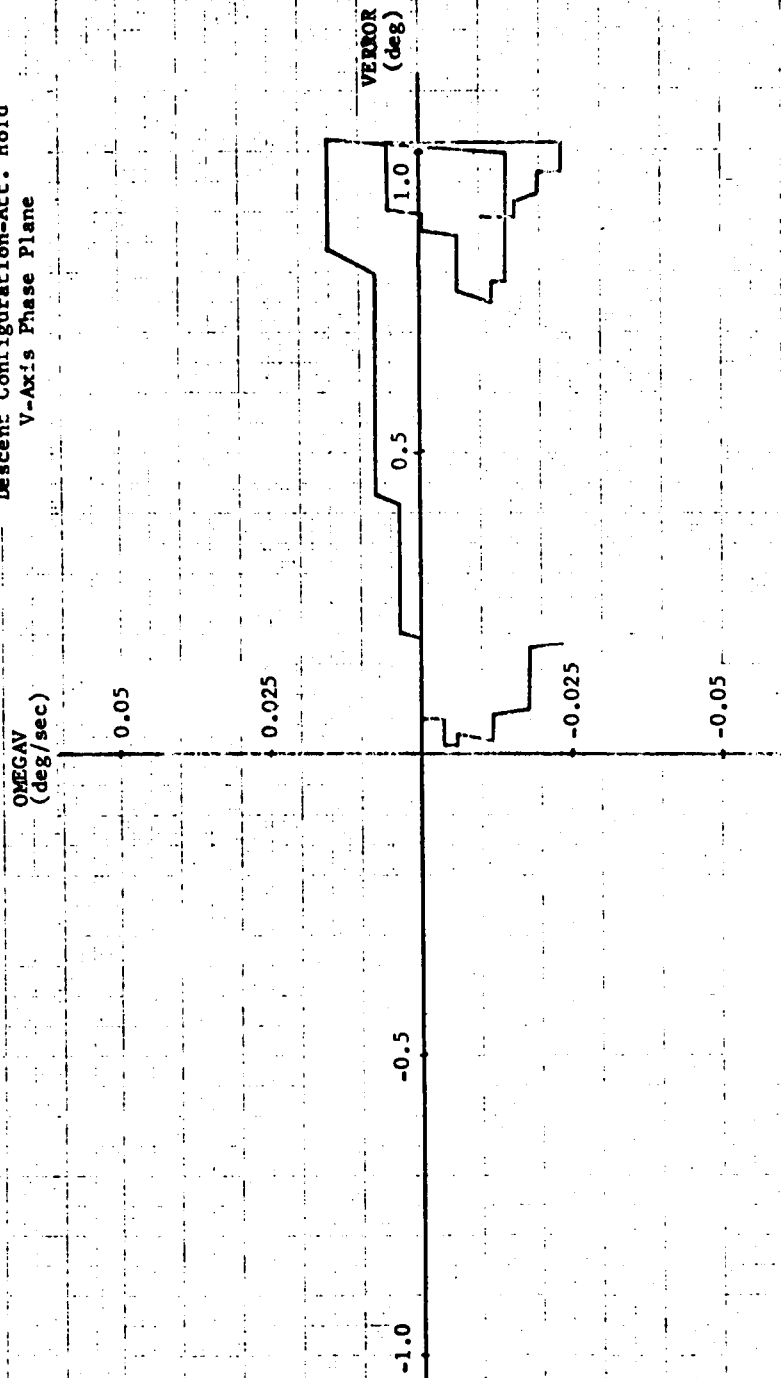
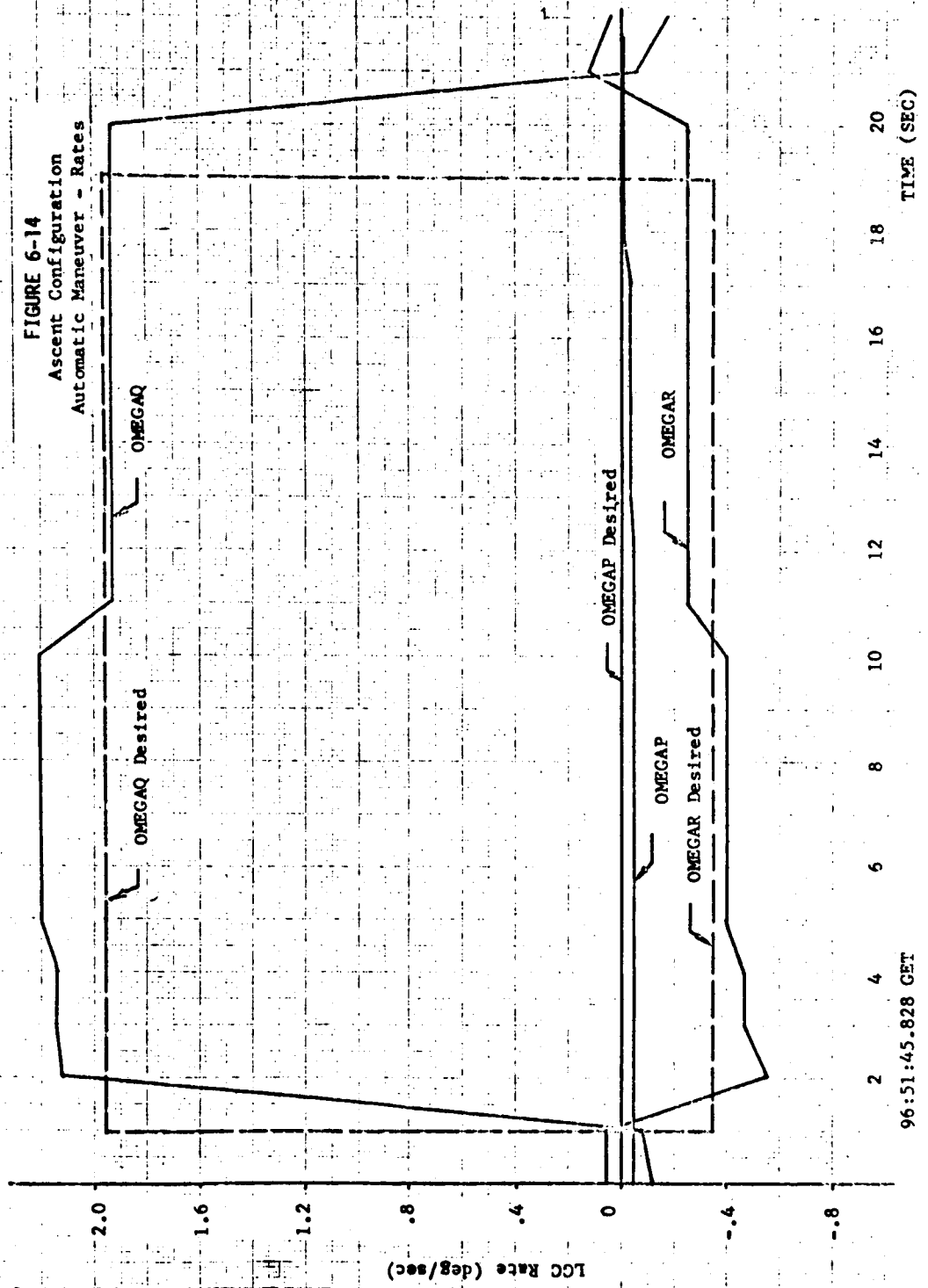
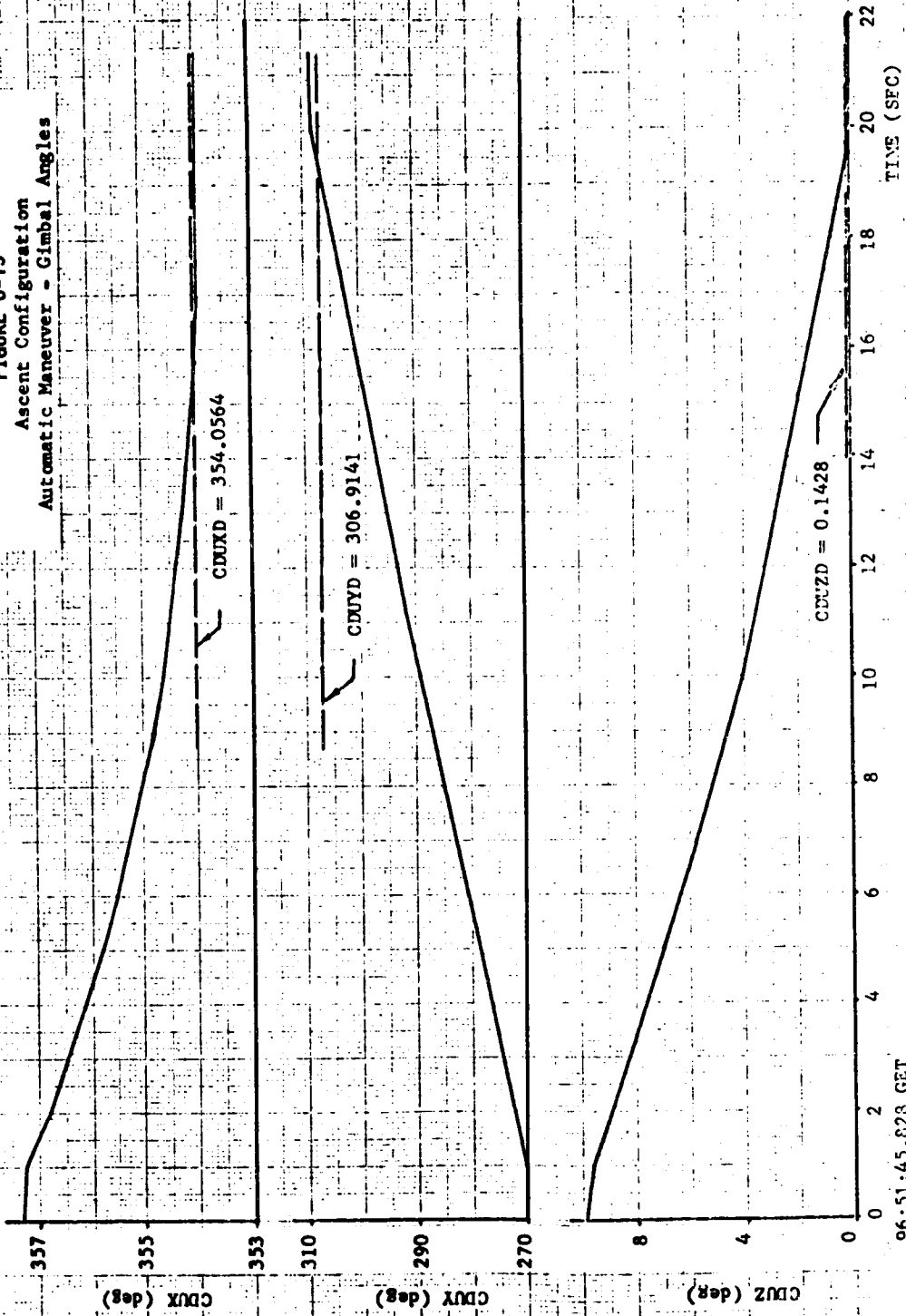


FIGURE 6-14  
 Ascent Configuration  
 Automatic Maneuver - Rates



96:51:45.828 GET

**FIGURE 6-15**  
**Ascent Configuration**  
**Automatic Maneuver - Gimbals Angles**





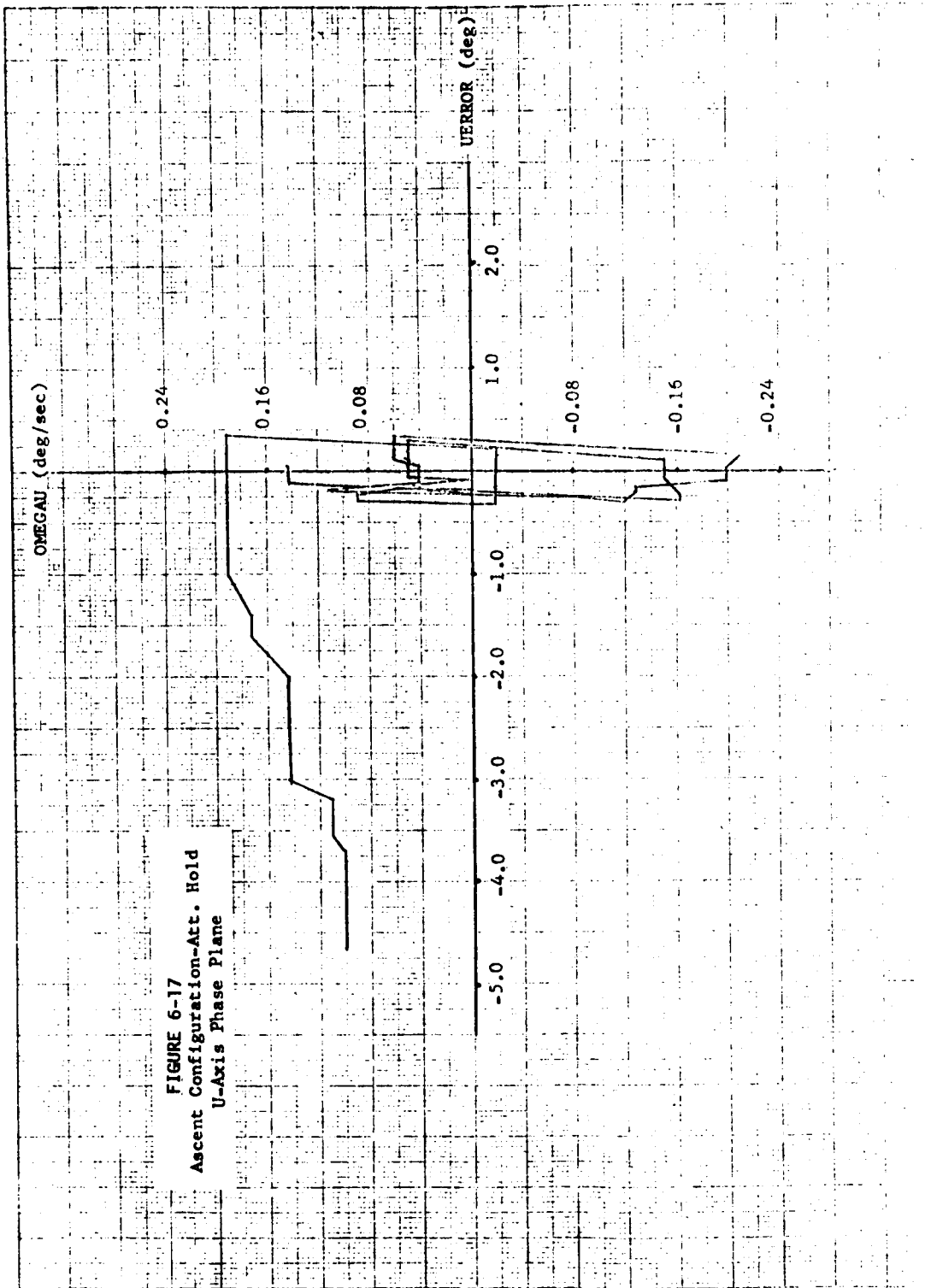
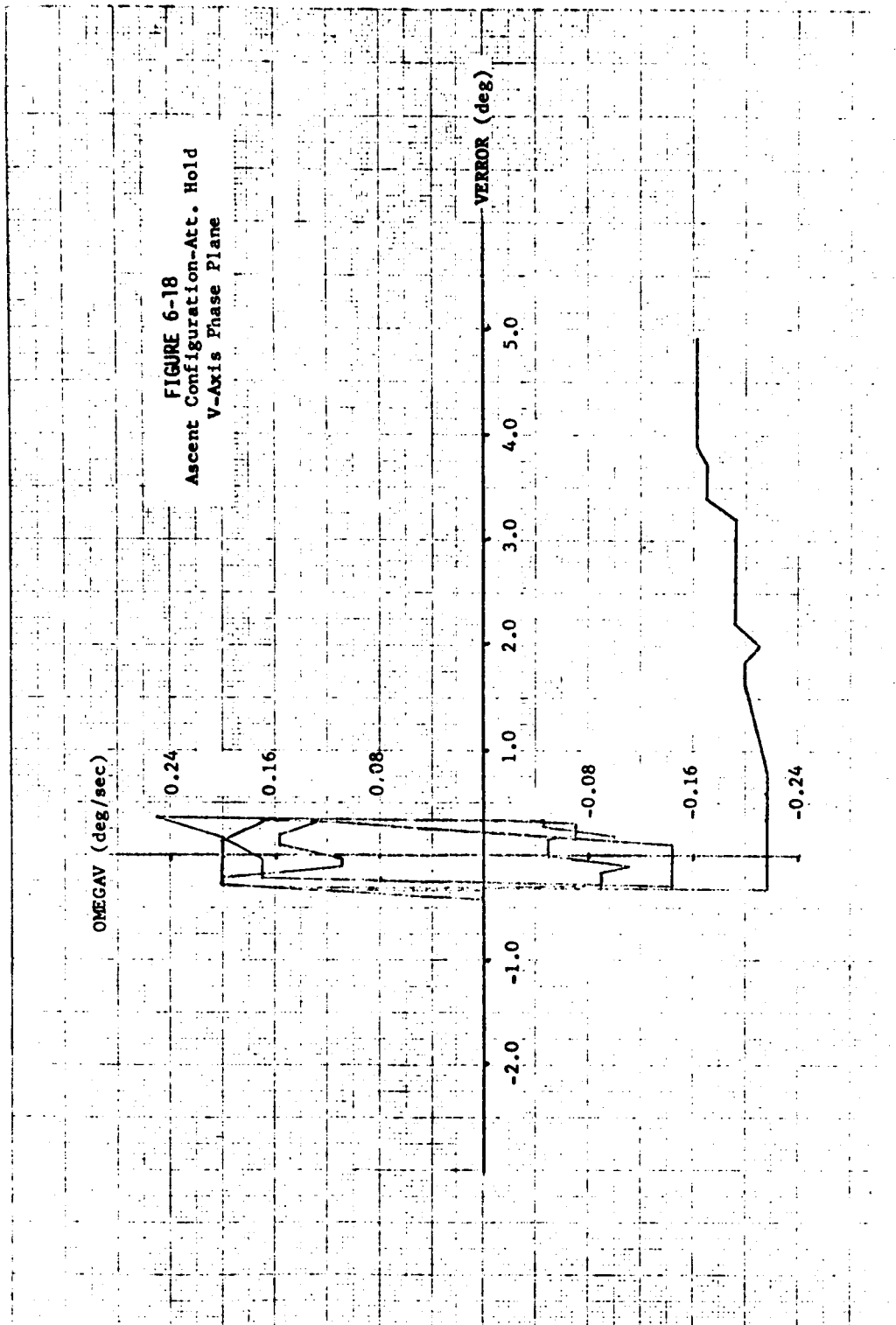
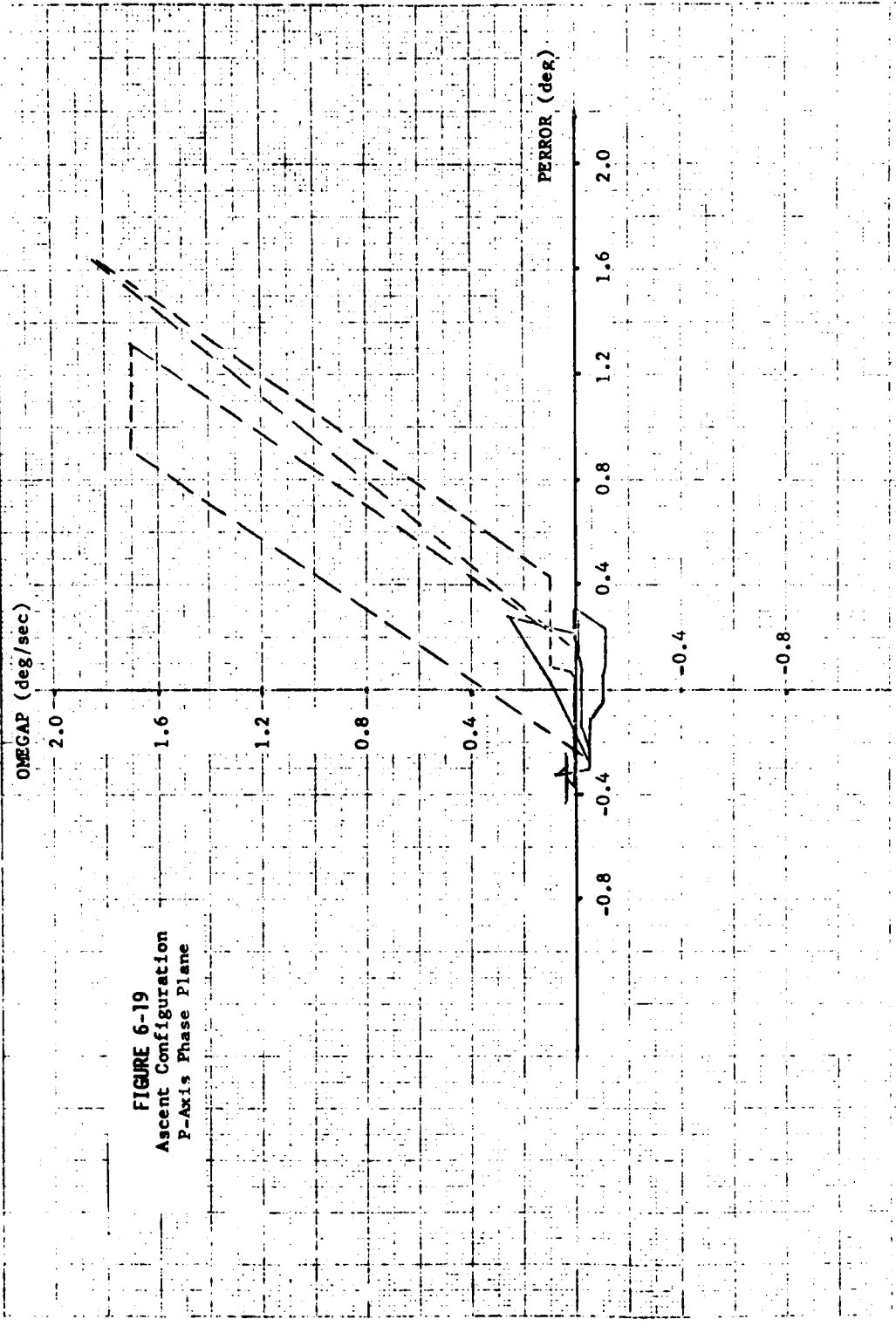


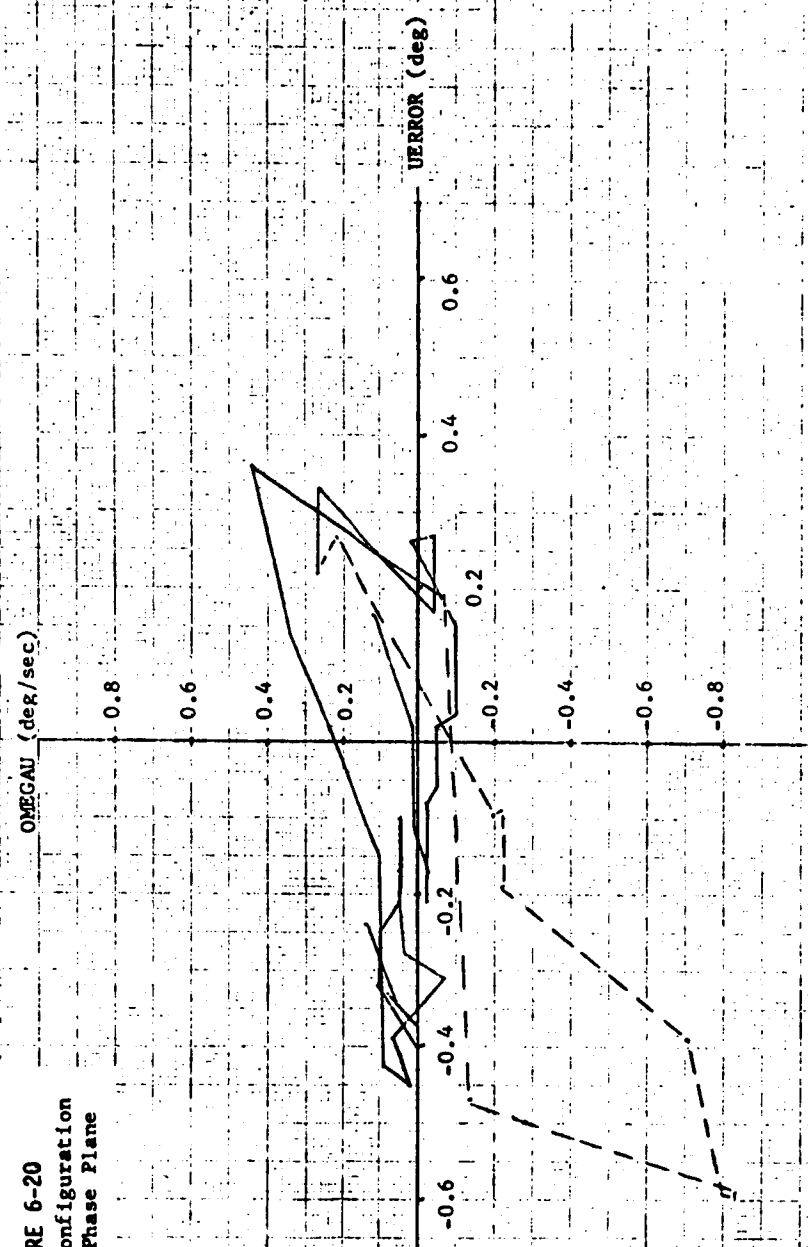
FIGURE 6-17  
Ascent Configuration-Att. Hold  
U-Axis Phase Plane





**FIGURE 6-19**  
 Ascent Configuration  
 P-Axis Phase Plane

**FIGURE 6-20**  
Ascent Configuration  
U-Axis Phase Plane



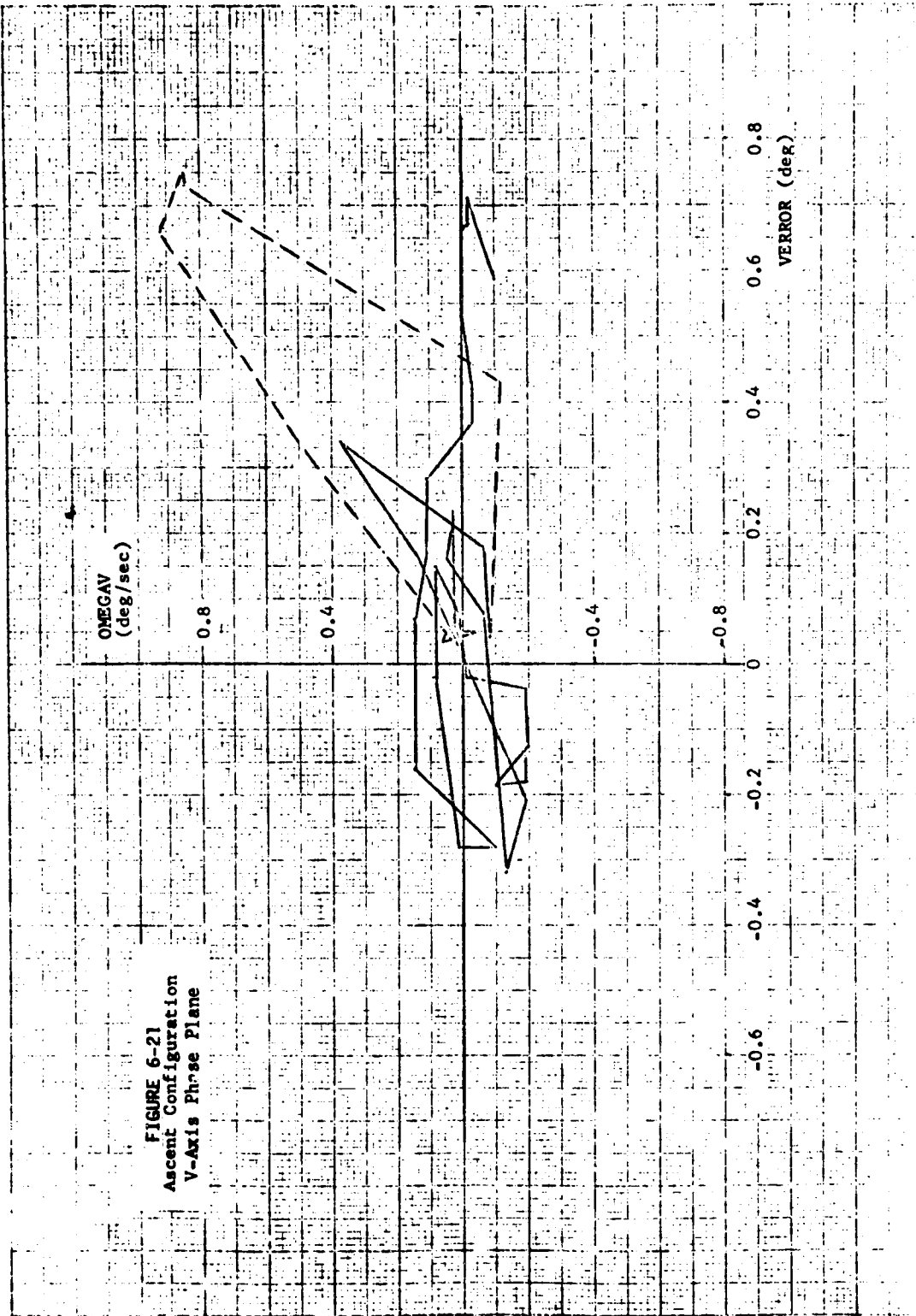


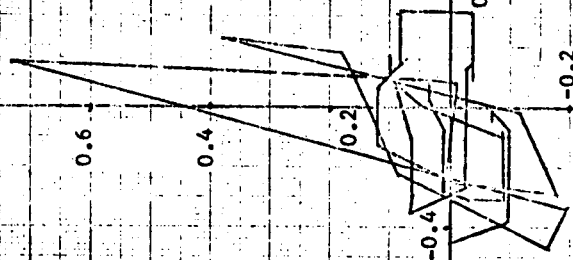
FIGURE 6-21  
Ascent Configuration  
V-Axis Phase Plane

OMEGAP (deg/sec)

FIGURE 6-22

CSI Burn

P-Axis Phase Plane



PERFOR (deg)

0.6

0.4

0.2

-1.2

-0.8

-0.4

0.4

0.8

1.2

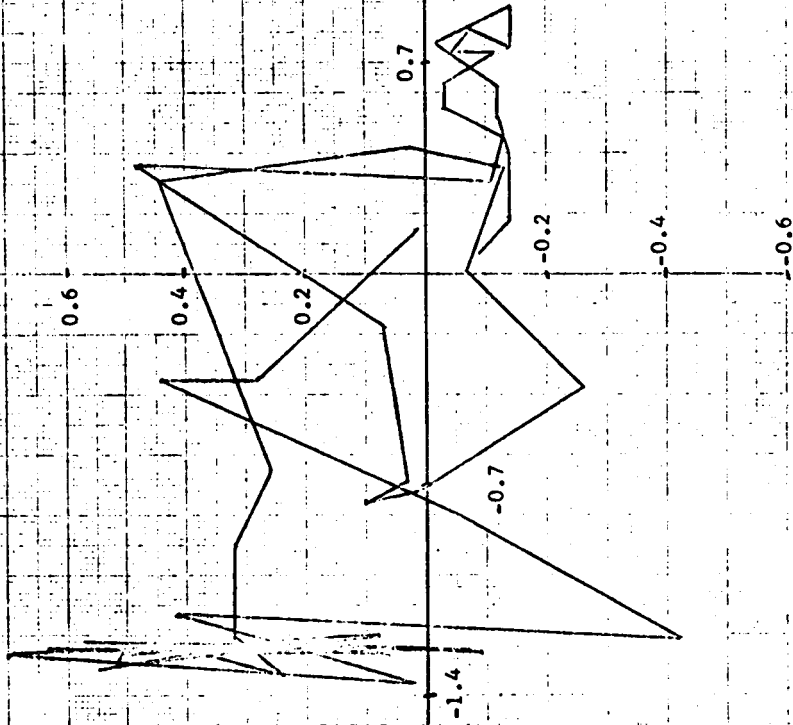
-0.2

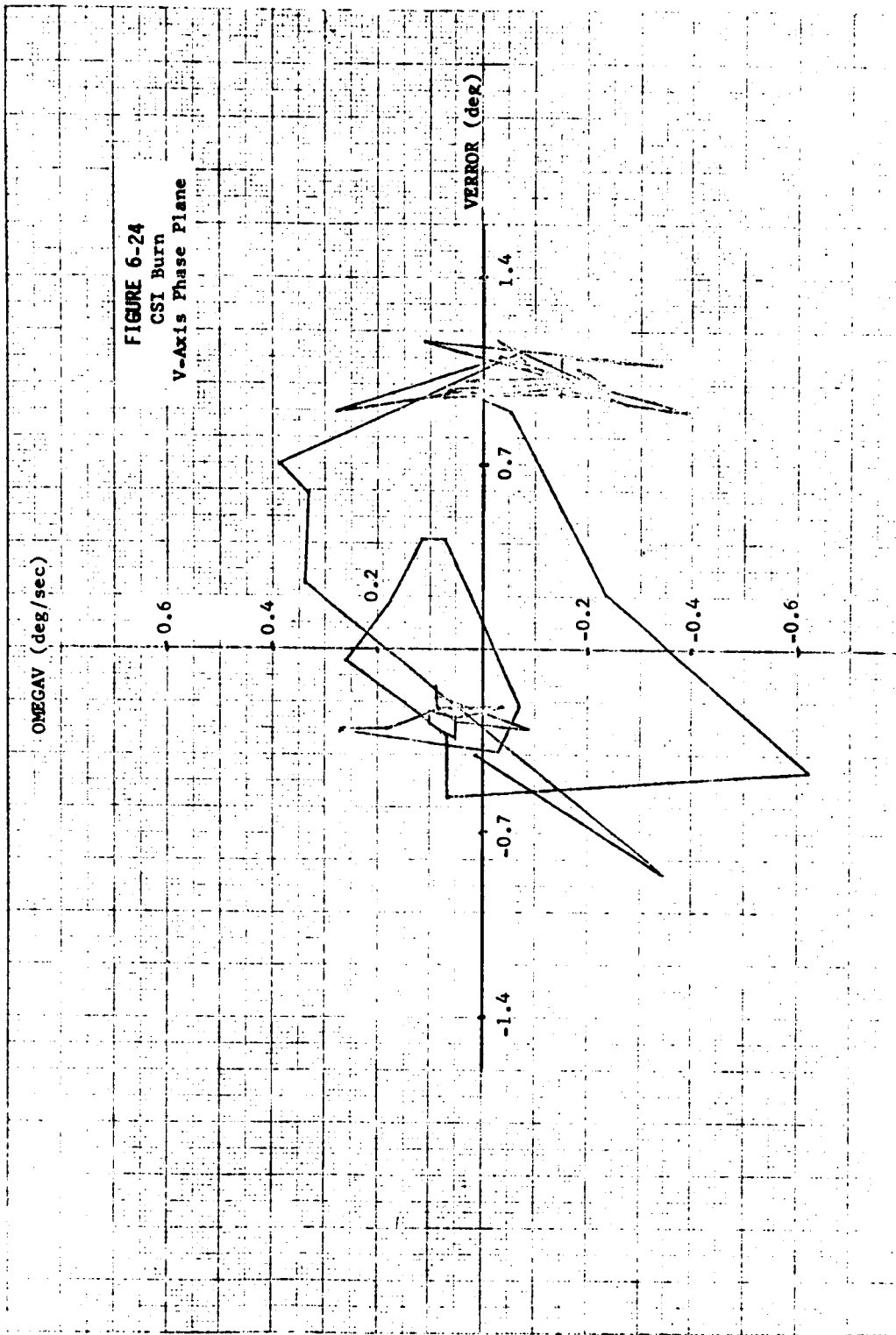
-0.4

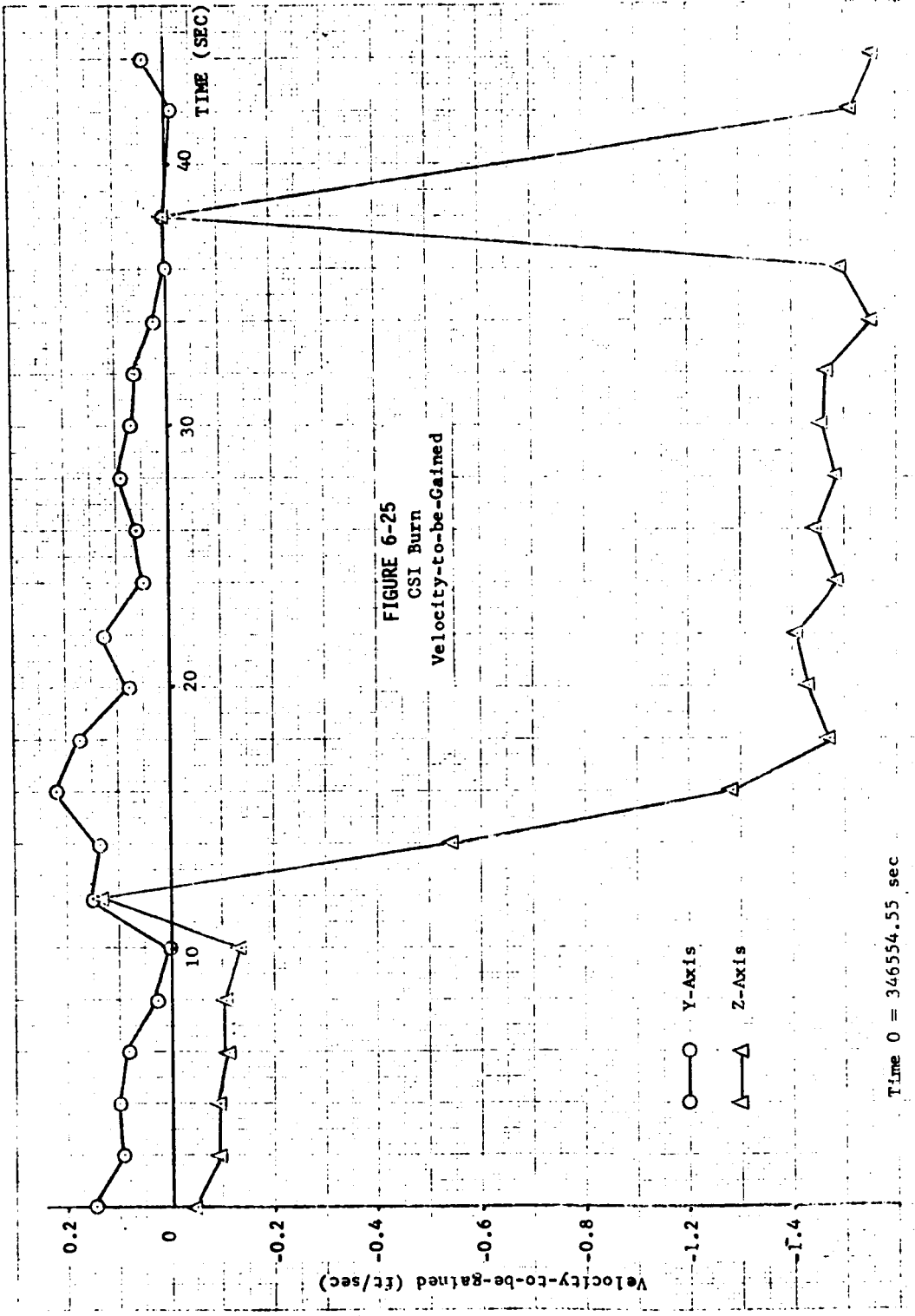
-0.6

FIGURE 6-23  
CSI Burn  
U-Axis Phase Plane

OMEGA (deg/sec)







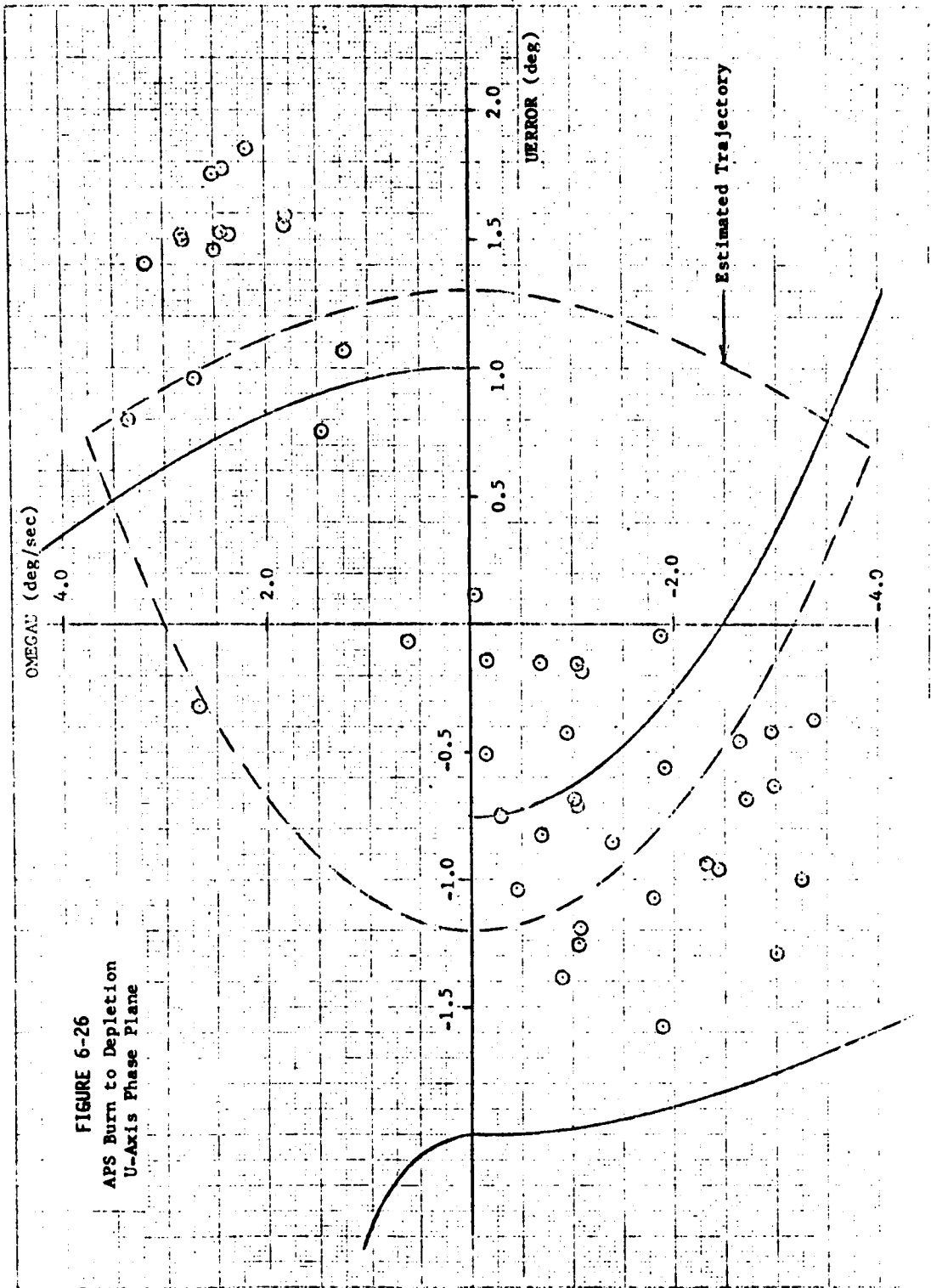


FIGURE 6-26  
 APS Burn to Depletion  
 U-Axis Phase Plane

**FIGURE 6-27**  
**APS Burn to Depletion**  
**U-Axis Attitude Errors & Jet Firings**

Time 0 = 101:57:44.940 GET

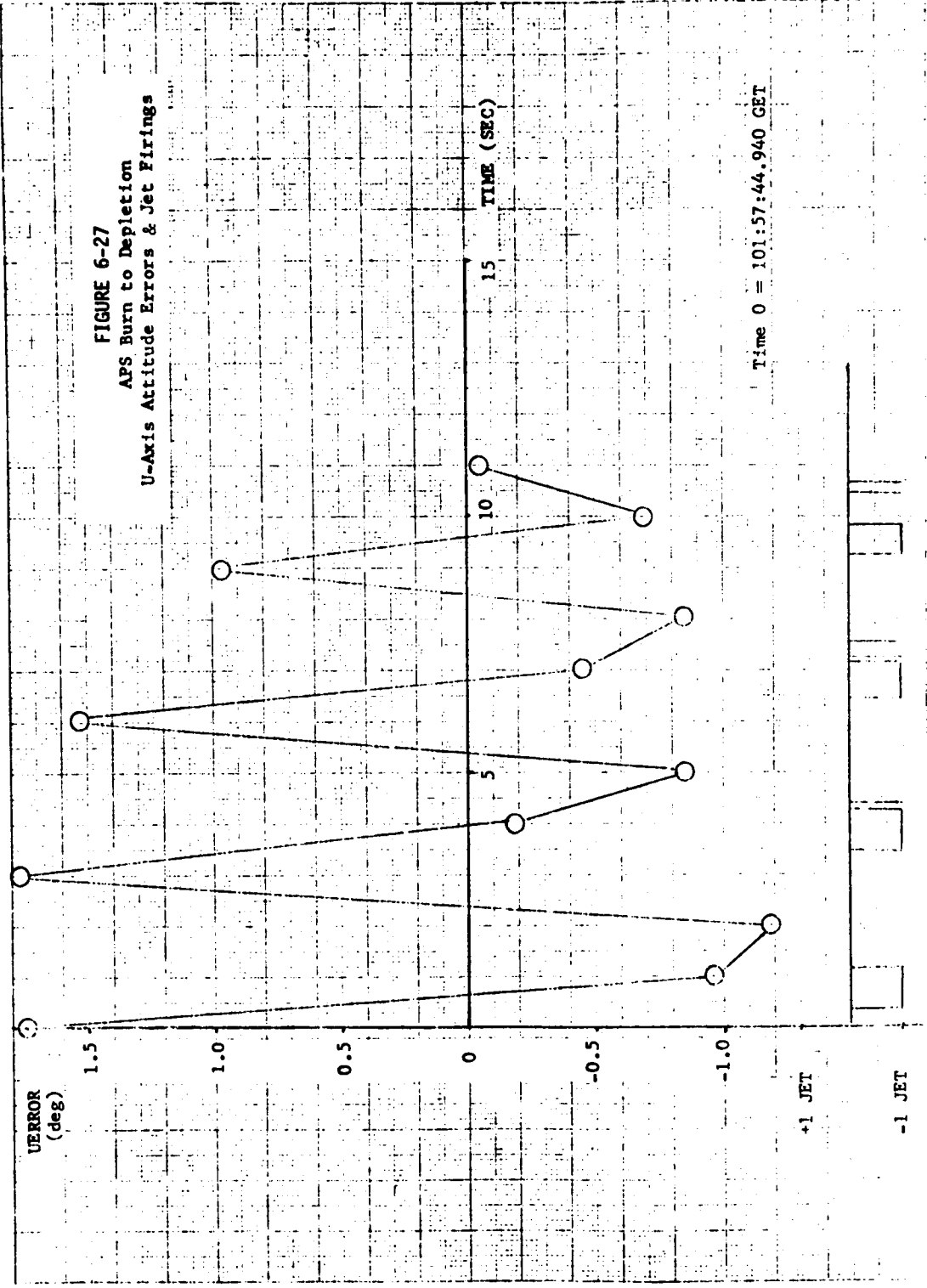
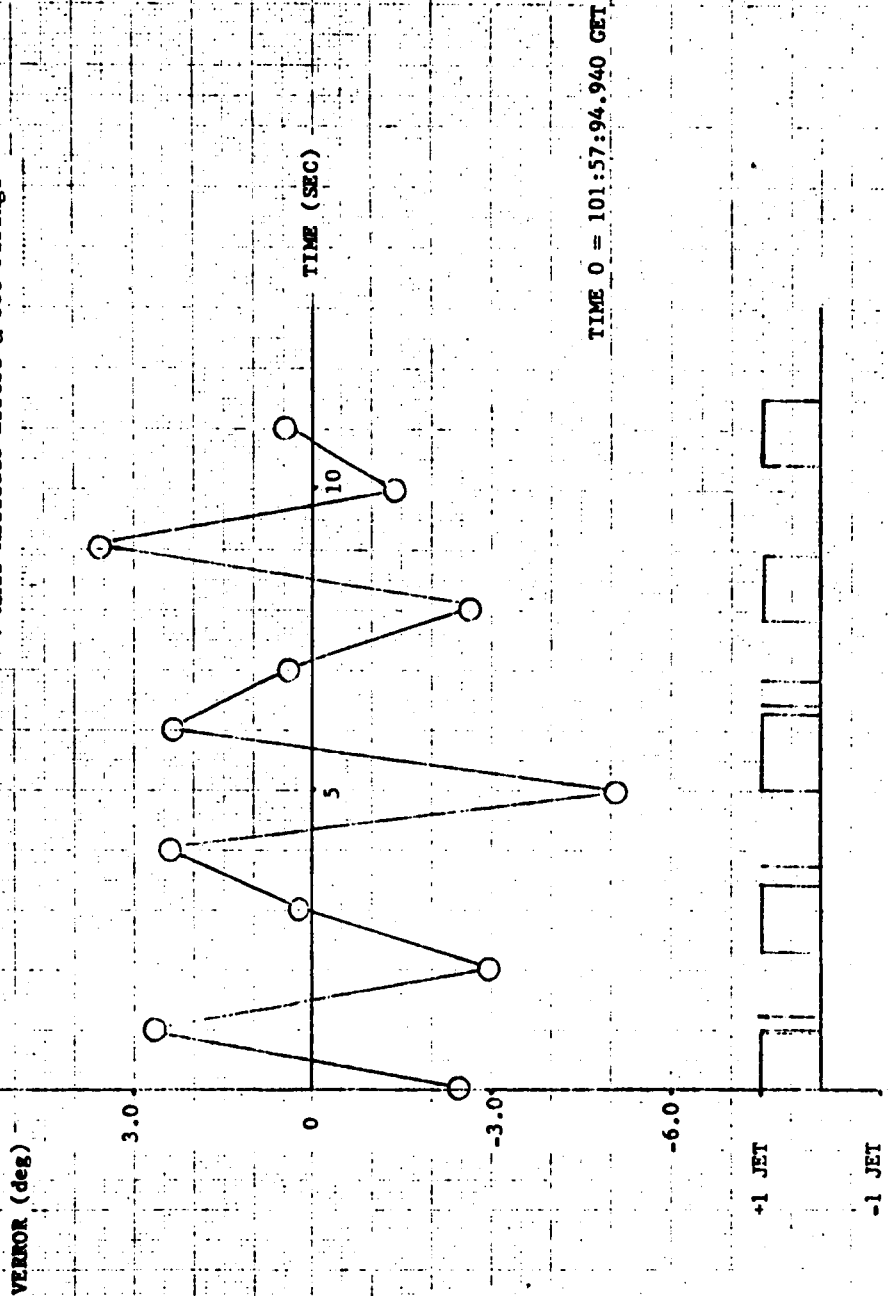


FIGURE 6-28  
 AFS Burn to Depletion  
 V-Axis Attitude Errors & Jet Firings



## 7.0 LM/AGS/CES CONTROLLABILITY

### 7.1 DPS PHASING BURN (AGS)

#### 7.1.1 Telemetry Quantization Versus the Rate-Attitude Phase Plane

The inflight telemetry data quantization was such that it made it impossible to determine with accuracy the Phase Plane about which the RCS system was operating. The telemetry encoder caused the rate channels increment to be 0.107 deg/sec\* and the attitude channels increment to be 0.092 deg\*. Figure 7-1 shows the theoretical phase plane. The cross-hatched areas is a typical deadband area of the attitude and rate telemetry resulting from the quantization employed. Figure 7-2 is based on theory and shows the logic volts generated by changes in rate and attitude commands. The cross-hatched area results from a typical telemetry quantization error and demonstrates how much the logic volts can change without an attitude or rate change being shown on telemetry.

The CES telemetry channels were sampled at a 0.1 second rate. This sample rate did not permit the accurate measurement of changes faster than about 2.5 Hz to be recorded.

The logic volt data was of greater value because the increment (because of the quantization) was 0.1 volts. This error was 20% of the theoretical 0.5 volt required to turn on a thruster pair, but less than 10% of the logic volts generally present when the thrusters were on, and less than 1% of the maximum logic volts. The rate data quantization error of 0.197 deg/sec was about 40% of the maximum rate shown by telemetry, and a much greater percentage of the "average" rate. For these reasons, it was decided to generate the rate from

---

$$* \frac{7.0 \text{ volts (rate and attitude scaling)}}{254 \text{ (TLM increments)}} = .02756 \text{ volts/TLM increment}$$

$$\frac{.02756 \text{ volts}}{.140 \text{ volts/deg/S}} = 0.197^\circ/\text{S/TLM increment}$$

$$\frac{.02756 \text{ volts}}{.30 \text{ volts/deg}} = 0.092 \text{ deg/TLM increment}$$

the logic volts in order to better determine the maximum rates present during the ullage and DPS-2 burn. However, because of the sampling rate, the result of the exercise was still only an approximation. Also, because of these inherent errors, approximations of angular accelerations were not considered.

Figure 7-3 shows the logic volts generated during the ullage and DPS-2 burn. (This figure and all subsequent figures were drawn from the flight data by the TRW 1800 computer.) Figure 7-4 shows the rates generated by solving the following expression.

$$\begin{aligned} \pm \dot{\theta}^* \\ \text{(Pitch \& Roll typical)} \end{aligned} = \frac{\frac{\text{logic volts}}{2} \pm 2.63}{\frac{9.597}{1.5}} \pm \theta$$

$$\begin{aligned} \pm \dot{\psi} \\ \text{(Yaw)} \end{aligned} = \frac{\frac{\text{logic volts}}{2} \pm 3.59}{\frac{9.597}{1.5}} \pm \theta$$

The (+) is dependent upon the recorded polarities. The value of  $\theta$  was taken from the recorded data and was assumed to be correct. This assumption was based on the fact that attitude error is a slow moving function compared to rate. Also, the attitude quantization error comprised only 1/3 of the phase plane deadband in pitch and roll (1/4 in yaw), while the rate quantization error comprised the entire phase plane deadband in pitch and roll (and 75% of the yaw deadband).

The pitch and roll rates recorded inflight are shown in Figures 7-5 and 7-7 (yaw rate not shown). These may be compared to the generated rates shown in Figure 7-4. The quantization caused a bias in both

---

\* Derived from the ATCA expression:

$$\text{Logic volts} = ([\pm (\theta) (0.3) (7) \pm (\theta) (.140) (22.5)] \cdot 4.57 \pm 2.63) \cdot 2$$

cases; therefore, the zeros were located manually. Comparison of the figures reveals that the generated rates are significantly larger than the recorded rates. In pitch, no other data of significance became apparent by this exercise, i.e., structural resonance or limit cycles, that were not apparent in the recorded data. However, in roll a significant difference exists. Theoretical deadbands of 0.2 deg/sec, pitch and roll, and 0.4 deg/sec for yaw are shown in Figures 7-4 and 7-5. Theoretically, any rates greater than these, with zero attitude error, would cause the thrusters to fire. Similarly, the attitude errors recorded during the ullage and burn are shown in Figure 7-6 (zeros were located manually). This figure has the theoretical attitude error deadbands indicated. By means of the maximum rates and attitude errors shown in Figures 7-4 and 7-6, the phase plane plot (Figure 7-1) was marked to show the extremes of attitude and rate control utilized in pitch, yaw and roll during the ullage and burn.

Of interest in the rate and attitude data is the apparent one-sided roll instability beginning at 93:47:46.6 and ending at 93:47:53.0 (see Figures 7-4 and 7-6). The end of the apparent divergence is coincident with engine cutoff. However, Figure 7-3 indicates (+) and (-) roll logic volts generated during this interval while the attitude and rate figures do not show an out-of-deadband signal that would generate a (+) logic voltage. This leads one to conclude that the telemetry quantization error is causing a false gyro null and the zeros were not located correctly. That is, the discrepancy is based on a mislocation of the attitude or rate zero point. Further, when the rate calculated from logic volts (Figure 7-4) is compared with the roll rates recorded in flight shown in Figure 7-7, one may observe that the roll rate from flight data does not show the rate peaks after 45 seconds that are shown on the calculated rate data. The disagreement of the plots is attributed to the telemetry quantization error. Therefore, the divergence did not exist.

Of other interest is the continued pitch down command, with a few roll left commands, throughout the ullage (see Figure 7-3). This could be explained by the position of the cg along (+) Y and (+) Z plus the hypothesis that the thrust of  $D_3$  was greater than that of  $D_1$ . However, this must remain a hypothesis in this analysis since angular accelerations, necessary to the proof, could not be obtained from the data because of the telemetry quantization error.

#### 7.1.2 GTS Performance

Figure 7-8 shows the motion of the DPS Engine through the DPS-2 burn. The slopes drawn on the figure are drawn to the nominal GDA rate of 0.198 deg/sec. The LM body acceleration produced by the engine motion is so described on the figure. The engine motions agree in time and polarity with the logic volts shown in Figure 7-3.

The first motion of the pitch GDA is observed at Gimbal Enable, 93:47:32.45 (32.45 on figure). The apparent slow engine motion subsequent to this time is a result of the telemetry sample rate and is not an anomaly attributable to the GDA. The GDA threshold was just overcome periodically at time increments much longer than the telemetry sample rate of 0.1 sample/second. As a result, the apparent slow GDA motion was recorded.

The GTS performance was satisfactory throughout the DPS-2 burn.

#### 7.1.3 CG Offsets

From Figure 7-8, it may be observed that static position of the engine moved (-) 0.234 degrees in pitch and (+) 0.641 degrees in roll between DPS-2 Start and DPS-2 Off. The polarities assigned to the above mentioned engine motions stem from the following facts:

- a) Pitch engine bell motion towards (-) Z causes body pitch up and positive going telemetry voltage.
- b) Roll engine bell motion towards (-) Y causes body roll right and positive going telemetry voltage.
- c) Pitch engine bell motion towards (-) Z is defined as (+)  $\delta_p$ .

d) Roll engine bell motion towards (+) Y is defined as (+)  $\delta_R$

The engine thrust is applied to the LM at station X = 154". Prior to the burn the cg is theoretically located near the X axis at X = 192.49" (Ref.1). From Figure 7-8 it may be observed that the engine was at (-) 1.97 degrees in the roll plane and (+) 1.49 degrees in the pitch plane prior to the burn. After the burn, the engine was at (-) 1.33 degrees in roll and (+) 1.26 degrees in pitch. By trigonometry,

Prior DPS-2, cg Y = +1.32"

cg Z = +1.00"

Post DPS-2, cg Y = +0.90"

cg Z = +0.85".

Resulting cg motion from start to end of burn:

Y cg motion, (-) 0.42" along (+) Y

Z cg motion, (-) 0.15" along (+) Z

This is the opposite direction from that predicted. There is no explanation for this discrepancy at this time. However, the change is small and could be the result of a cg mistrim at the start of the burn since the previous burn (DPS 1) was with the docked configuration.

## 7.2 DESCENT STAGE ATTITUDE HOLD (AGS)

### 7.2.1 Propellant Consumption

The telemetered data (received by Ship Mercury in the Pacific) was extremely noisy. As a result, there were many false thruster firings indicated. The following listing was derived from a count of indicated firings vs. duration in the recorded 4-minute and 45-second attitude hold period prior to DPS-2.

<u>Number of Indicated Firings</u>	<u>Indicated Firing Duration (Seconds)</u>
478	0.014
55	0.020
2	0.030
1	0.050
7	0.070

<u>Number of Indicated Firings</u>	<u>Indicated Firing Duration (Seconds)</u>
8	0.080
1	0.100
4	0.150
7	0.200
2	0.250
2	0.300
2	0.400
1	0.500
1	0.600
1	0.800

However, after the data were screened of theoretically impossible thrust combinations plus thrust on indications when logic volts were not greater than 0.5 volts, the above tabulation was reduced to the following one.

<u>Number of Indicated Firings</u>	<u>Indicated Firing Duration (Seconds)</u>
24	0.014
30	0.020
1	0.050
1	0.080

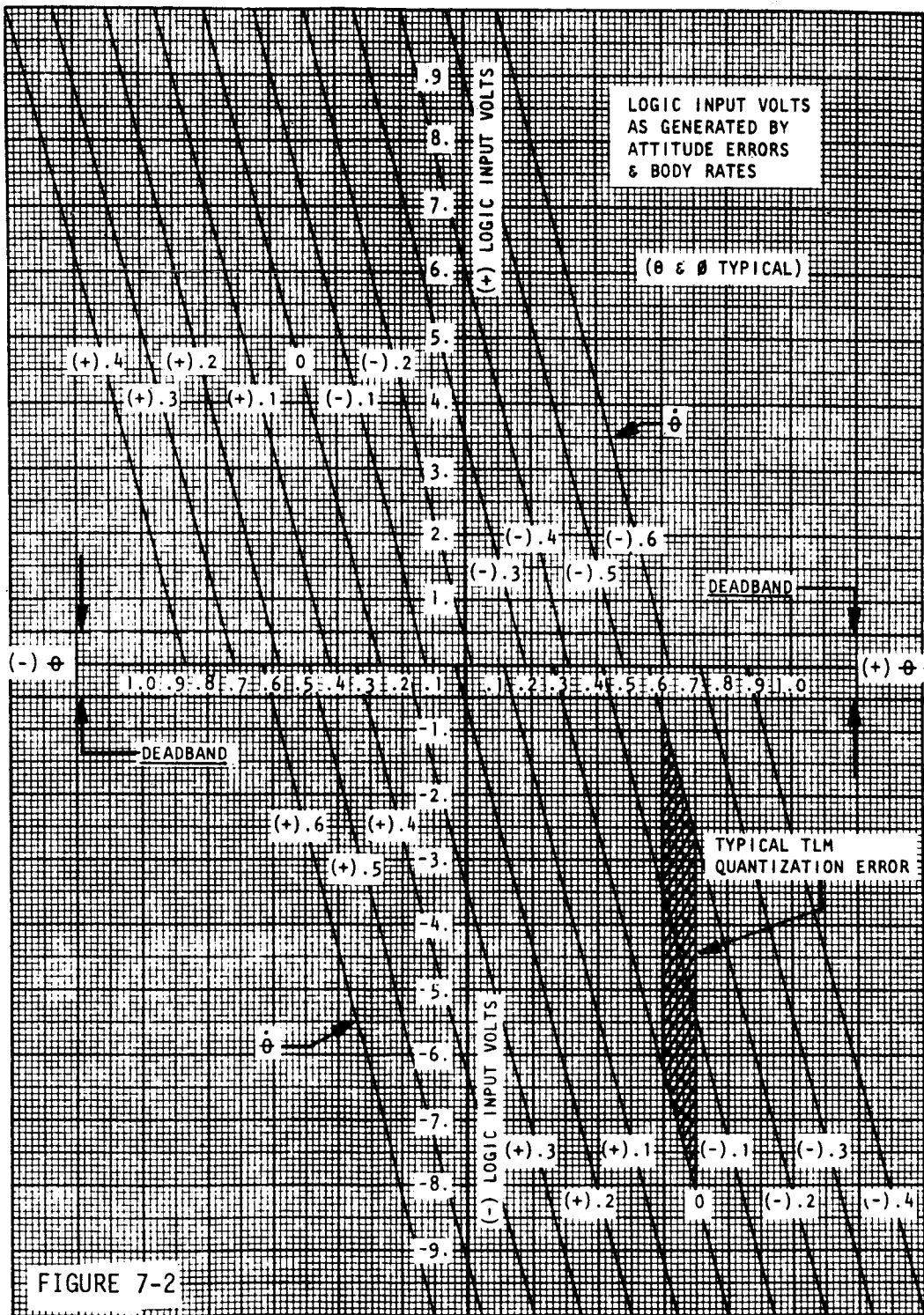
Propellant usage per thruster on time was extracted from the Spacecraft Operational Data Book, Volume II. By this means the following tabulation was devised.

Length of Thruster Firing (Seconds)	Pounds of Propellant Used	Number of Firings	Total Pounds Used
0.014	0.0075	24	0.180
0.020	0.0097	30	0.290
0.050	0.0203	1	0.020
0.080	0.0295	1	<u>0.030</u>
			$\Sigma = 0.520$

$$\frac{.520 \text{ lb}}{285 \text{ sec}} \times \frac{60 \text{ sec}}{\text{min}} = 0.109 \frac{\text{lb}}{\text{min}}$$

The Spacecraft Operational Data Book, Volume II, predicted 0.114 lb/min. Therefore, it is concluded that the propellant consumption was satisfactory as a result of a satisfactory CES attitude hold performance.





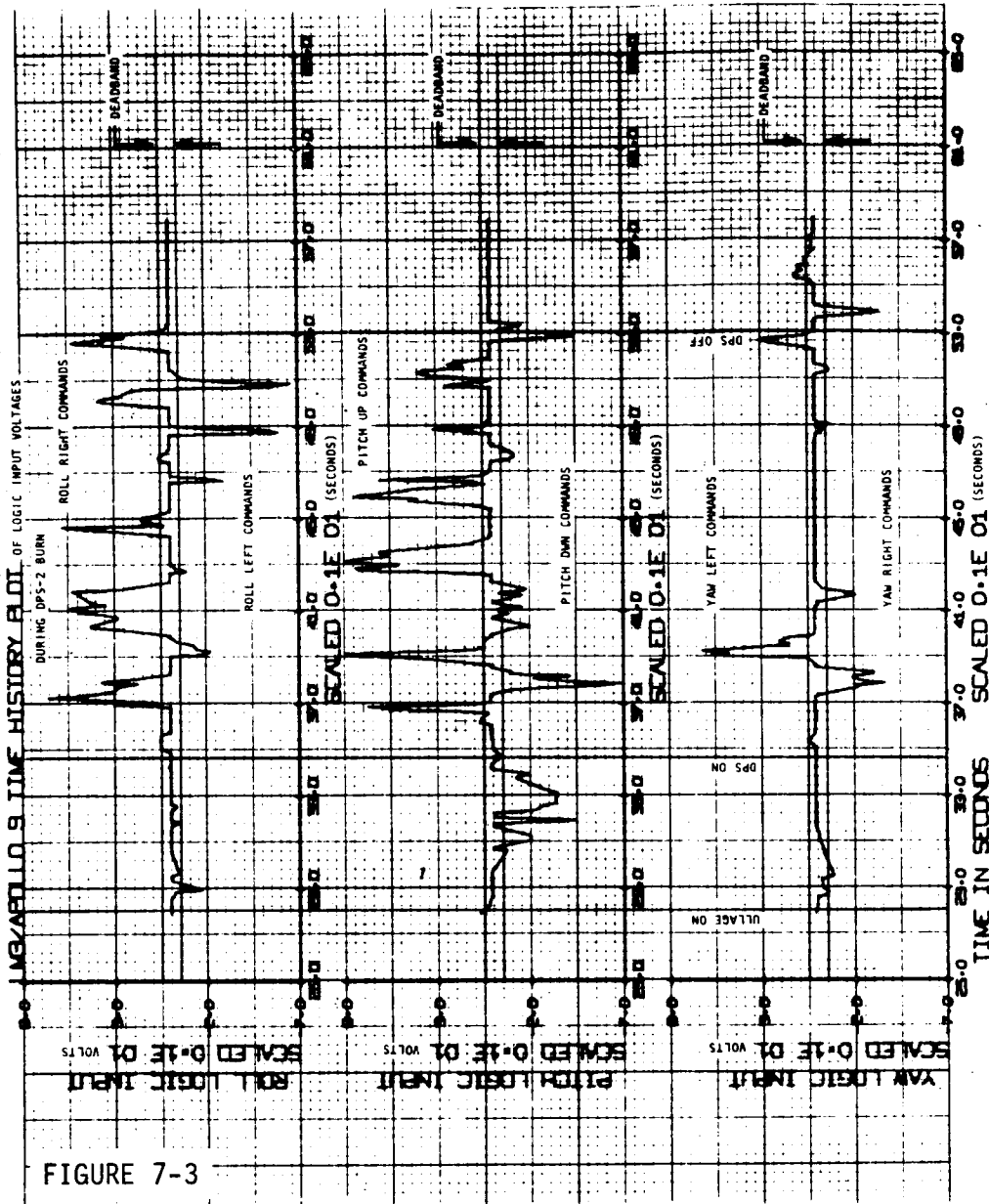


FIGURE 7-3

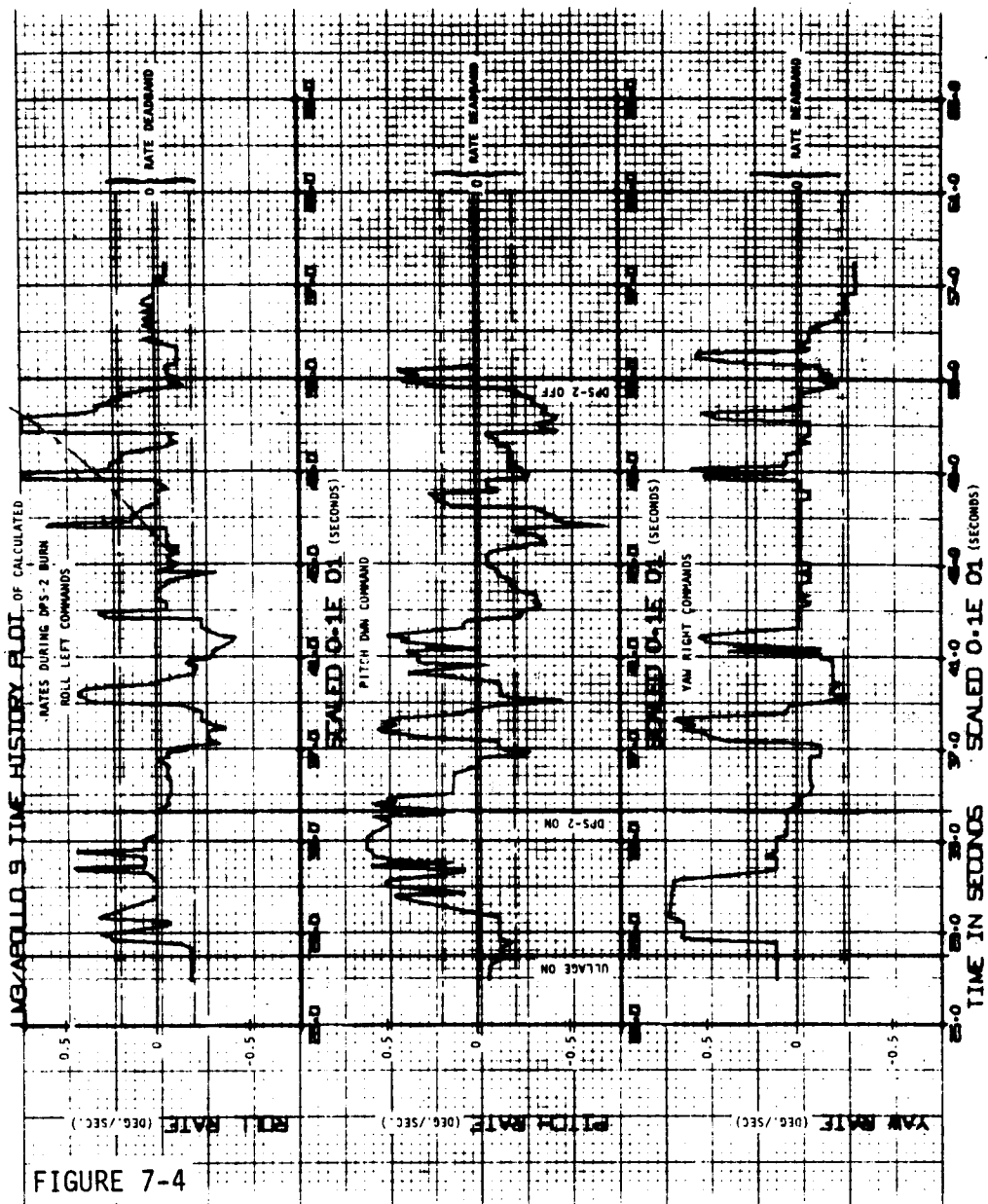


FIGURE 7-4



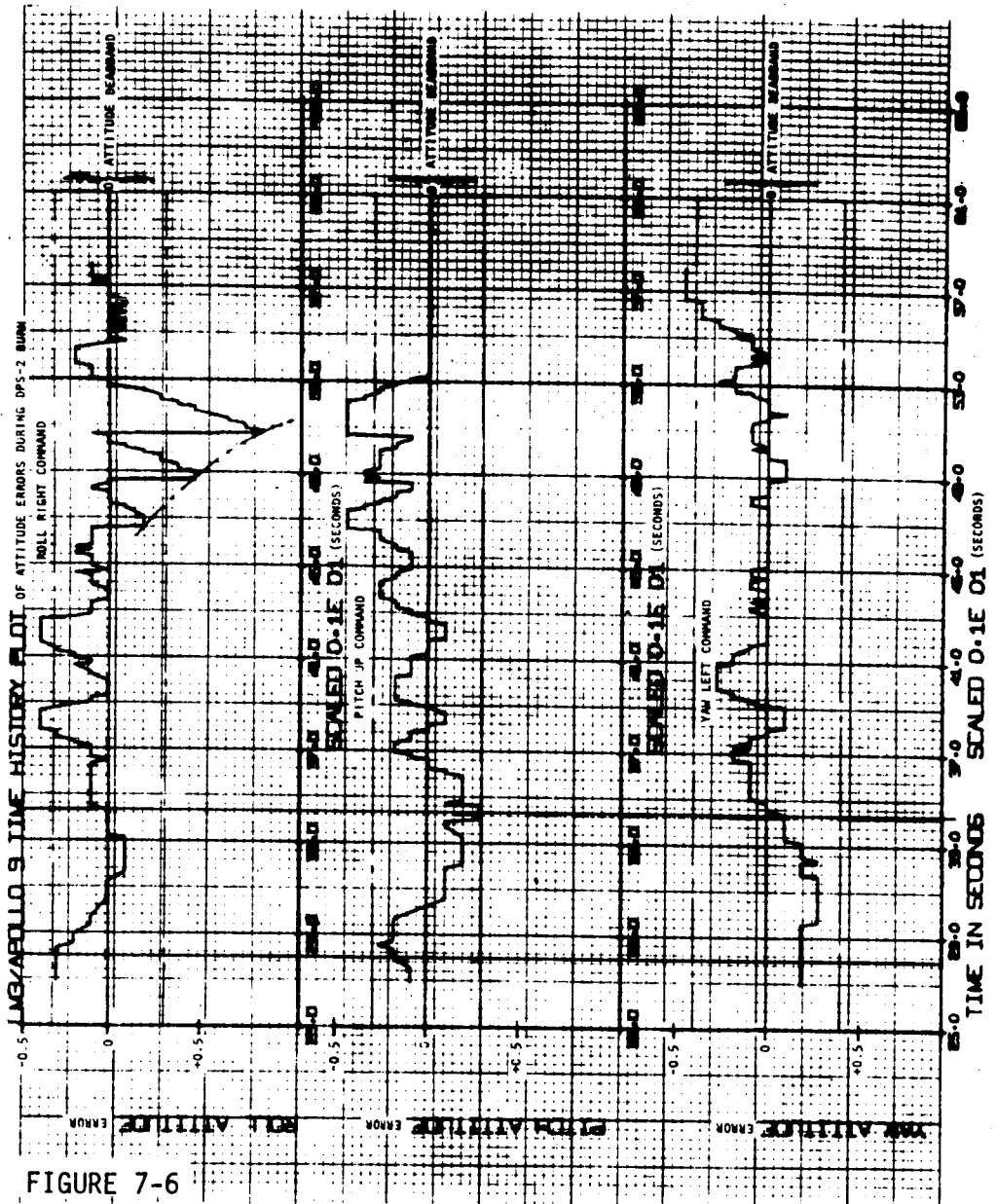


FIGURE 7-6

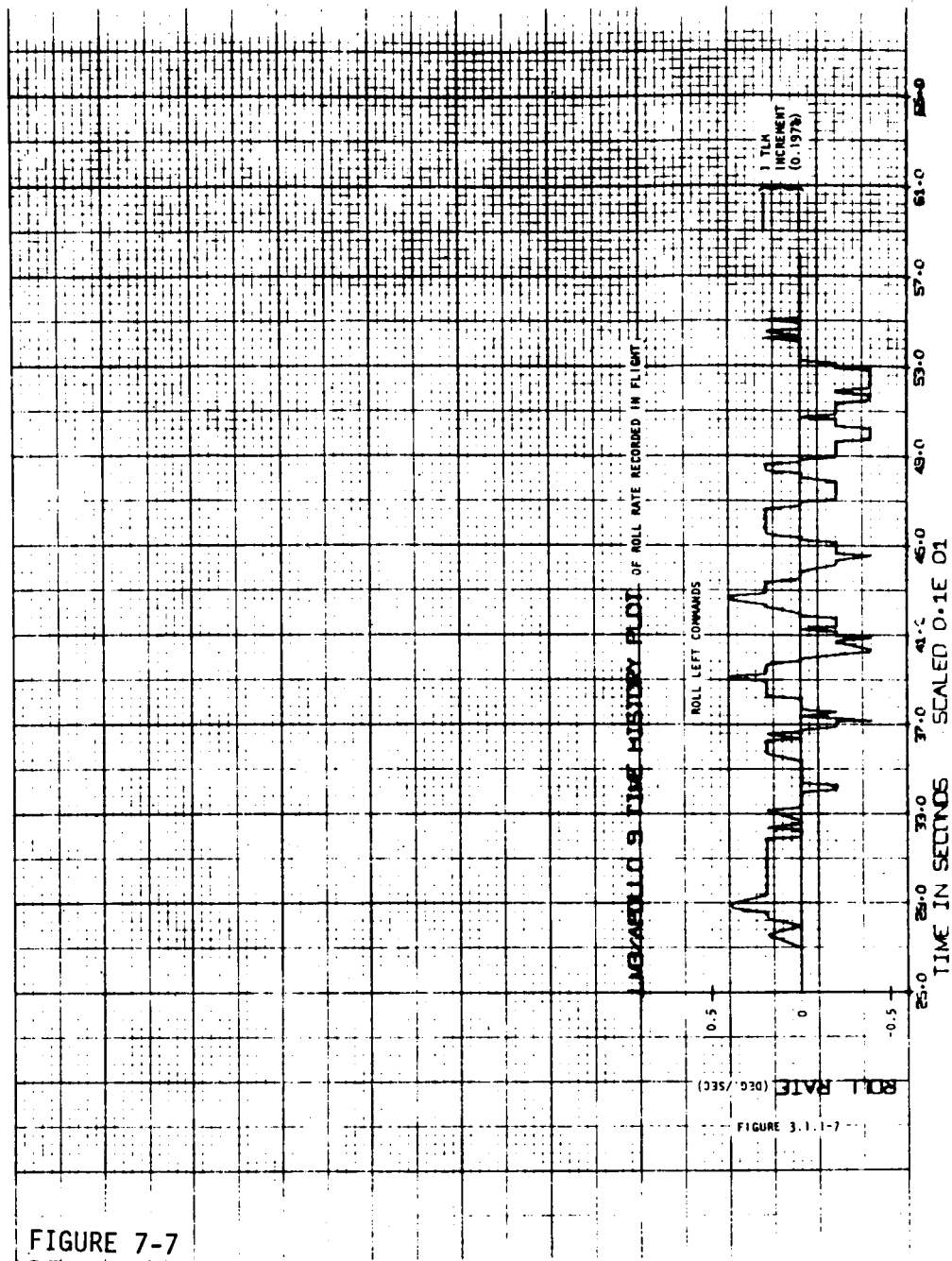


FIGURE 7-7

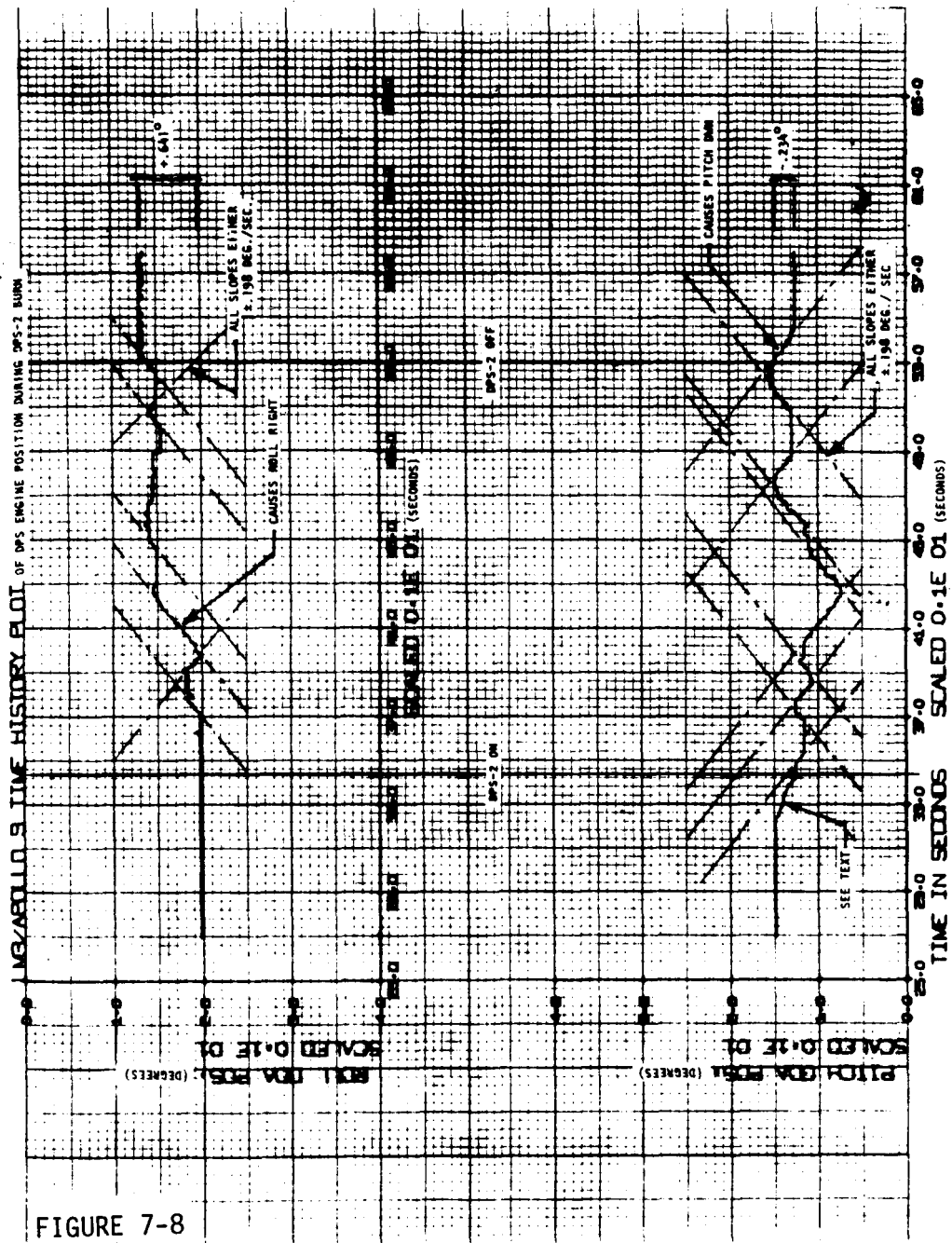


FIGURE 7-8

## 8.0 RENDEZVOUS

### 8.1 ONBOARD NAVIGATION

Performance of the spacecraft navigation systems during the rendezvous period was excellent. All updates supplied to the LM Guidance Computer (LGC) during the rendezvous were from the onboard rendezvous radar. Figure 8-1 to 8-6 present a comparison of LM state vector components after CSI with the TRW HOPE Program and the integrated state vector components. The integrated state vectors show how the onboard states would have propagated in the absence of rendezvous radar observations. From the data, the tendency was for the state vectors to converge on the BET state vectors as radar marks were incorporated.

During the LM separation period, the command module pilot was making sextant sightings when the LM was visible and updating the LM state vector in the Command Module Computer (CMC). Figures 8-7 to 8-9 present the CMC relative (CSM/LM) state vector components and the preliminary BET relative vector components during the rendezvous period. Although minimal CMC data were available during the rendezvous period, those which were obtained show close agreement with the BET relative state vectors.

### 8.2 RENDEZVOUS TARGETING

Comparisons of all executed  $\Delta V$  solutions during the rendezvous with the pre-mission nominal  $\Delta V$ 's are shown in Table 8.1. The total  $\Delta V$  required to perform the LM maneuvers was within 4 percent of the nominal  $\Delta V$ .

During the rendezvous sequence, various maneuver solutions were available to the LM crew. These additional solutions were available as a comparison for evaluating the primary solution and for backup purposes. The RTCC was calculating a solution based on the RTCC trajectory, onboard chart solutions were calculated, and the CSM had a capability to solve for TPI and midcourse maneuvers. Due to the near perfect relative trajectory and the accurate onboard navigation, all solutions were equally good and any one would have produced approximately the same results. All of the available solutions are presented in Table 8.2.

### 8.2.1 CSI Maneuver Evaluation

Three CSI solutions were available; the LGC solution, the RTCC solution and the charts. Each of these solutions impulsively summed with the LGC LM states and then propagating both LM and CSM orbits to the time of CDH yields nearly identical  $\Delta H$  results as shown in Table 8.3.

### 8.2.2 TPI Maneuver Evaluation

For TPI, four solutions were available; the LGC, CMC, RTCC and chart solution. All would have produced equally good results as shown in Table 8.4. Starting from the TPI maneuver, the LGC state vectors (obtained by integrating forward from the last available LGC state vectors) were propagated out to the Distance of Closest Approach (DCA) based on precision integration of the CSM orbit and by incorporating separately into the LM trajectory each of the available TPI solutions as impulsive maneuvers. Also determined was the time at which the DCA occurred and the  $\Delta V$  required to match orbits at that same time. The  $\Delta V$  required is equivalent to the braking  $\Delta V$ . The DCA time was put in the form of a shift from the expected time for braking (TTPF) since time shifts from nominal are critical due to lighting constraints during the braking period. Accuracy of the LGC solution (the burn actually used) is further substantiated by the small midcourse corrections (<4 ft/sec) actually required after TPI.

The CSM would have performed the TPI maneuver as a mirror image burn had the LM become incapacitated or had the LM primary and backup solutions failed GO/NO-GO tests. To evaluate the CSM TPI solution, the mirror image burn was simulated one minute after the actual TPI time using the CSM  $\Delta V$  solution and using the CSM onboard state vectors. The run indicated the CSM trajectory distance of closest approach to the LM would have been 4200 ft and the required braking would have been 29 ft/sec (nominal 30 ft/sec). The time of intercept would have been within one minute of predicted intercept time. These errors are reasonable and are expected due to the imperfections in the targeting scheme.

A CSI to intercept evaluation of the LGC targeting was evaluated through simulation by re-flying each of the actual rendezvous solutions and by integrating out the passive vehicle trajectory. Starting with the LGC onboard state vectors immediately prior to CSI, the CSI  $\Delta V$  was applied as an impulse to the LM velocity state and the trajectory was propagated to CDH time. As shown in Table 8.3, the error between the nominal differential altitude at CDH time and  $\Delta h$  from the CSI targeting is 0.90 n.m., a reasonable error considering the imperfections in the targeting scheme and preflight simulation error predictions. At CDH time, the CDH  $\Delta V$  was impulsively applied and the states were propagated to the time of TPI. Since considerable rendezvous radar updating was accomplished between CSI and TPI, it was considered unrealistic to use the propagated states. Therefore, the LM states were updated to the onboard values. The values used were the last available onboard states (10 minutes prior to TPI) before loss of station coverage. At the time of TPI, the TPI  $\Delta V$  solution was impulsively applied and the distance of closest approach to the target vehicle determined (Table 8.5). Next the TPI solution and the first midcourse solution trajectory was determined. Also, the TPI and both TPM solutions were used to solve for a trajectory propagated to intercept. Results of both cases are also shown in the table. The rendezvous targeting errors are within preflight simulation error predictions.

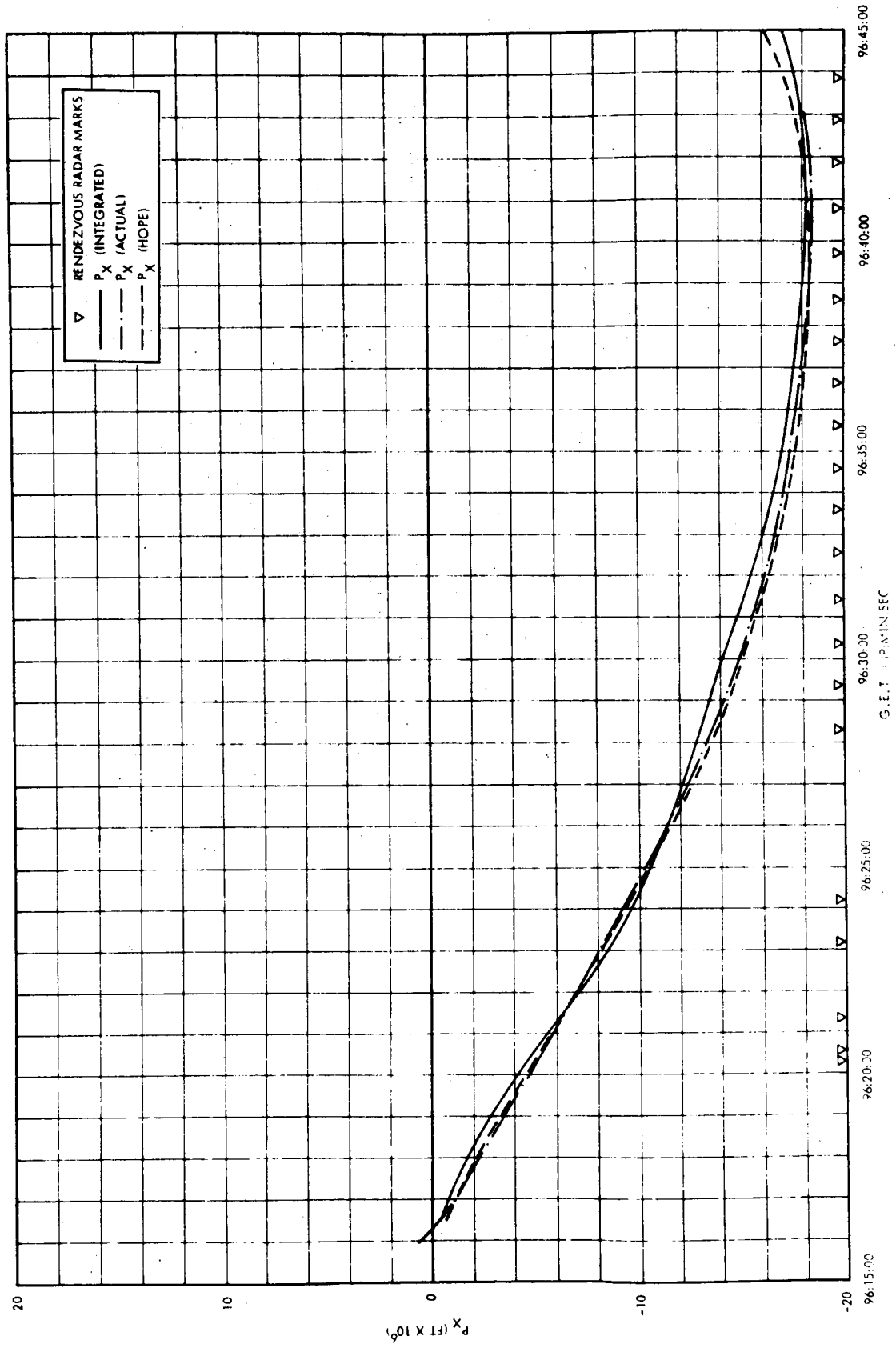


Figure 8.1 STATE VECTOR COMPARISON VERSUS RENDEZVOUS RADAR MARKS - P<sub>X</sub>

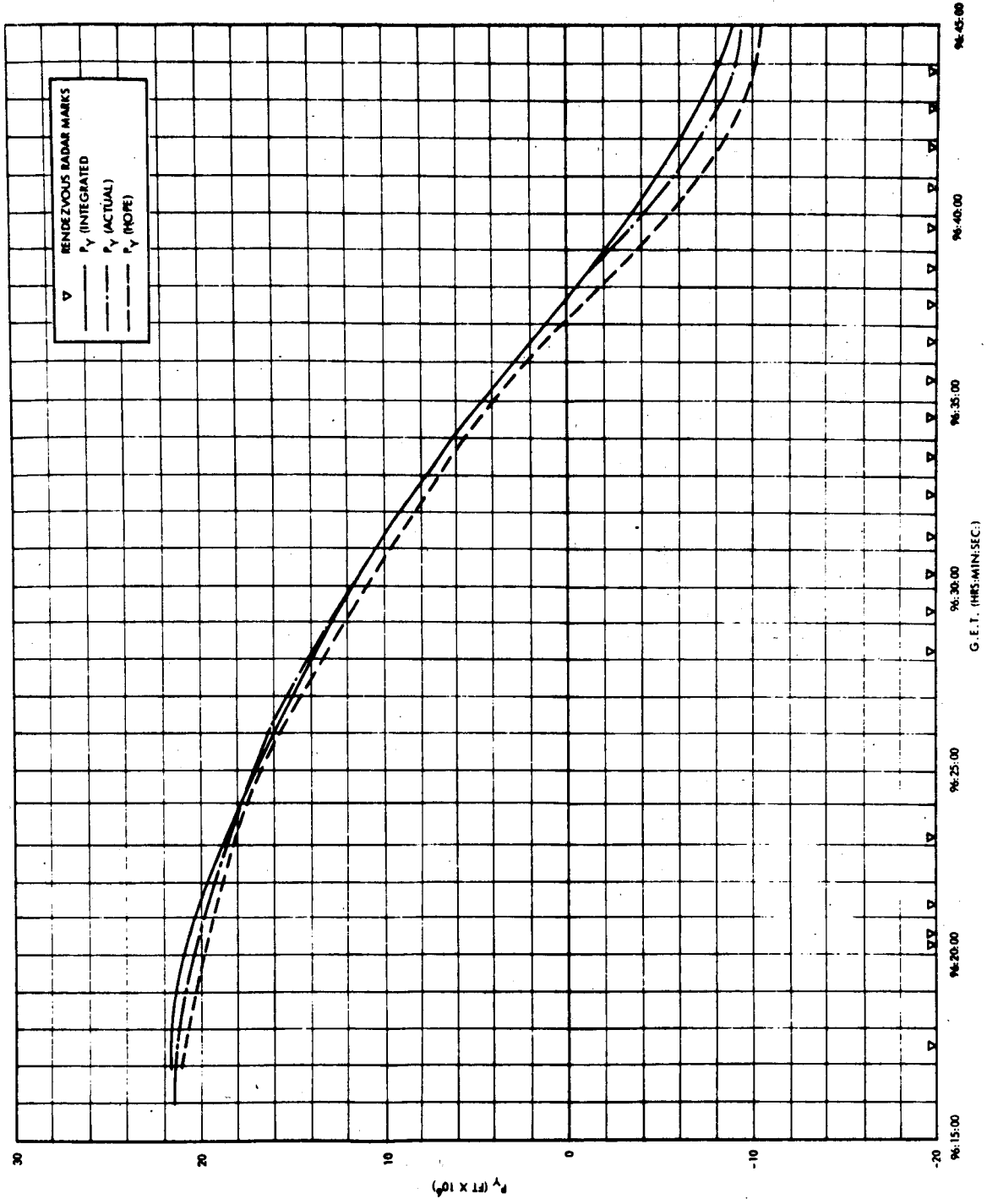


Figure 8.2 STATE VECTOR COMPARISON VERSUS RENDEZVOUS RADAR MARKS -  $P_y$

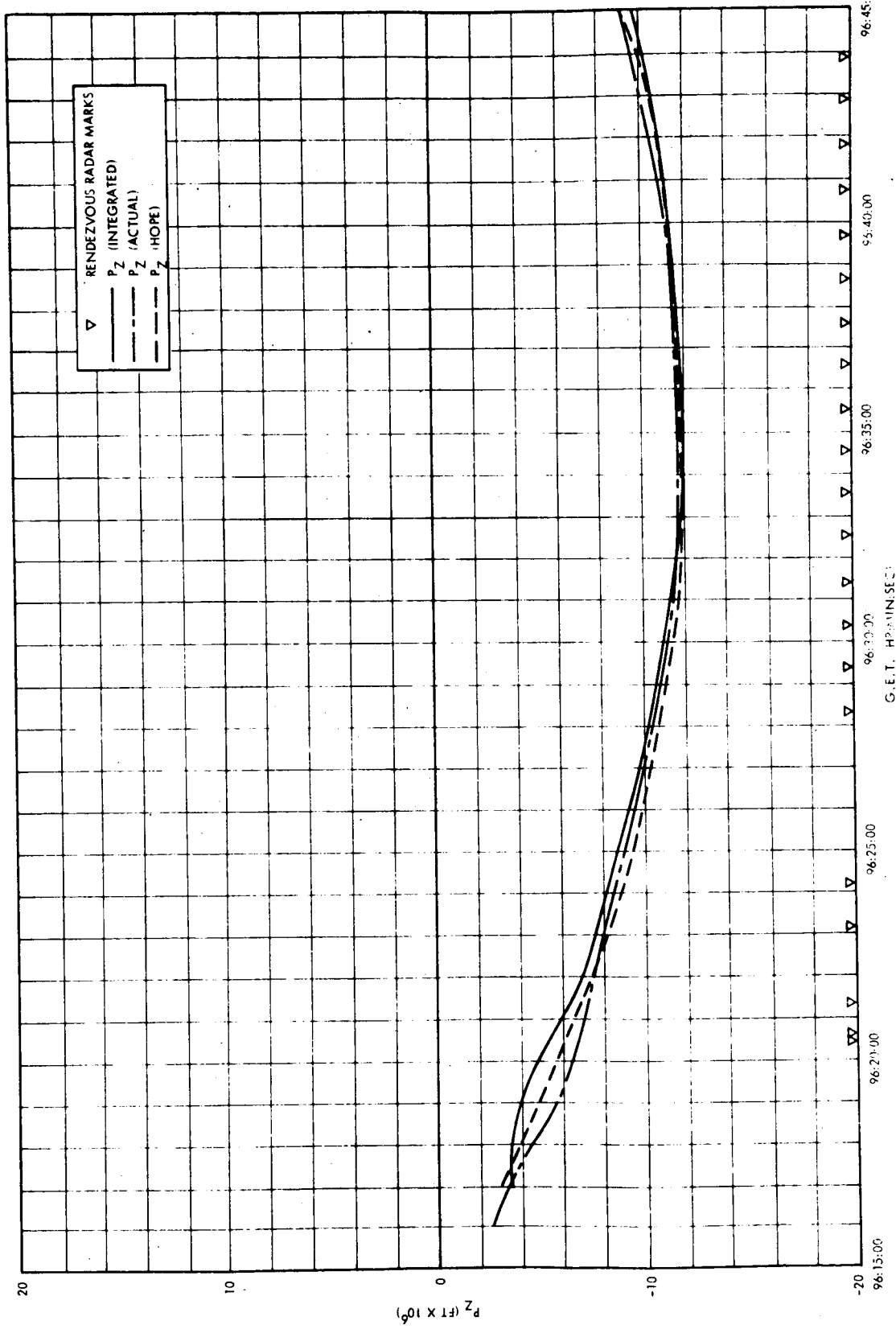


Figure 8.3 STATE VECTOR COMPARISON VERSUS RENDEZVOUS RADAR MARKS - PZ

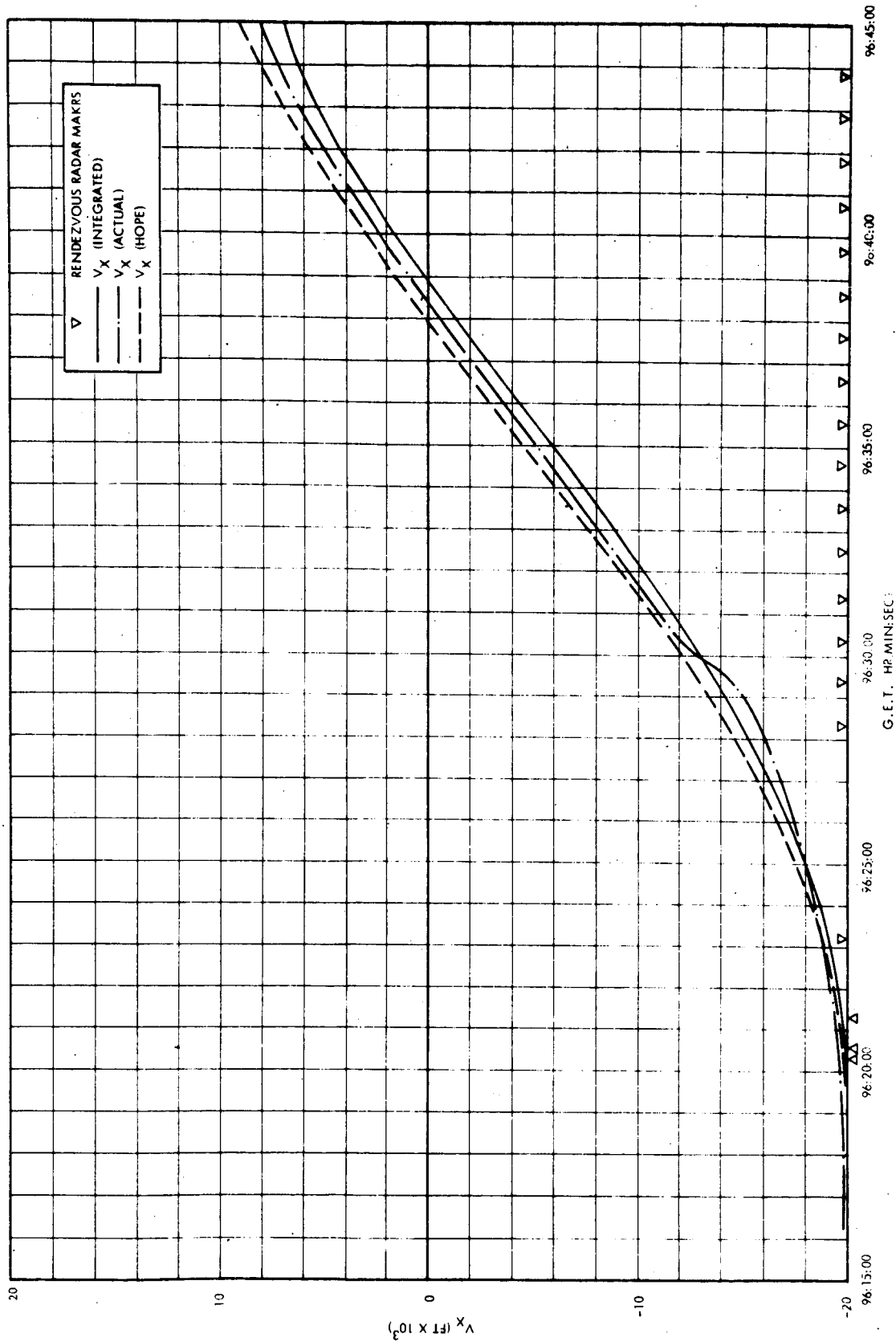


Figure 8.4 STATE VECTOR COMPARISON VERSUS RENDEZVOUS RADAR MARKS -  $V_x$

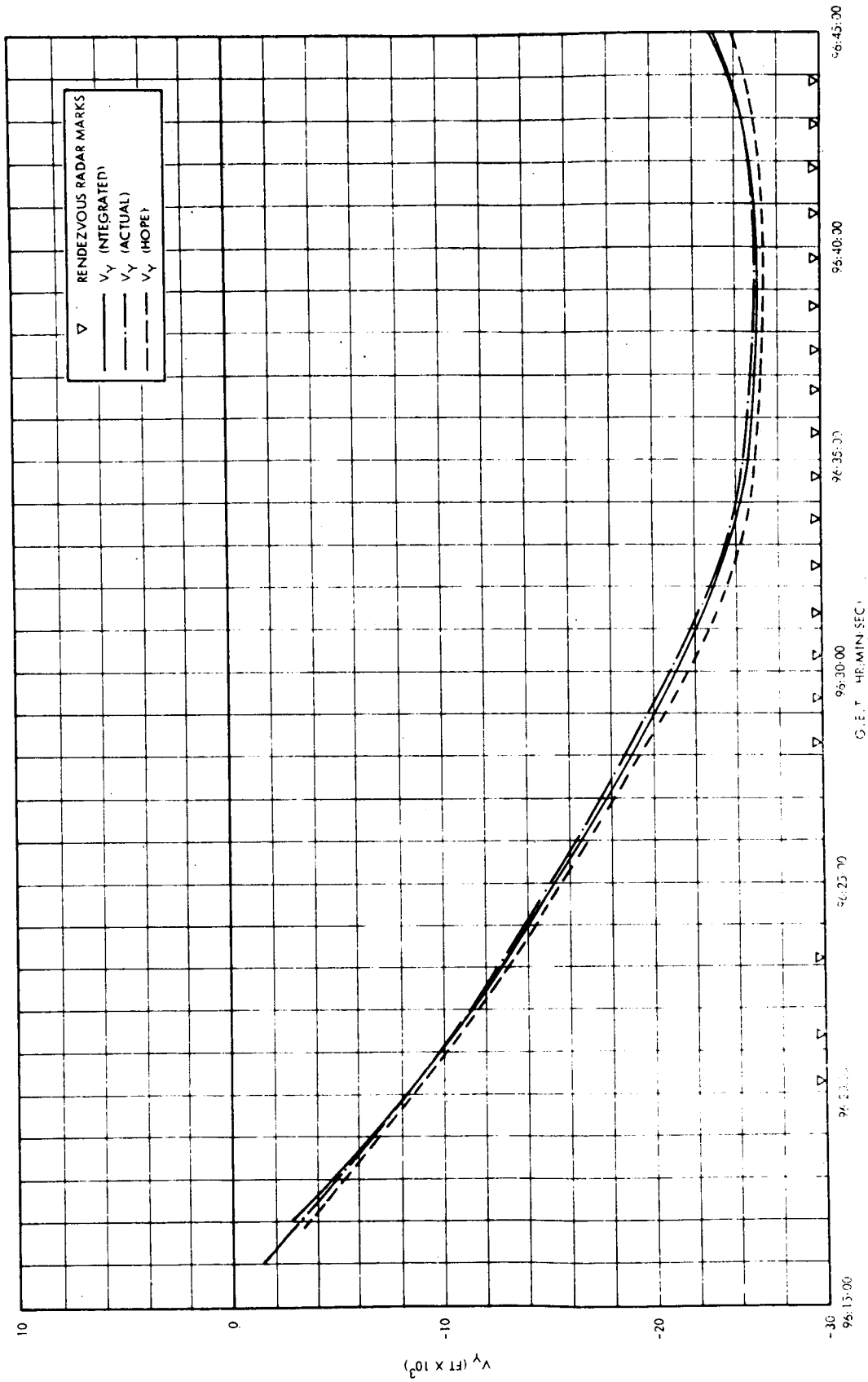


Figure 8.5 STATE VECTOR COMPARISON VERSUS RENDEZVOUS RADAR MARKS -  $V_y$

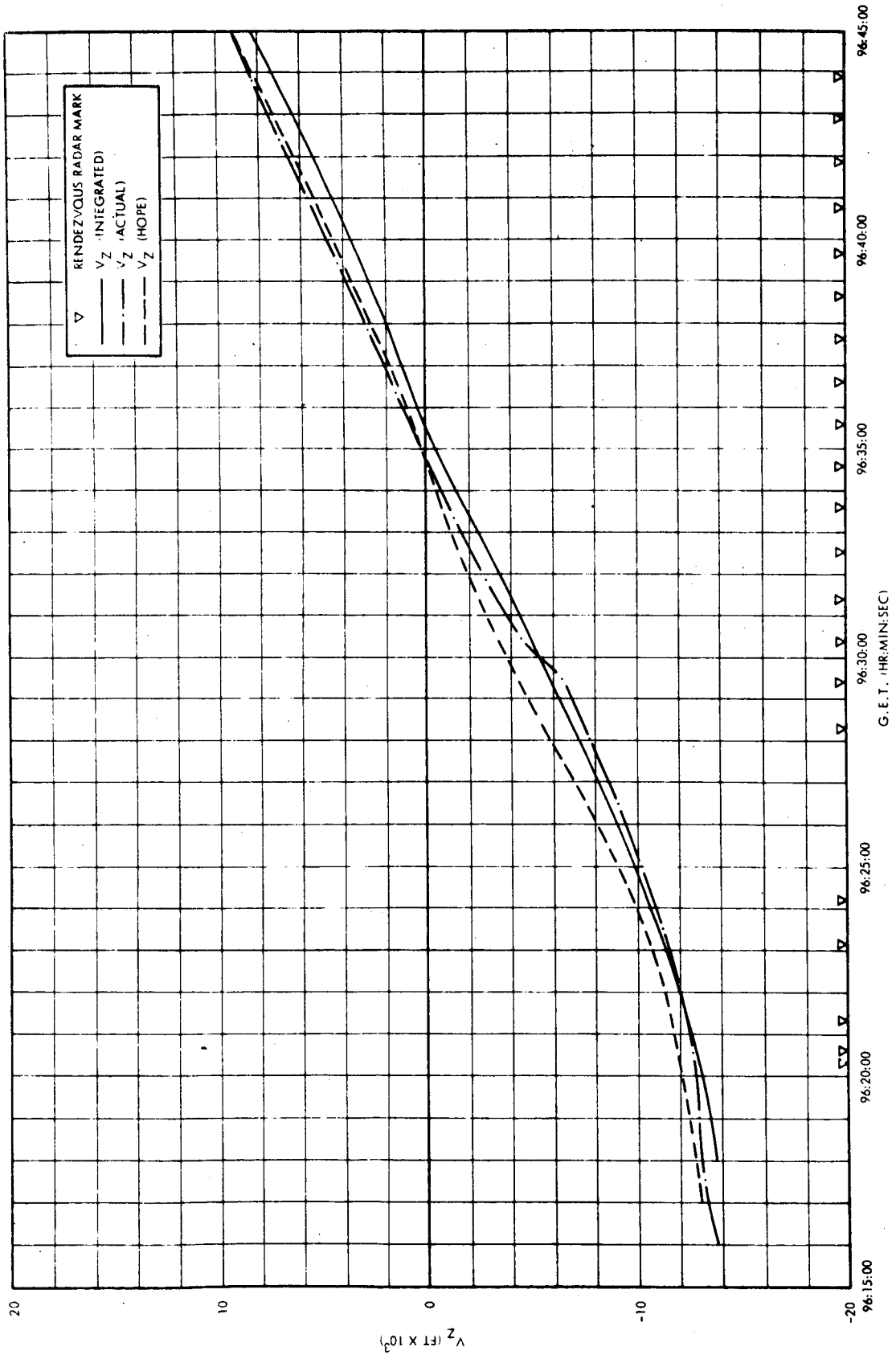


Figure 8-6 STATE VECTOR COMPARISON VERSUS RENDEZVOUS RADAR MARKS -  $V_z$

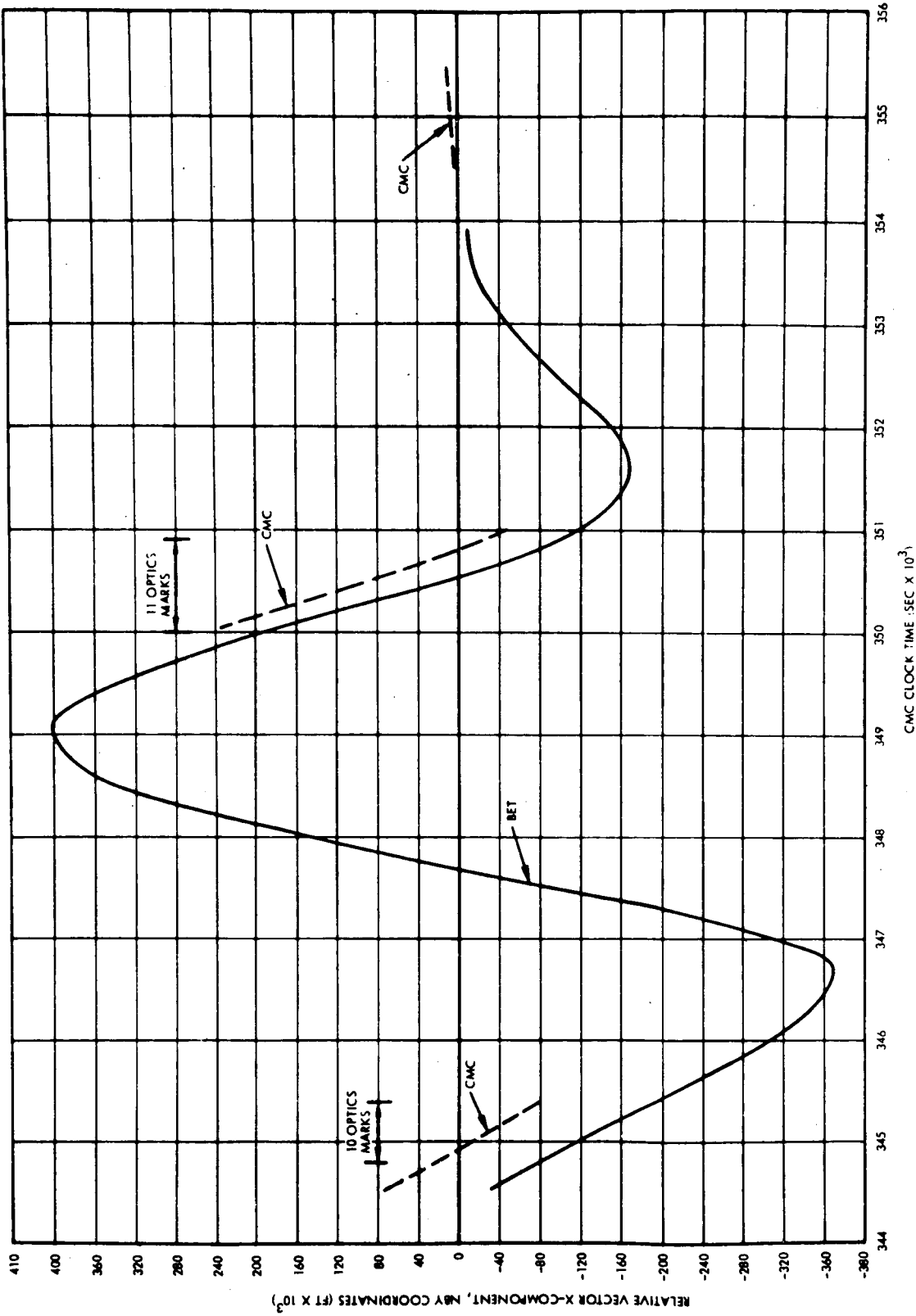


Figure 8-7 COMPARISON OF CMC AND BET RELATIVE POSITION VECTOR - X COMPONENT (NBY COORDINATES)

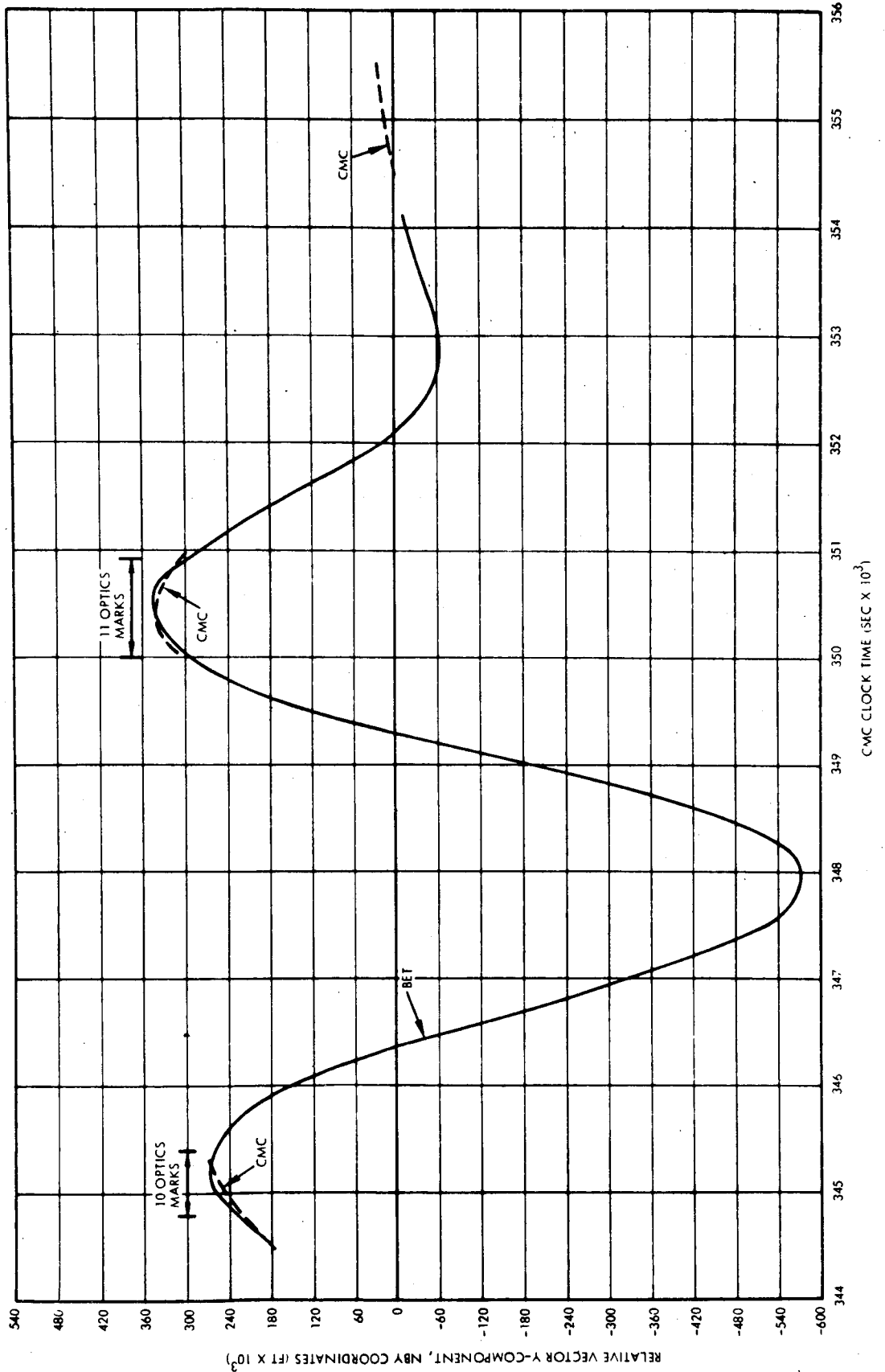


Figure 8-8 COMPARISON OF CMC AND BET RELATIVE POSITION VECTOR - Y COMPONENT (NBY COORDINATES)

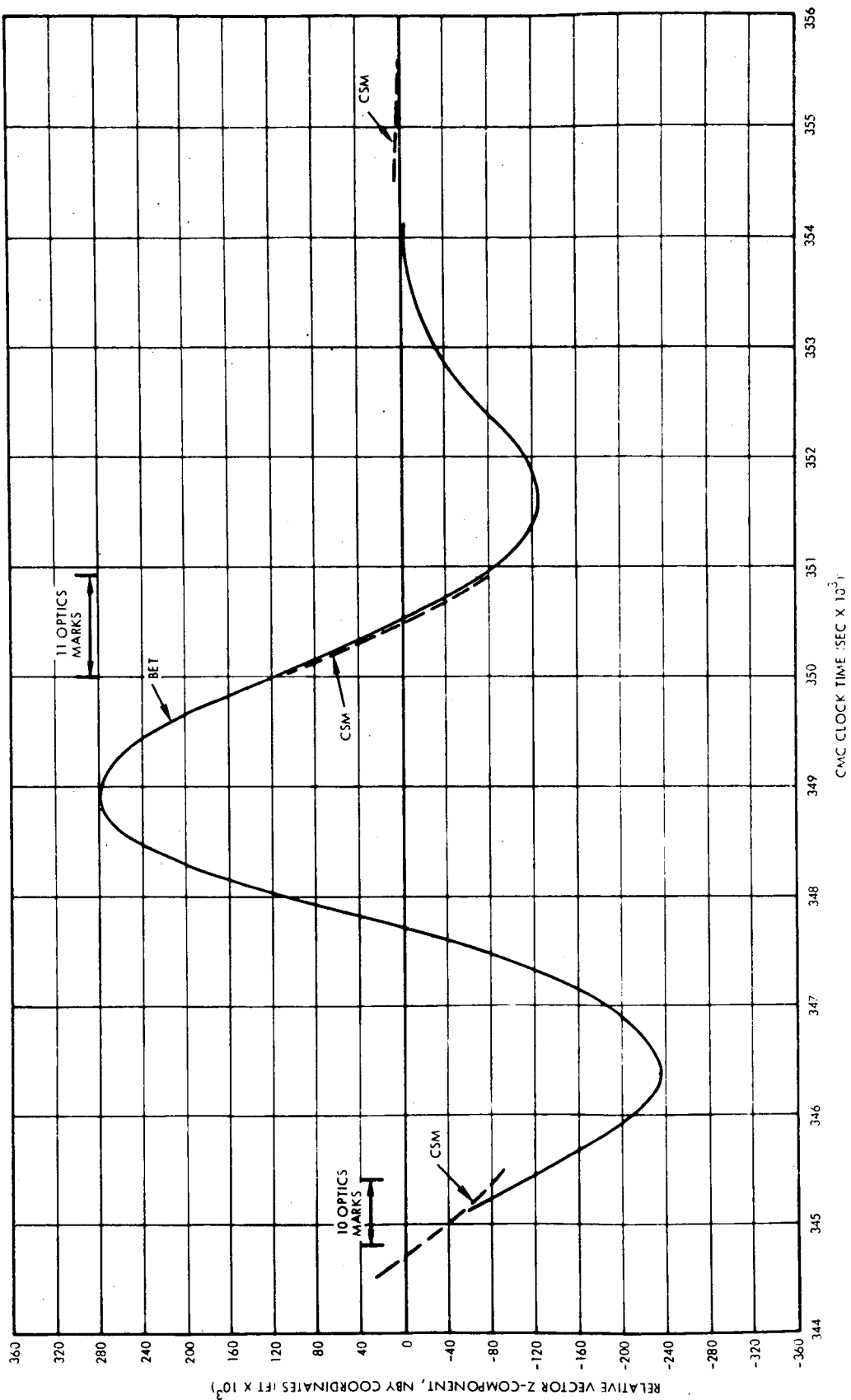


Figure 8-9 COMPARISON OF CMC AND BET RELATIVE POSITION VECTOR - Z COMPONENT ( NBY COORDINATES)

TABLE 8.1  
RENDEZVOUS TARGETING SUMMARY

Maneuver	$\Delta V$ Nominal*(Ft/Sec)	$\Delta V$ Actual (Ft/Sec)	Solution Executed
CSM Separation	5.0	5.0	RTCC
Phasing	88.8	90.5	RTCC
Insertion	41.8	43.1	RTCC
CSI	38.9	40.0	LGC
CDH	39.1	41.5	LGC
TPI	22.9	22.3	LGC
MCC 1	0	1.4	LGC
MCC 2	0	2.0	LGC
Braking	28.7	27.8	
<b>TOTAL</b>	<b>266.2</b>	<b>273.2</b>	

Percent Above Nominal = 3.2

\*Apollo 9 Spacecraft Operational Trajectory, Revision 2, 20 February 1969

**TABLE 8.2**  
RENDEZVOUS TARGETING  
SOLUTION

Source Maneuver	RTCC		CMC		LGC		AEA		CHARTS	
Separation	$\Delta V_X=0$ $\Delta V_Y=0$ $\Delta V_Z=+5.0$	RSS +5.0								
Phasing	$\Delta V_X=+0.9$ $\Delta V_Y=0$ $\Delta V_Z=-90.7$	RSS 90.704								
TPI <sub>o</sub>	$\Delta V_X=-20.2$ $\Delta V_Y=+0.4$ $\Delta V_Z=-1.5$	RSS 20.259	$\Delta V_X=19.6$ $\Delta V_Y=0.6$ $\Delta V_Z=-3.3$	RSS 19.884	$\Delta V_X=-20.1$ $\Delta V_Y=0$ $\Delta V_Z=1.8$	RSS 20.180				
Insertion	$\Delta V_X=43.1$ $\Delta V_Y=0$ $\Delta V_Z=0.8$	RSS 43.107								
CSI	$\Delta V_X=-39.3$ $\Delta V_Y=0.6$ $\Delta V_Z=0$	RSS 39.304			$\Delta V_X=-40.0$ $\Delta V_Y=0$ $\Delta V_Z=0$	RSS 40.0	No Solution		$\Delta V_X=-40.7$ $\Delta V_Y=0$ $\Delta V_Z=0$	RSS 40.7
CDH	$\Delta V_X=-38.2$ $\Delta V_Y=-0.9$ $\Delta V_Z=-15.1$	RSS 41.086			$\Delta V_X=-39.2$ $\Delta V_Y=0.1$ $\Delta V_Z=-13.7$	RSS 41.525	$\Delta V_X=-40$ $\Delta V_Y=0$ $\Delta V_Z=-14$	RSS 42.379	$\Delta V_X=-39$ $\Delta V_Y=0$ $\Delta V_Z=-14$	RSS 42.077
TPI	$\Delta V_X=19.6$ $\Delta V_Y=0.1$ $\Delta V_Z=-10.5$	RSS 22.235	$\Delta V_X=-19.5$ $\Delta V_Y=-0.5$ $\Delta V_Z=9.0$	RSS 21.482	$\Delta V_X=19.4$ $\Delta V_Y=0.4$ $\Delta V_Z=9.7$	RSS 21.693			F 20.0 D 1.0	
MCC #1			$\Delta V_X=-0.6$ $\Delta V_Y=0.5$ $\Delta V_Z=2.3$	RSS 2.45	$\Delta V_X=-1.0$ $\Delta V_Y=-0.3$ $\Delta V_Z=0.9$	RSS 1.38			A 6.0 D 0.0	
MCC #2					$\Delta V_X=0.2$ $\Delta V_Y=-0.9$ $\Delta V_Z=-1.8$	RSS 2.022			F 1.0 U 0.0	
TPF				29.3		27.8		29		

TABLE 8.3  
CSI MANEUVER EVALUATION

<u>SOLUTION</u>	<u>ΔH AT CDH TIG (349094 SEC)</u>
LGC	9.9 n.m.
RTCC	9.5 n.m.
CHARTS	10.4 n.m.
Postflight BET	10.5 n.m.

NOTE: Nominal Δh = 10.8 n.m.

TABLE 8.4  
COMPARISON OF TPI SOLUTIONS

<u>SOLUTION</u>	<u>DISTANCE OF CLOSEST APPROACH (FT)</u>	<u>REQUIRED BRAKING ΔV (FT/SEC)</u>	<u>INTERCEPT TIME SLIP (SEC)</u>
LGC	2081	31.2	72 early
CMC	657	29.5	32 early
RTCC	3973	34.8	140 early
CHARTS	1291	21.2	267 late

NOTE 1 - LGC predicted intercept time: TTPF = 354587.67 secs

NOTE 2 - Actual ΔV braking was 27.8 ft/sec.

TABLE 8.5  
PGNCS TPI MANEUVER EVALUATION

Maneuver	Distance of Closest Approach (ft)	Required Braking $\Delta V$ (ft/sec)	Intercept Time Slip (sec)
TPI Only	3585	33.0	94 early
TPI & TPM	3050	27.9	1 late
TPI, TPM 1 & 2	2926	30.5	37 early

NOTE 1 - LGC predicted intercept time: TTPF = 354587.67 sec.

## REFERENCES

1. NASA SNA-B-D-027 (II) Rev. 1, "CSM/LM Spacecraft Operational Data Book, Vol II LM Data Book Part 1, Revision 1, 15 March 1969
2. NASA SNA-8-D-027 (II) Rev 1, CSM/LM Spacecraft Operational Data Book, Vol III Mass Properties, Revision 1, November 1968.
3. MIT IL E-2377, LM Digital Autopilot Simulation Results Using Program SUNDANCE, January 1969.